Tampere University

Joni Vuorinen

AXIAL FUEL MIXING IN CIRCULATING FLUIDIZED BED BOILER – MEASUREMENTS AND MODELLING

Faculty of Engineering and Natural Sciences
Master of Science Thesis
July 2019

ABSTRACT

JONI VUORINEN: Axial fuel mixing in circulating fluidized bed boiler – measurements and modelling
Tampere University
Master of Science Thesis, 93 pages
July 2019
Master's Degree Programme in Mechanical Engineering
Major: Applied Mechanics and Thermal Sciences
Examiner: University Lecturer Henrik Tolvanen, Professor Jukka Konttinen

Keywords: Circulating fluidized bed, modelling, fuel mixing, temperature profile, terminal velocity

Efforts to decrease greenhouse gas emissions have led to growing interest in biomass usage as energy source. The circulating fluidized bed (CFB) boiler has been proven a viable option for different kinds of bio-based fuels and other challenging fuels. In addition, fluidization technologies provide a cost-effective way to reduce SO_x and NO_x emissions. Thus, CFB boilers can be thought as a feasible option to reduce emissions compared to some other combustion technologies. Accurate modelling can help improve the design, operation and safety of boilers, and it is seen as an important tool in the development of boilers.

The goals of this thesis were to improve the accuracy of the temperature modelling in a comprehensive CFB model and to increase the knowledge on axial fuel mixing in CFB boilers. Large-scale measurements were done in a commercial CFB boiler to acquire temperature profiles when the fuels used were coal and biomass. Terminal velocities of these two different fuels were measured with and without bed material in laboratory-scale units. Image analysis was conducted for the elutriated fuel samples to obtain knowledge on size and shape of fuel particles. These measurement results were used as help when analysing the axial fuel mixing in the comprehensive CFB model.

The measurements showed that bed material affects the terminal velocity of fuel particles significantly. At the solids concentrations used, it was observed that the terminal velocity of devolatilized biomass could drop to a quarter from the measurements without the bed material. The measurements without the bed material showed that the terminal velocity of biomass changes more than terminal velocity of coal, during conversion from as received to devolatilized.

Based on the measurements and analysis of the comprehensive model, a new method for calculating the temperature profile was introduced in this thesis. The new method is based on a limiter for volatile combustion which allows more oxygen to go through the bottom bed and splash zone of the furnace. In addition, the fuel mixing model was manipulated so that more fuel can be elutriated to the transport zone. Results show that the modelling of the temperature profile improved with the new method. However, more research should be done relating to fuel mixing, gas mixing and biomass deformation during combustion, based on the results of this thesis.

The originality of this thesis has been checked using the Turnitin OriginalityCheck service

TIIVISTELMÄ

JONI VUORINEN: Polttoaineen aksiaalinen sekoittuminen kiertoleijukattilassa – Mittaukset ja mallintaminen
Tampereen yliopisto
Diplomityö, 93 sivua
Heinäkuu 2019
Konetekniikan diplomi-insinöörin tutkinto-ohjelma
Pääaine: Sovellettu mekaniikka ja lämpötekniikka
Tarkastajat: yliopistonlehtori Henrik Tolvanen, professori Jukka Konttinen

Avainsanat: Kiertoleijukattila, mallintaminen, polttoaineen sekoittuminen, lämpötilaprofiili, terminaalinopeus

Tavoitteet vähentää kasvihuonekaasupäästöjä ovat johtaneet kasvavaan kiinnostukseen biomassan energiakäyttöä kohti. Kiertoleijukattila on osoittautunut toimivaksi ratkaisuksi erilaisille biopohjaisille ja muille haastaville polttoaineille. Lisäksi kiertoleijukattila tarjoaa kustannustehokkaan tavan vähentää SO_x ja NO_x päästöjä. Näistä syistä kiertoleijukattilaa voidaan pitää toimivana ratkaisuna vähentää päästöjä verrattuna muihin polttotekniikoihin. Luotettava mallinnus voi auttaa parantamaan kattiloiden rakennetta, toimintaa sekä turvallisuutta. Näistä syistä mallintaminen nähdään tärkeänä työkaluna kattiloiden kehittämisessä.

Tämän työn tavoitteena oli parantaa lämpötilan mallintamisen tarkkuutta kokonaisvaltaisessa kiertoleijukattilamallissa sekä lisätä tietämystä aksiaalisesta polttoaineen sekoittumisesta kiertoleijukattilassa. Lämpötilaprofiilimittauksia tehtiin teollisen kokoluokan kiertoleijukattilassa, kun polttoaineina käytettiin hiiltä sekä biomassaa. Näiden polttoaineiden terminaalinopeus mitattiin ilman petimateriaalia ja petimateriaalin kanssa laboratoriolaitteistolla. Kuva-analyysi suoritettiin testatuille polttoaineille, jotta saatiin tietoa partikkelien koosta ja muodosta. Näitä tuloksia käytettiin apuna analysoidessa polttoaineen sekoittumista kokonaisvaltaisessa kiertoleijukattilamallissa.

Mittaukset osoittivat, että petimateriaali vaikuttaa polttoaineen terminaalinopeuteen merkittävästi. Käytetyillä kiintoainetiheyksillä koksatun biomassan terminaalinopeus tippui neljäsosaan mittauksista ilman petimateriaalia. Mittaukset ilman petimateriaalia osoittivat, että biomassan terminaalinopeus muuttuu enemmän kuin hiilen terminaalinopeus konversiossa tuoreesta polttoaineesta koksiksi.

Mittausten ja kokonaisvaltaisen mallin analyysin perusteella uusi menetelmä lämpötilaprofiilin laskemiseksi kehitettiin tässä työssä. Uusi menetelmä perustuu rajoittimeen, joka mahdollistaa suuremman happimäärän kulkemisen pohjapedin ja roiskealueen (splash zone) läpi. Lisäksi polttoaineen sekoittumismallia muokattiin siten, että enemmän polttoainetta voi kulkeutua roiskealueen yläpuolelle. Tulokset osoittavat, että lämpötilaprofiilin mallintaminen parani uudella menetelmällä. Tämän diplomityön tulosten perusteella lisää tutkimusta kuitenkin tarvitaan liittyen polttoaineen ja kaasun sekoittumiseen sekä biomassan muodonmuutokseen palamisen aikana.

PREFACE

This thesis has been done in the R&D department of the Pulp & Energy business line in Valmet Technologies. I would like to thank all my co-workers for the joyful working atmosphere every day. Especially I would like to thank Mr. Ville Ylä-Outinen and Dr. Sonja Enestam for giving me the opportunity to do my thesis at Valmet. Ville's help and thoughts during the whole thesis project are greatly appreciated. I would also like to thank the whole personnel in the Valmet's R&D Center for the help during work done there. Special thanks go to Mr. Tarmo Toivonen for arranging the facilities there. In addition, I would like to thank Dr. Aino Vettenranta for the feedback and help with the text of this thesis.

I would like to thank University Lecturer Henrik Tolvanen for the help especially with the structure and presentation style of the thesis. Your feedback has helped to keep me focused in correct things during the thesis. I would also like to thank Professor Jukka Konttinen for being the second examiner for my thesis.

I would like to express my gratitude for Chalmers University of Technology and especially Associate Professor David Pallarès for making the measurements there possible and Mr. Jesper Aronsson for help during measurements. In addition, I would like to thank the power plant which allowed measurements at their boiler.

This thesis project was only a part of my studies in Tampere University and thus I would also like to thank friends from the university for help and friendship during the studies. Finally, and especially, I would like to thank my family for always supporting me in my studies from the first day of primary school to this day.

Tampere, 11.7.2019

Joni Vuorinen

CONTENTS

LIST OF SYMBOLS AND ABBREVIATIONS

A.R.	As received
BFB	Bubbling fluidized bed
CCS	Carbon capture and storage
CFB	Circulating fluidized bed
CFD	Computational fluid dynamics
CG	Centre of gravity
CP	Centre of pressure
CUT	Chalmers University of Technology
daf	Dry ash free
EU	European Union
HHV	Higher heating value
LHV	Lower heating value
LUT	Lappeenranta University of Technology
PCTL	Percentile
PF	Pulverized firing
PSD	Particle size distribution
TUHH	Hamburg University of Technology
0D	0-dimensional
1D	1-dimensional
1.5D	1.5-dimensional
2D	2-dimensional
3D	3-dimensional

a	Splash zone decay constant	-
a_1	Variable in equation 21	-
A_p	Particle's projected area	m^2
A_{part}	Area of the particle's surface	m^2
AR	Aspect ratio	-
$A_{sph,eq\,V}$	Area of sphere with equivalent volume as particle	m^2
b	Exponent in heat transfer coefficient formulation	-
b_1	Variable in equation 21	-
c	Coefficient in heat transfer coefficient formulation	-
c_1	Variable in equation 21	-
$c2d$	Portion of entrainable particles which behave according to ballistic decay	-
C	Fuel concentration	kg m^{-3}
C_{bal}	Ballistic fuel concentration	kg m^{-3}
C_{Cox}	Circularity, Cox	-
C_D	Drag coefficient	-
C_{disp}	Dispersive fuel concentration	kg m^{-3}
C_{H_b}	Fuel concentration at dense bed surface	kg m^{-3}
C_{Riley}	Circularity, Riley	-
d	Diameter	m
D	Diameter of tube	m
d_a	Diameter of active fuel particle	m
d_b	Diameter of inert bed particle	m

d_c	Diameter of smallest circumscribed circle	m
d_i	Diameter of largest inscribed circle	m
d_{max}	Maximum dimensional distance	m
d_{mean}	Intermediate dimensional distance	m
d_{min}	Minimum dimensional distance	m
d_p	Diameter of particle	m
d_p^*	Dimensionless particle diameter	-
$d_{sph,eq\ A_p}$	Diameter of sphere with equivalent projected area as particle	m
$d_{sph,eq\ V}$	Diameter of sphere with equivalent volume as particle	m
F_B	Buoyancy force	N
F_D	Drag force	N
F_G	Gravitational force	N
F_L	Lift force	N
F_N	Newton shape descriptor	-
F_S	Stokes form factor	-
g	Acceleration due to gravity	m s^{-2}
h	Heat transfer coefficient	W m^{-2} K^{-1}
H_b	Dense bed height	m
k_N	Newton's drag correction	-
k_S	Stoke's drag correction	-
K	Transport zone decay constant	-
L_p	Characteristic length of the particle	m
m_a	Mass of active fuel particle	kg
m_b	Mass of inert bed particle	kg
P	Perimeter	m
Re	Reynolds number	-
Re_a	Reynolds number of active fuel particle	-
R_P	Roundness, Pentland	-
t	Time	s
u_f	Fluid velocity	m s^{-1}
u_p	Particle velocity	m s^{-1}
u_{slip}	Slip velocity	m s^{-1}
u_t	Terminal velocity of a particle	m s^{-1}
u_t^*	Dimensionless terminal velocity	-
$u_{t,a}$	Terminal velocity of active fuel particle	m s^{-1}
$u_{t,b}$	Terminal velocity of inert bed particle	m s^{-1}
$u_{t,c}$	Terminal velocity of a particle in cold conditions	m s^{-1}
$u_{t,h}$	Terminal velocity of a particle in hot conditions	m s^{-1}
V_p	Volume of the particle	m^3
X	Coefficient	-
z	Height	m
ε_{core}	Voidage at core region	-
μ_f	Dynamic viscosity of the fluid	kg m^{-1} s^{-1}
$\mu_{f,c}$	Dynamic viscosity of the fluid in cold conditions	kg m^{-1} s^{-1}
$\mu_{f,h}$	Dynamic viscosity of the fluid in hot conditions	kg m^{-1} s^{-1}

ν_f	Kinematic viscosity of the fluid	$m^2\ s^{-1}$
ρ_f	Density of the fluid	$kg\ m^{-3}$
$\rho_{f,c}$	Density of the fluid in cold conditions	$kg\ m^{-3}$
$\rho_{f,h}$	Density of the fluid in hot conditions	$kg\ m^{-3}$
ρ_p	Density of the particle	$kg\ m^{-3}$
ρ_s	Solids concentration	$kg\ m^{-3}$
$\rho_{s,core}$	Solids concentration at core region	$kg\ m^{-3}$
$\rho_{s,entr}$	Amount of solids entrained from the dense bed to the transport zone	$kg\ m^{-3}$
ρ_{s,H_b}	Solids concentration in the dense bed	$kg\ m^{-3}$
φ	Sphericity	-
$\varphi_\perp$	Crosswise sphericity	-
$\varphi_\parallel$	Lengthwise sphericity	-
Ψ_C	Corey shape factor	-

1. INTRODUCTION

The first research on the impact of greenhouse gases to the global thermal balance was made in the 1800s, most notably by Fourier and Arrhenius (Arrhenius 1896; Fourier 2013). Scientific consensus grew during the 1900s about the effects of human activities to the climate change and in 2015, an intergovernmental Paris Agreement was agreed upon to limit the increase in global average temperature to well below 2 °C compared to the pre-industrial levels (Paris Agreement 2015). To date, the agreement is ratified by 185 countries out of 197 parties of the convention (United Nations Climate Change 2019). According to the Intergovernmental Panel on Climate Change (2018), the current goal of limiting the increase in global average temperature below 1.5 °C requires CO_2 emission decline by 45% from 2010 level by 2030, and emissions should reach net zero around 2050. The European Union (EU) has set its own emission reduction target to be at least 40% by the year 2030, and 80% by the year of 2050 compared to the greenhouse gas emissions in 1990 (European Commission). In addition to these emission reduction targets, EU has set a target to produce at least 27% of energy from renewable sources and China, for example, has set a target to produce 20% of energy from non-fossil sources by the year 2030 (European Commission; Jiankun et al. 2012; Climate Action Tracker).

Biomass usage can have a significant impact in reducing the life cycle carbon dioxide equivalent emissions in the energy production compared to fossil fuels (Eriksson et al. 2007; Intergovernmental Panel on Climate Change 2014, p. 539; Macedo et al. 2015, pp. 582–616; Souza et al. 2017; Vakkilainen 2017, p. 19; Charry et al. 2018; He et al. 2018; Rautiainen et al. 2018; Suopajärvi et al. 2018). However, there are also arguments against the usage of biomass in energy production, typically based on short time span calculations or considering biomass usage as separate from other industries (Konttinen et al. 2018; Orasuo 2018). But as stated above, biomass usage is mainly considered to decrease carbon dioxide equivalent emissions compared to fossil fuels. Scientific interest towards biomass usage as energy source has grown continuously and the usage of biomass as a primary energy source in power generation is expected to rise 6% annually for the next 4 years while international targets demand the decrease of coal generated power (International Energy Agency; Mao et al. 2018). Biomass combustion with carbon capture and storage (CCS) can also be utilized as a negative emission technology even though CCS still has some unsolved problems regarding its economic and technical feasibility which have limited its industrial scale use (Teir et al. 2011; Koornneef et al. 2012; Mclaren 2012; Kemper 2015; Rootzén & Johnsson 2015; Budinis et al. 2018; Durmaz 2018; Fridahl & Lehtveer 2018; Lee & Choi 2018).

Fluidized bed combustion has been proven to be a viable option for energy conversion from both biomass and coal. Fluidized bed combustion occurs in a furnace where air is

blown from the bottom of the furnace through a bed that consists of sand and ash particles. Air fluidizes the bed and fuel is fed into the bed where combustion occurs. Circulating fluidized bed (CFB) is a certain type of fluidization technology which is utilized in chemical and energy engineering. In CFB boilers bed material is entrained to the top of the furnace and from there out of the furnace to the particle separator where combustion air and bed material are separated. Bed material is then fed back to the furnace through a fluidized loop seal while flue gases exit the hot loop. The CFB technology is presented in more detail in Chapter 2.

The benefits of computer-aided engineering are widely known and, for example, computational fluid dynamics (CFD) techniques have numerous advantages over experience-based design. These benefits include reduction of lead times and costs of new design, ability to study systems where experiments are difficult to perform and ability to study system's behaviour under hazardous conditions and beyond their normal operating conditions (Versteeg & Malalasekera 2007, p. 2). In CFB boilers, there exists a complex multiphase flow with continuous thermochemical reactions and heat transfer. Thus, measurements are difficult to perform inside the furnace. This also means that a holistic model from CFB boiler with CFD would require very long calculation times and that is why it is not feasible in an industrial use (Kallio et al. 2015; Nikku 2015). Nikku et al. (2017) reported that a CFD-simulation of a laboratory-scale cold-model CFB required calculation times between 120–290 hours depending on software and calculation model with 2 Intel Xeon E5-2698 processors (Nikku et al. 2017).

For the above-mentioned reasons, there has been an interest to develop a comprehensive models which could offer reasonable results with reasonable computational times. The development for the first comprehensive models started in the late 1980s and currently there are three three-dimensional (3D) holistic semiempirical models in the open literature (Pallarès & Johnsson 2013). However, these models do not provide completely accurate results from different phenomena in the boiler. Thus, development has to be done to increase the accuracy and reliability of these models.

This thesis focuses on axial fuel mixing in the CFB boiler, which has been subject of research lately (Pallarès & Johnsson 2008b, Korhonen 2012; Nikku et al. 2014; Nikku 2015; Nikku et al. 2016; Köhler et al. 2017; Soriano Sánchez 2019). The goal is to obtain knowledge on axial fuel mixing and study axial fuel mixing in a comprehensive CFB model and its effects on axial temperature profile. The primary goal of this thesis is to improve the modelling of axial temperature profile and to identify the development targets related to axial fuel mixing and temperature profile in a comprehensive CFB model, which is developed in Chalmers University of Technology (CUT) in co-operation with Valmet (formerly known as Metso Power).

The theoretical background of this work is discussed with a focus on CFB fluid dynamics, fuel behaviour in combustion, heat transfer, and particle behaviour in flow. In addition,

comprehensive CFB models and fuel mixing models are presented in Chapter 4. The experimental research focuses on terminal velocity of fuel particles with and without bed material, which affects directly the fuel mixing in the CUT model. Similar kind of experimental research has been done previously by Korhonen (2012), Nikku et al. (2014) and Soriano Sánchez (2019). In addition, temperature distribution is measured from a large-scale CFB boiler to get knowledge on the temperature distribution with coal and biomass as fuels. This information is also used as a validation data in the modelling part. In the modelling part, the most crucial variables in fuel mixing model are identified with sensitivity analysis. Information from the measurements and sensitivity analysis is then used in analysing and improving the accuracy of the CFB model. Research questions that will be discussed are:

- *How biomass differs from coal with respect to fuel mixing and combustion in a CFB boiler?*
- *What kind of information can be obtained from measuring terminal velocity of fuel particles?*
- *Does information from terminal velocity measurements improve CFB modelling efforts?*
- *Does temperature profile of the comprehensive model correspond to the measured temperature profile?*

The first research question is discussed on theoretical basis in Chapters 2 and 3. The experimental results from fuel elutriation are presented in Chapter 6. The results from terminal velocity measurements and information obtained through them and image analysis is presented in Chapter 6. Third research question is addressed mostly in Chapter 7 but the results which lead to the conclusions are presented in Chapter 6. Final research question is addressed in Chapter 6.

2. CIRCULATING FLUIDIZED BED BOILER

2.1 Circulating fluidized bed boiler overview

Fluidized bed technology development can be dated back to 1920s for Winkler's coal gasifier. In the 1960s efforts to find an alternative combustion system for low-grade coal lead to the development of fluidized bed combustion. In Finland the interest for fluidized bed combustion came from the interest in burning other low-grade fuels like peat, wood waste and sludge. In the mid-1970s began the research and development for circulating fluidized bed combustion in Germany which was soon followed by Finland, Sweden and the USA. First commercial CFB boiler (5 MW_e) started in 1979 and to date largest ones are in the range of 600 MW_e (Wall et al. 2012; Nuortimo 2015; Cai et al. 2017). (Kunii & Levenspiel 1991, pp. 15–59; Koornneef et al. 2007)

Regardless of the manufacturer, CFB boilers typically share the same basic configurations. Largest differences come from solid separator, external heat exchanger and air feeding system (Koornneef et al. 2007). Regarding solid separation, cyclone is the most used particle separator, but one manufacturer uses impact separator which is inexpensive and more simple construction but offers poorer collection efficiency than a cyclone (Basu 2015, p. 220). Major differences come also from the cooling of the cyclone since some manufacturers offer non-cooled cyclones which require thicker refractory and leads to higher heat loss (Basu 2015, p. 215). There are also differences in the positioning of the cyclone since one manufacturer offers so called compact separator which reduces area required for the hot loop (Chen & Jiang 2011). Also loop seal design causes differences between designs since the loop seal can be designed to have different number of sections and include also a superheater to avoid corrosion and fouling for example with biomass as fuel. Certain manufacturer can also have different designs for different fuels and different power outputs starting from heat exchanger surfaces to the number of cyclones required (Uusitalo et al. 2018). Figure 1 illustrates Valmet's Cymic CFB boiler.

Fluidized bed combustion has numerous advantages over pulverized firing (PF): primarily fuel flexibility, emission control and good load-following capability (Basu 2015 pp. 7–12). Circulating fluidized bed boilers typically have combustion temperature between 800 °C and 900 °C while PF boilers have combustion temperatures between 1300 °C and 1400 °C. Thus, CFB boilers produce much less NO_x emissions (Utt & Giglio 2012). In comparison to PF boilers CFB boilers also offer possibility for in-furnace sulphur capture by adding limestone to the furnace.

Fuel flexibility has been proven to be important feature regarding CFB boilers. Inert bed material works as a thermal "flywheel" in a CFB boiler which gives the CFB boiler better ability to tolerate variations in fuel quality and burn wider range of fuels (Utt & Giglio

2012). Fuel flexibility concerns also particle size of the fuel since CFB boilers can tolerate fuels with wide particle size distribution (PSD). In comparison to pulverized fuel burners which demand biomass particles to be less than 1 mm on diameter CFB boilers can burn particles which vary typically from microns to multiple centimetres (Kastberg & Nilsson 2002; Koornneef et al. (2007); Nikku et al. 2014; Hurskainen & Vainikka 2015, p. 183). Thus, need for energy intensive excessive biomass milling is much smaller in CFB boilers (Priyanto et al. 2017; Riaza 2017). Figure 6 compares typical fuel ranges of CFB and PF boilers while demonstrating heating value and burning difficulty of different fuels (Utt & Giglio 2012). It should be noted that pulverized coal boilers can co-fire biomass with their primary fuel, but the levels of co-firing are typically between 5–10% (IEA-ETSAP 2013). Increasing the amount of biomass used, leads to several problems in PF boilers, one becoming from the fact that biomass particles remain significantly larger than 1 mm even through the same milling process as coal (Agbor et al. 2014). PF boilers are also more sensitive to the biomass quality they use in co-firing since for example moisture content in fuel should be less than 20 weight% in PF boilers (Agbor et al. 2014; Roni et al. 2017).

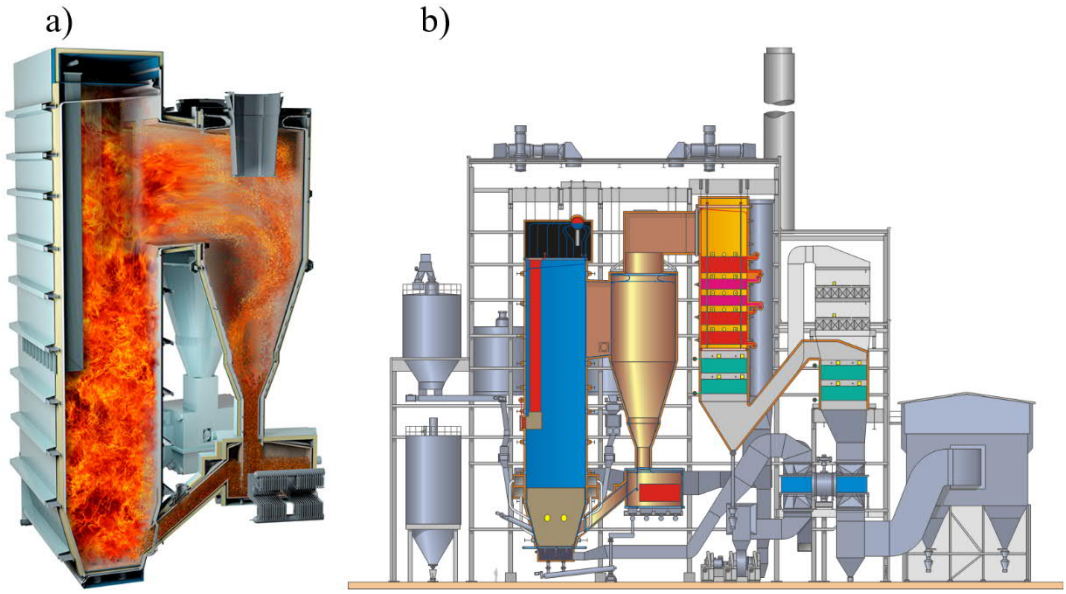

Figure 1. *Illustration of circulating fluidized bed boiler's hot loop in operation (a) and whole boiler (b). Figures in courtesy of Valmet.*

In comparison to grate firing, fluidized bed combustion has better efficiency and among fluidized bed technologies CFB has better efficiency than bubbling fluidized bed (BFB) combustion (van den Broek et al. 1996; Yin et al. 2008; Basu 2015; Yin & Li 2017). Biggest difference in CFB and BFB operation is that in BFB boilers superficial gas velocity is much slower and thus bed material is not entrained out of the furnace. In comparison to grate firing, CFB boilers allow both low SO_x and NO_x emissions due to low combustion temperature and in-furnace sulphur capture (Yin et al. 2008; Yin & Li 2017). CFB boilers also have higher heat-release rate per grate area than grate firing or BFB boilers which allows smaller furnace cross sections for same power output (Yin et al. 2008; Basu 2015, p. 5).

2.2 Fluid dynamics

Circulating fluidized bed boiler includes complex multiphase flow which has great impact on boiler's operation. In gas flow particles of different shapes and sizes are fluidized by air injections from evenly distributed primary air nozzles on the furnace floor and secondary air nozzles on the furnace walls. Primary air's function is to provide combustion air and fluidize the bed. Primary air's amount is between 40–80% from the stoichiometric amount (Basu 2015, p. 107). When load is increased the proportion of primary air is increased in relation to secondary air. Secondary air injections are typically 1.5–4 m above the grate. Secondary air injections function is to provide rest of the combustion air to the furnace for staged combustion. Furnace also receives air from the fluidization air from the loop seal and some air is pushed to the furnace with fuel. Some boilers can also have openings near the furnace floor for recycled flue gas for better combustion control. (Basu 2015; Valmet MyAcademy)

Fluidized bed material consists mostly of sand and ash from fuel. The relation between amounts of ash and sand depends a lot from the fuel used. For fuels which contain lots of ash like coal the bed has a lot greater amount of ash than for biomass which does not produce as much ash as coal (Basu 2015, p. 309). Majority of bed particles can be classified to group B in Geldart classification (Geldart 1973; Kunii & Levenspiel, pp. 77-79; Basu 2015, pp.342-343). Figure 2 presents a PSDs for solid material in industrial scale CFB boilers. In addition, Figure 2 has separation efficiency curve for cyclone separator. Typically, in multiphase flows PSD is modelled with Gaussian distribution, log-normal distribution or Rosin-Rammler distribution (also known as Weibull distribution) (Wang & Fan 2013). To author's knowledge the latter one is considered the most suitable for PSD in CFB boiler (Yang et al. 2003; Yang et al. 2004).

Fluidization behaviour of the bed depends mainly on superficial gas velocity, particle size and density difference between particles and fluidization medium. Thus, for the same bed material the behaviour of the bed depends on the fluidization velocity. CFB boilers operate typically on state of fast fluidization. In this state particle entrainment is significant and thus there is no distinct bed surface. In fast beds solids move upwards in the core region of the furnace and have a downward flux next to walls. Particles typically form clusters to dilute suspension according to Figure 3. Causes for this phenomenon are presented in Chapter 3.3. (Kunii & Levenspiel 1991; Basu 2105; Grace 2017)

Different fluid dynamical zones can be identified at different heights of a CFB boiler. These different zones are defined based on solids behaviour in areas in question. These different regions are presented in Figure 4. When solids inventory is large enough, the furnace floor has dense bed which resembles a bubbling fluidized bed. Time-averaged solids concentration in dense bed is constant along the height of the dense bed. Recent results have shown that dense bed can be maintained with gas velocities at least twice greater than the terminal velocity of an average bed particle if pressure drop along the

riser height is enough i.e. particle inventory is large enough (Djerf et al. 2018). Dense bed height is small compared to the total riser height (<0.5 m) but it is shown that it affects solids concentration also above its own surface. (Johnsson & Leckner 1995; Svensson et al. 1996; Djerf et al. 2018);

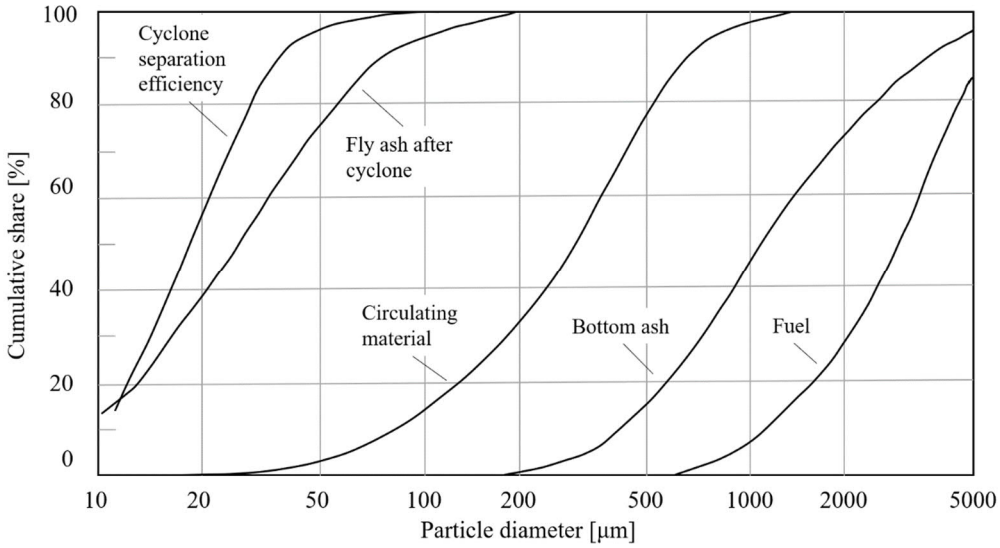

Figure 2. *Cyclone separation efficiency and particle size distributions of solid material in commercial CFB boiler. Adapted from Hyppänen & Raiko (2002).*

Dense bed consists of emulsion phase where most of the solids exist at minimum fluidization conditions and bubble phase where large fraction of primary air passes through the dense bed with large velocity. Bubbles create so called bubble paths in which most of the bubbles rise to the top of the dense bed (Pallarès & Johnsson 2006b). For velocities well above the minimum fluidization velocity so called through flow exists through and between the bubbles (Grace & Clift 1974, according to Pallarès & Johnsson 2013). It is shown that for fluidization velocities far greater than the minimum fluidization velocity most of the primary air passes the dense bed as through flow leading to local velocities several times higher than the average fluidization velocity (Clift & Grace 1985, according to Pallarès & Johnsson 2013; Hilligardt & Werther 1986, according to Pallarès & Johnsson 2013; Olowson & Almstedt 1990). Thus, dense bed is very inhomogeneous with very different behaviour depending on time and place.

Varying gas velocity and bursting bubbles on the dense bed surface cause a splash zone above dense bed surface. In splash zone erupting bubbles eject particles upward into the freeboard where particles might fall to the bed due to gravity or be entrained to the higher parts of the furnace. Splash zone has strong solids back-mixing phenomenon and bulk of particles have ballistic movement. Thus, solids concentration decreases significantly in the length of splash zone.

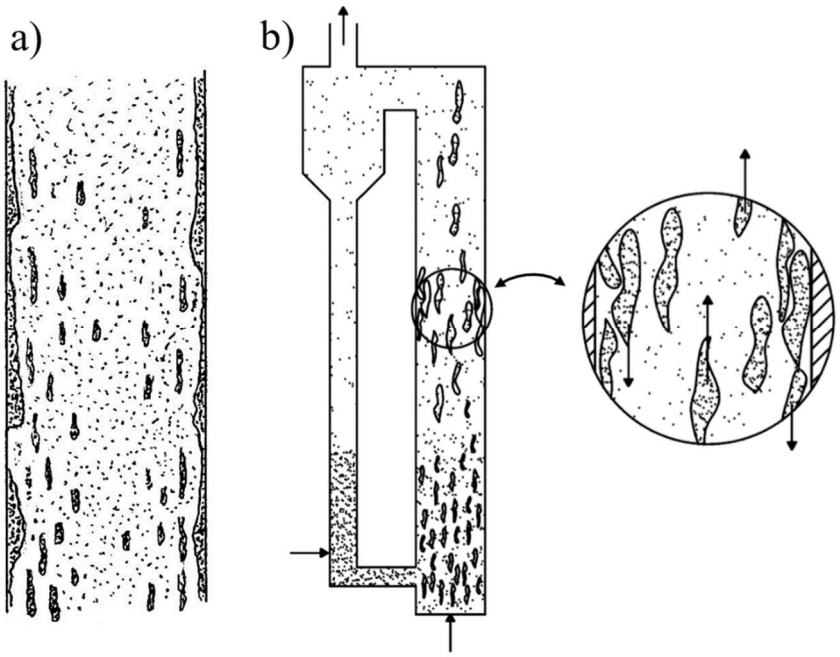

Figure 3. *Solids in the core-annulus flow in fast fluidization a) (Davidson 2000). Particle clustering in a fast fluidized bed b). Upward arrows present the upward flow in the core region and downward arrows present the downward flow next to walls. Adapted from Basu (2015, p. 30).*

Transport zone above splash zone has significantly smaller decay of solids concentration than splash zone. At transport zone exists a core-annulus structure in the flow where particles flow upward in the core of the furnace in dilute suspension. Next to walls exists a downward flow which has greater solids flux than upward flow (Davidson 2000). Figure 3 presents a typical solids distribution in the transport zone where core has dilute suspension with particle clusters and wall region has film flow downwards.

When the solids reach the top part of the furnace, they are either entrained to the cyclone via exit duct or enter the downflow in the wall layer. Solids behaviour in the exit zone includes more uncertainty than other areas of the freeboard (Pallarès & Johnsson 2006a). Highly dilute conditions in the exit zone cause pressure measurements to be unreliable. Thus, experimental knowledge on exit zone behaviour in the industrial scale CFB boilers is limited to visual observations in the scale models. Proportion of particles entering the cyclone have great impact on the operation of a CFB boiler (Pallarès & Johnsson 2006a). Industrial scale CFB boilers typically have one or more cyclone entrances with T-shape configurations where there is so called top hat above the cyclone entrance. Effect of exit zone geometry has been proven to have great impact on the segregation efficiency of a small CFB unit (Brereton & Grace 1993, according to Pallarès & Johnsson 2006a; Zhao et al. 2015; Zhang et al. 2018). However, these observations concern smaller CFBs than this thesis and it is argued that exit zone geometry has less significant impact in the industrial size CFB boilers (Johnsson et al. 1999; Lackermeier & Werther 2002). As stated above the amount of backflow from the exit zone has great impact to the operation of the CFB boiler. If less particles are entrained to the cyclone, particles have on average longer

residence times in the furnace. On the other hand, very low flows to the cyclone might affect boiler's operation for example if loop seal superheater is in use.

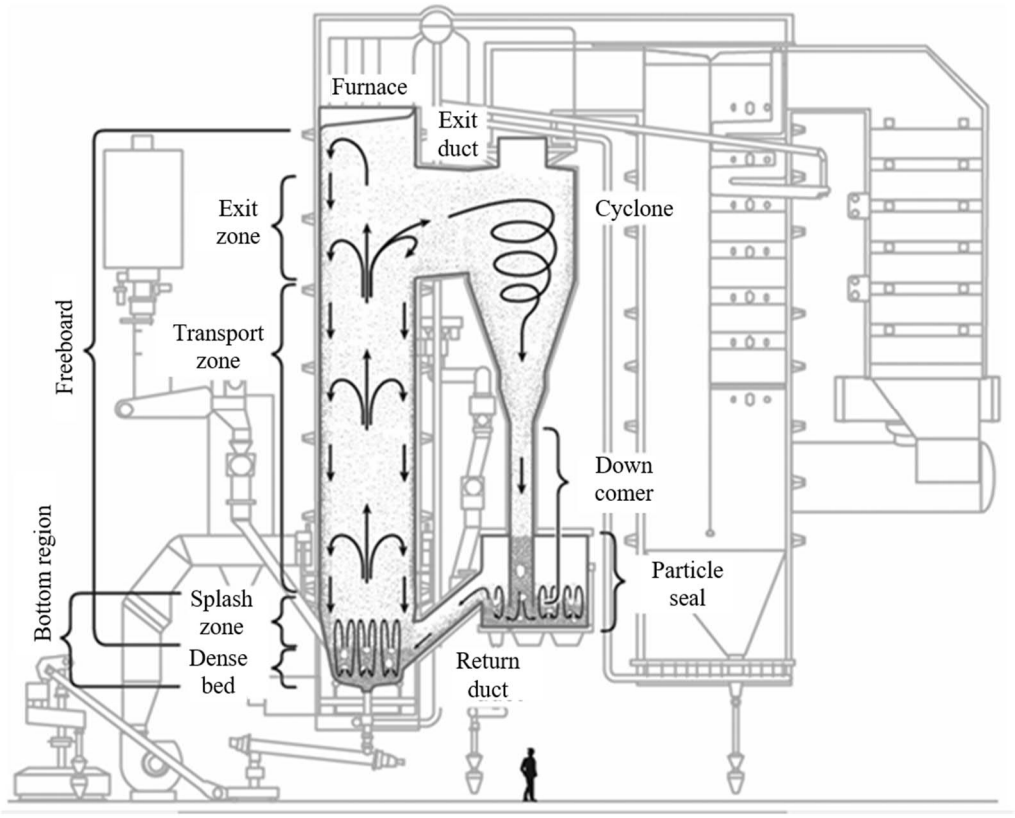

Figure 4. *Different zones in the hot loop of a CFB boiler. Adapted from Pallarès & Johnsson (2013).*

In the cyclone solids are separated from the gas flow. Solids are directed to loop seal via down comer. Loop seal is kept in state of bubbling fluidization from where solids travel back to the furnace. Depending on the cyclone's separation efficiency some particle sizes end up out of the hot loop with flue gas. In principal cyclone's separation efficiency improves with larger particles. Typical overall cyclone efficiency is over 99.9% and cut point size is 10–30 µm (Hyppänen & Raiko 2002). Figure 2 illustrates a typical cyclone separation efficiency curve.

Back-mixing of solids yields to an exponential decay of solids concentration in the furnace. Johnsson and Leckner (1995) argued that there exist two different decay constants for the vertical solids concentration profile. Splash zone decay is dominated by the splash zone decay constant a and transport zone by the decay constant K. Thus, solids concentration profile can be evaluated with an equation (1)

$$\rho_s(z) = \left(\rho_{s,H_b} - \rho_{s,entr}\right)e^{-a(z-H_b)} + \rho_{s,entr}e^{-K(z-H_b)} \qquad z \geq H_b \quad (1)$$

where ρ_s is solids concentration, ρ_{s,H_b} is the solids concentration in the dense bed, $\rho_{s,entr}$ is the amount of solids entrained from the dense bed to the transport zone, H_b is the dense

bed height and z is the height of calculation point. Figure 5 presents typical solids concentration and meaning of these variables more precisely. Johnsson and Leckner (1995) presented formulas for decay constants a and K to be

$$a = 4\frac{u_t}{u_f} \tag{2}$$

$$K = \frac{0.23}{u_f - u_t} \tag{3}$$

where u_t is terminal velocity of the particle and u_f is velocity of the fluid. However, these values cannot be taken as certain since there is still uncertainty regarding the decay constants and research is being done to focus on them (Pallarès & Johnsson 2013, Djerf et al. 2018).

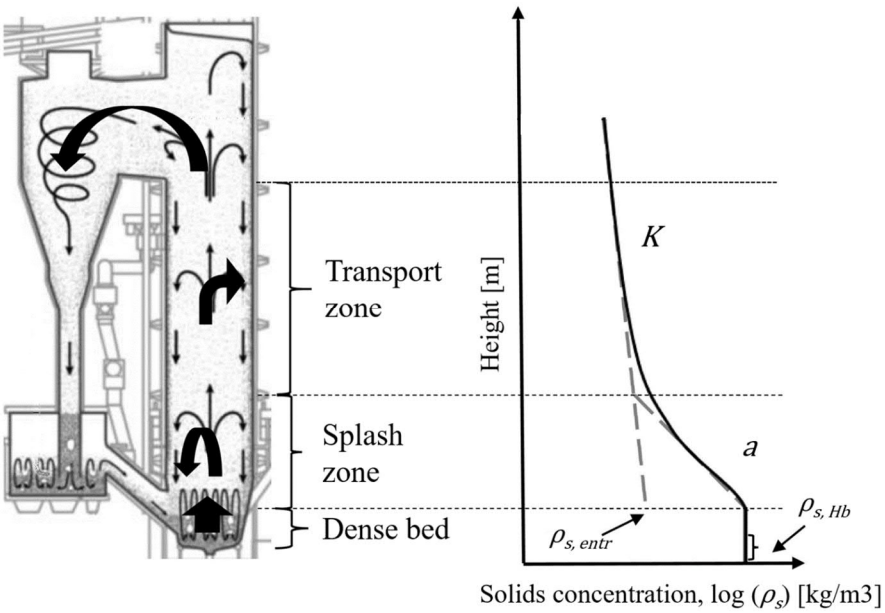

***Figure 5**. Solids concentration and decay constants in different parts of furnace. Dashed grey lines indicate the influence of the decay constants on the concentration profile. Solid black line illustrates typical solids concentration in furnace. Adapted from Djerf et al. (2018).*

2.3 Fuel and combustion

CFB boilers can utilize wide range of fuels with varying burning difficulty. This means fuels from different ranks of coal to biomass, sludges and waste as illustrated in Figure 6. Different fuels have different contents of moisture, volatiles, char and ash. While moisture and volatiles are released quickly from the particle, char combustion happens lot more slowly. Thus, content of the fuel has impact on where energy is released from the particle. Typically, biomass and peat have higher volatile and moisture content than coal (Vassilev et al. 2010). Respectively biomass and peat also have lower char content and

energy density compared to coal. Figure 7 presents higher heating value (HHV), volatile matter, carbon and hydrogen shares for different dry ash free (daf) solid fuels.

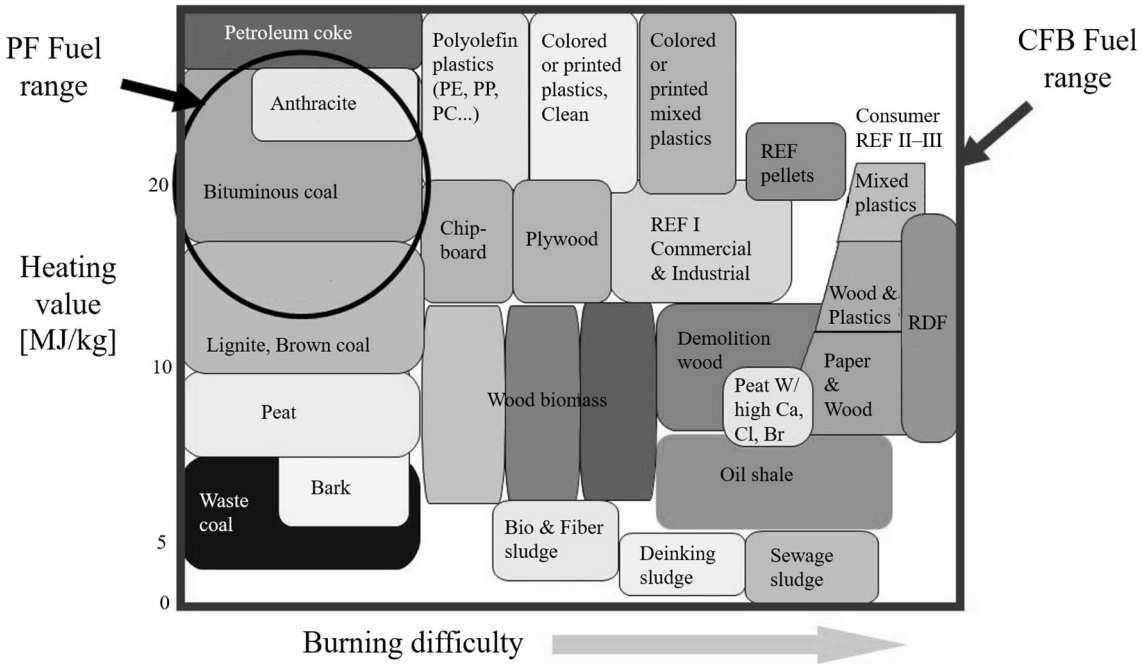

Figure 6. *Illustration of typical PF boiler's and CFB boiler's fuel ranges. Adapted from Utt & Giglio (2012).*

Typical moisture contents vary for fuels and very different moisture contents can have significant impact on the boiler performance. As a principle coal has lot smaller moisture content than biomass. Coals with low moisture content have 2–10 weight% of water content. Brown coals typically have wider range of moisture content ranging from 2–70 weight% of water. Moisture content of biomass depends a lot on the pre-treatment of the fuel. Wood pellets can have moisture content of only 8 weight% while fresh wood has 50–60 weight% of water. Fresh straw has moisture content of 30–60 weight% but the combustion usually occurs with less than 20 weight% moisture content. (Spliethoff 2010 pp. 15–56; Alakangas et al. 2016)

Ash content of the fuel impacts the solids inventory in the CFB riser. For low ash fuels such as biomass the solids inventory could include lot more make-up material than for fuels with higher ash content. Typical ash content for wood and forest residue is between 0.4–3 weight% of the dry matter while straw and reed canary grass have higher ash contents with 5–9 weight%. For coals the ash content from the dry matter is typically in the range of 5–17 weight%. (Spliethoff 2010 pp. 15 – 56; Alakangas 2016)

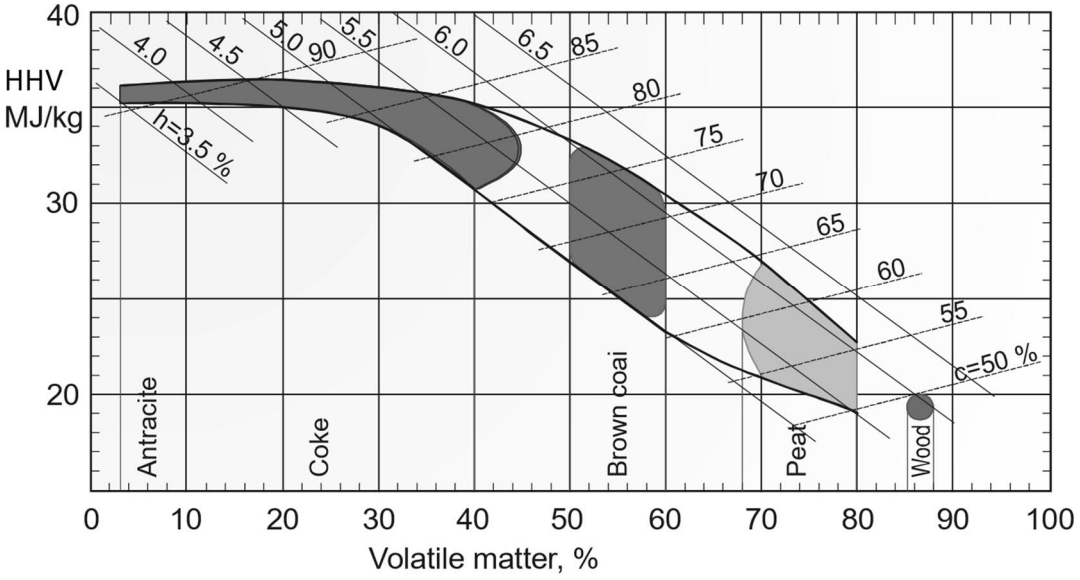

Figure 7. *Comparison of higher heating value and dry ash free based volatile matter for different fuels. Figure also has comparison of hydrogen (h) and carbon (c) content. Adapted from Alakangas (2005 p. 82).*

Depending on the fuel, the fuel particles can have variety of different shapes and sizes. Coal particles have rather spherical, though irregular shape while biomass particles are typically non-spherical with irregular shapes, possibly even being very elongated (Luckos & Koekemoer 2014; Nikku et al. 2014; Ulusoy & Igathinathane 2014). However, very small biomass particles are typically less elongated than larger ones (Guo et al. 2012). Fuel PSDs used in CFB boilers can be relatively wide. Biomass PSD can vary from very fine particles to very coarse particles. This means that the particle size can be in order of micron or 10 cm (Nikku et al. 2014). However, particles to be in the larger end of the PSD are usually very elongated. Hurskainen & Vainikka (2015, p. 183) recommended biomass particle size to be less than 40 mm in CFB boilers and Koornneef et al. (2007) said fuel particle size to be in general between 0 and 25 mm in CFB boilers. Coal PSDs used in CFB boilers are typically narrower than those of biomass. Typically coal particle size in CFB boilers is under 10 mm with most of particles being between 1–5 mm (Bartok & Sarofim 1991, according to Lind 1999; Lind et al. 1995, according to Lind 1999; Basu 2006 p. 337). Densities of coal and biomass have also significant differences between each other's. Coal typically has significantly higher density than biomass. Material densities of different fuels and bed material are presented in Table 1.

During combustion fuel particles undergo deformation and density changes. During moisture release fuel's density decreases due to evaporation of moisture. Respectively fuel's density decreases during devolatilization due to volatile matter released even though fuel particle can have some shrinkage or swelling during devolatilization. During char combustion the particle will either shrink in size at approximately constant density or decrease in density and have approximately constant particle size. (Pallarès 2008a p. 17; Vakkilainen 2017 p. 32)

Table 1. *Densities for different materials.*

Material	Density [kg/m^3]	Reference	Material	Density [kg/m^3]	Reference
Birch; sweet, yellow; air dry	705	(a)	Charcoal, oak	529	(a)
Pine; Norway; air dry	545	(a)	Charcoal, pine	368	(a)
Spruce; white, red; air dry	449	(a)	Anthracite	1554	(a)
Forest residue; dried	510	(b)	Lignite	1249	(a)
Sawdust	650	(c)	Bituminous coal, char	1850-1950	(f)
Biomass particle	644	(d)	Crushed limestone	2100-2600	(g)
Peat, turf; dry	753	(a)	Silica sand	2600	(g)
Peat (dried)	340	(b)	Crushed sandstone	2000-2600	(g)
Softwood char	299	(e)	Quartz; flint	2643	(a)

(a) Liley et al. (1997)
(b) Nikku et al. (2014)
(c) Lu et al. (2010)
(d) Fotovat et al. (2015)
(e) Gupta et al. (2002)
(f) Kleinhans et al. (2018)
(g) Wang & Fan (2013)

Deformation of coal and biomass during combustion process have significant differences. Riaza et al. (2017) reported that during pyrolysis biomass particle changed to a more rounded shape and bent over itself while no detectable swelling was occurring. In the same study it was concluded that during char combustion biomass particle pulls its mass together leading to an even more spherical shape while diameter of the particle shrinks. Holmgren et al. (2017) concluded that during rapid devolatilization pine wood particles formed plasticized hollow spheres and wheat straw particles curled and did not shrink as much as pine wood particles. Same research also reported that circularity of stem wood and wheat straw particles increased during devolatilization. However, stem wood's increase was reported to be greater according to used evaluation methods. Also, Tolvanen et al. (2013) concluded that in their tests torrefied wood particles seemed to change from elongated to spherical and that same particles did not have swelling during devolatilization. Cetin et al. (2004) investigated the effect of ambient conditions to the behaviour of biomass particle during conversion. They reported that high heating rates (≈ 500 °C/s) result in melting of biomass char particles. Thus, for example pine saw dust lost practically its cell structure during devolatilization and had plastic transformations. With lower heating rates the natural porosity of the material allowed the volatile gases to flow and no major morphological changes did occur. Same research also concluded that softwood melts easier than hardwood while bagasse was the most resistant to melting. Holmgren et al. (2017) concluded that density changes during devolatilization can vary significantly between biofuels. In their research density of pine stem wood remained rather constant while wheat straw had significant decrease in density during conversion.

During devolatilization coal particles could swell since the evaporating gases inside the particle increase the pressure inside the particle (Basu 2015, p. 105; Steer et al. 2015;

Riaza et al. 2017). Coal particles have higher density and lower porosity than biomass particles. Thus, volatile gases are not able to flow out of the particle as freely in coal as in biomass (Riaza et al. 2017). Therefore, coal particles typically swell during devolatilization and volatile gases can exit the coal particle as jets. This internal pressure inside the particle can also cause fragmentation where particle breaks into multiple pieces (Basu 2015, p. 105). Levendis et al. (2011) reported that fragmentation could occur also prior to ignition. Steer et al. (2015) reported that smaller coal particles tend to swell while larger particles fragmentate more easily. Luckos & Koekemoer (2014) reported that devolatilized coal had slightly decreased sphericity compared to raw particles with average values of 0.749 and 0.798 respectively. Highly porous coal char can also have fragmentation during char burning called secondary fragmentation (Basu 2015, p. 105). While combustion happens on the pore surfaces of the char the sizes of the pores increase. Thus, carbon wall bridge between pores weakens and when it is weak enough external forces can break the particle into fragments.

Burnout time of a particle depends on many aspects: ambient conditions, chemical and mechanical properties of the particle and size and shape of the particle (Momeni et al. 2013; Basu 2015, p. 108). Thus, burnout times for coal and biomass are very different. Biomass particles burn out typically lot quicker than coal particles. Riaza et al. (2017) reported that burnout time for the same mass of high volatile bituminous coal can be multiple times longer than the burnout time for biomass. The same research also compared burnout times for particles with same diameter and concluded that mean burnout time for particles in range of 600–710 µm and 710–1000 µm were 4.1 s and 6.6 s respectively for coal and 1.5 s and 1.7 s respectively for biomass.

Burnout times also vary between coals and not just between biomass and coal. Riaza et al. (2014) reported that burnout times for bituminous coal content was much shorter than for anthracitic particles. Same research stated that this may be due to the higher volatile matter content and higher reactivity of the bituminous coal. Bituminous coal also had lot more swelling which also increases the surface area and therefore enhances particle reactivity (Riaza et al. 2014).

2.4 Heat transfer and temperature profile

As stated earlier, circulating fluidized bed boiler differs from pulverised coal boilers in two major ways. Combustion temperature is lower in CFB boilers (typically 800–900 °C) and solid concentration is higher (Oka 2004, p. 147). Thus, heat transfer happens in addition to radiation and convection through conduction when particles collide with each other's and heat transfer surfaces (Basu 2015, p. 57). Walls of CFB boiler function as heat transfer surfaces which are manufactured from pipes and membrane panels between pipes. There can also be other heat transfer surfaces in the furnace to absorb more heat. Most typical solutions are so called wing walls which enter the furnace through its wall

and exit through the ceiling and division wall which goes through the entire height of the furnace. Wing walls can be seen on Figure 1. Typically heat transfer surfaces in the furnace are evaporators but wing walls could also be used as superheaters (Basu 2015, p. 179). At the most wearing locations the furnace is lined with refractory which reduces the heat transfer in these areas significantly. These areas concern the bottom of the furnace approximately to the secondary air injection height or above, lower end of wing walls and division wall and cyclone inlet (Basu 2015).

The cyclone and the loop seal walls can also be water cooled but they are typically lined with refractory so the heat transfer through these surfaces is small compared to one from furnace. However, a heat exchanger can be also located inside the loop seal's fluidized bed. Thus, boiler's fuel flexibility and load control capability can be enhanced. This kind of a loop seal superheater can be seen in Figure 1. (Basu 2015)

Suspension density is the most dominant factor influencing the heat transfer to the walls. If conduction and convection are considered as a whole and called convection Breitholtz et al. (2001) stated that higher the average suspension density higher the share of convective heat transfer is from the total heat transfer. Figure 8 illustrates the total heat transfer coefficient and estimated convective share as a function of suspension density by Breitholtz et al. (2001). According to Hyppänen & Raiko (2002) heat transfer coefficients vary typically between 50 and 250 W m^{-2} K^{-1} inside the furnace. Since the combustion temperature in CFB boiler is typically smaller than the melting temperature of ash slagging is not a major problem in CFB boilers (Skrifvars & Hupa 2002; Basu 2015, p. 321). Thus, the heat transfer in the hot loop does not reduce significantly due to slagging of water walls. However, it should be noted that alkali metals reduce the melting point of ash which may result in more slagging with high-alkali fuels (Hiltunen et al. 2003; Spliethoff 2010, pp. 47–48).

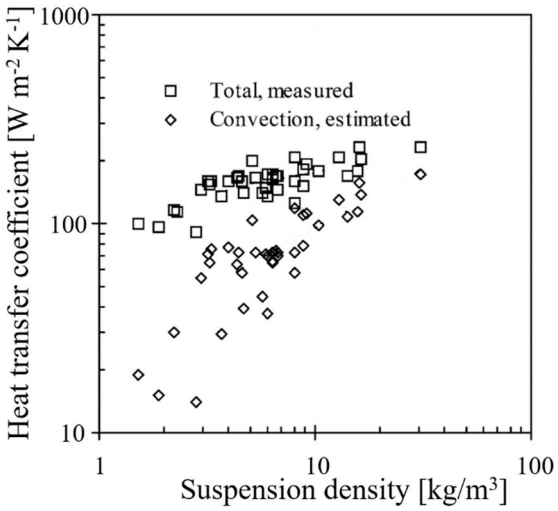

Figure 8. *Total and convective heat transfer coefficient as a function of suspension density. Adapted from Breitholtz et al. (2001).*

There has not been plenty of researches which have published results from axial temperature distribution from industrial scale CFB boiler. La Nauze (1987, according to Nikku 2015) published results from smaller scale for the effect of different fuels for axial temperature. Niklasson et al. (2006) published results from co-firing of biomass and coal in 12 MW_{th} CFB boiler. Vepsäläinen et al. (2009) published temperature profile from their measurement campaign in 50 kW CFB boiler. Blaszczuk et al. (2012) published temperature profiles for different loads from 460 MW_e supercritical boiler with bituminous coal as fuel. Nikku (2015) published profiles from large-scale CFB boiler with biomass as fuel. Zhou et al. (2015) reported temperature profiles of different operational conditions for 400–600 kW_{th} boiler with Shenmu char as fuel.

Variables which affect axial temperature profile are numerous. In addition to already presented factors like heat transfer surfaces and suspension density, operational conditions and fuel plays a significant role. Different fuels have different fluid dynamical properties throughout their combustion process. Thus, different fuels are prone to elutriate better from the bottom of the furnace than other fuels resulting in more heat release in upper parts of the furnace. La Nauze (1987, according to Nikku 2015) presented results for effect of different fuels on temperature distribution in CFB boiler. These results are illustrated in Figure 9. Typically, temperature profile for coal is relatively even and bed temperature is higher than for biofuels. This difference between wood chips and coal was explained by the high volatile content of biomass which results in above-bed combustion. Nikku (2015) stated that while char combustion has effect on temperature profiles, combustion of volatile gases has stronger influence. He added that fuel properties determine where the volatiles are released and thus also fuel size and shape affect the temperature profile.

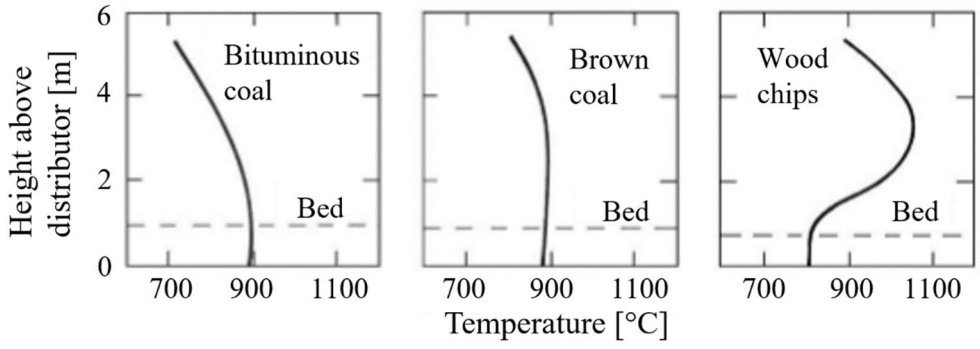

Figure 9. *Axial temperature profiles for different fuels. Adapted from La Nauze (1987) and Nikku (2015).*

Fuel is injected to the furnace at low heights in the refractory lined part of the furnace. Thus, air injection and gas-solid mixing have significant impact to temperature profile. If oxygen does not reach fuel or volatilized gases, combustion cannot occur. Thus, secondary air's share of combustion air and injection heights can alter temperature profile with mixing of gases and solid particles. According to Basu (2015, p. 173) high-volatile fuels

combust nearer to fuel feed ports than low-volatile fuels since low volatile fuels burn more slowly. Thus, they have more time to spread away from the fuel ports.

When determining the average axial profile, the effect of horizontal profile should also be noticed. Largest temperature gradients in CFB boiler occur next to heat transfer surfaces so measurements near these surfaces could distort the results for average core temperatures. Yet these thermal boundary layers are not very wide, typically in the range of 10–30 cm (Basu & Nag 1996; Hyppänen & Raiko 2002; Hartge et al. 2005). Temperature gradients can be great in the thermal boundary layer since temperatures at the wall can be under 400 °C while core temperature outside the boundary layer can be over 800 °C (Basu & Nag 1996; Hartge et al. 2005). Figure 10 illustrates horizontal temperature profiles near water wall at different heights in 235 MW_e CFB boiler.

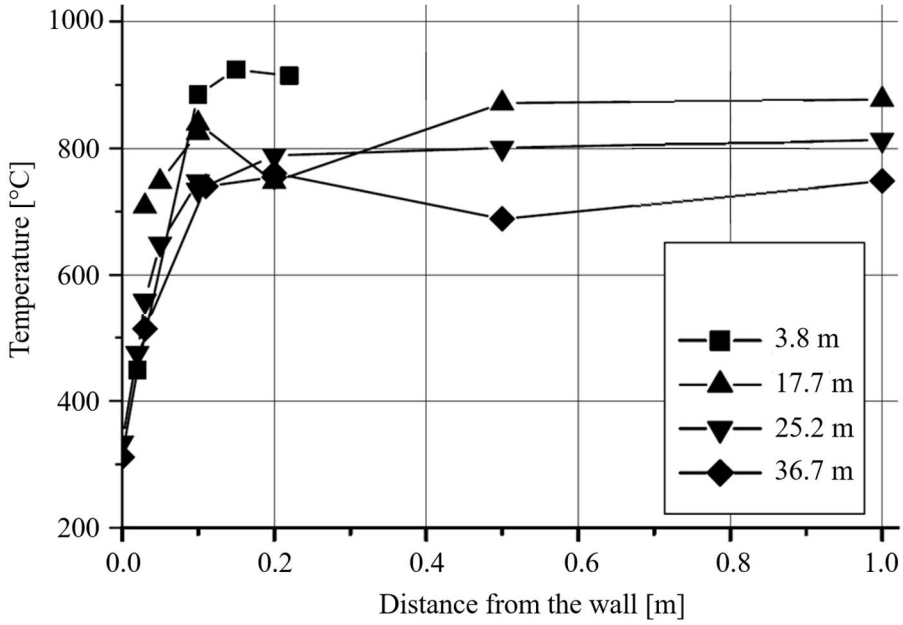

Figure 10. *Horizontal temperature profiles at different heights near wall in a commercial CFB boiler. Adapted from Hartge et al. (2005).*

According to Myöhänen & Hyppänen (2011, according to Pallarès et al. 2012) internal heat transfer surfaces in the core area cause a solids downflow near these surfaces. Thus, solids concentration near these walls would differ from the core area and naturally thermal boundary layer is formed next to them. Dutta & Basu (2002) reported that in their measurements in pilot scale cold CFB unit wing walls had downward solids flux only if the wing wall was placed at the top of the riser. When wing wall was located further away from the roof no downward solids flow was noticed. If solids concentration near the wing wall is lower than next to water walls, then it could be argued that also the heat transfer coefficient is smaller for the wing walls.

3. CHARACTERIZATION AND MOTION OF FUEL PARTICLES

3.1 Fuel particle characterization

Particles and especially fuel particles used in CFB boilers have countless number of different shapes and sizes. These properties have great impact on their flow behaviour inside the boiler. Thus, it is important to be able to characterize these properties from particles. Most accurate particle shape and size measurements are achieved with 3D measurements. However, these measurements are demanding and time consuming for irregular non-spherical particles (Bagheri et al. 2015). Thus, accurate 3D measurements of PSDs used in CFB boilers are not feasible in the industrial environment. In addition, using 3D information about fuel particles in modelling is very complicated and time consuming in large CFB units. Thus, fuel particles are most typically measured with 2-dimensional (2D) image analysis or by sieving. Sieving is simple way of identifying PSD for particles. However, for example biomass particles can be very elongated and thus they may find orientations in which they pass very small sieve openings when compared to their maximum diameter. Thus, Nikku et al. (2014) stated that biomass may be unsuitable for sieve analysis. (Nikku et al. 2014)

Particles are typically characterized by using different shape factors. Shape factor means that a particle is compared to a sphere and the particle's characteristic dimension is adjusted to a sphere with shape factor. Thus, different shapes can be compared for example when calculating terminal velocity of a particle. In literature there are numerous of different shape factors for particles. Most common shape factor is sphericity where area of a sphere with same volume as the particle is divided by the actual particle area (Wadell 1933). However, Cavarretta et al. (2009) concluded that 2D images are a good approximation of the 3D shape sphericity if particle is spherical or very elongated and very flat. Thus, fuel sphericities are not necessary caught accurately with 2D measurements. In addition to the difficulty in measurement of sphericity, two different shapes can have same values for sphericity. Mandø & Rosendahl (2010) argued that the most likely reason for the popularity of the sphericity is that it seems to be the most elegant way of quantifying the shape of an arbitrary particle. Table 2 presents some values for sphericities for different particles. From the table it is obvious that bio-based fuels (if not pelletized) have lot smaller sphericity than coal or bed material. Table 2 presents also values for fly ash from coal. These values suggest that the fly ash is very spherical and it is reported that fly ash sphericity remains quite similar also in co-combustion of coal and biomass when biomass energy content is one third of the total energy content of the fuel (Saraber & van den Berg 2004, according to García -Galindo et al. 2019).

Table 2. *Sphericity values for different particles.*

Particle		Sphericity	Reference	Particle		Sphericity	Reference
Sphere		1	(a)	Sand			
Half Sphere		0.84	(a)		Round	0.86	(c)
Octahedron		0.85	(a)		Sharp	0.66	(c)
Cube		0.81	(a)	Coal			
Tetrahedron		0.67	(a)		Anthracite	0.63	(c)
Cylinder					Bituminous	0.63	(c)
	z = d	0.87	(a)		Natural dust	0.65	(d)
	z = 10d	0.58	(a)		Pulverized	0.73	(d)
Disk				Peat		0.26-0.55	(e)
	z = d/3	0.76	(a)	Woodchip		0.13-0.33	(e)
	z = d/10	0.47	(a)	Wood pellet		0.87	(f)
Wheat		0.85	(b)	Fly ash from coal		0.92-0.97	(g)

(a) Geometrical considerations
(b) Kunii & Levenspiel (1991)
(c) Leva et al. (1948), according to Kunii & Levenspiel (1991)
(d) Carman (1937), according to Kunii & Levenspiel (1991)
(e) Korhonen (2012)
(f) Arce et al. (2013)
(g) Usui et al. (2001)

Table 3 presents some other shape factors that can be used to describe fuel particles. Bagheri et al. (2015) concluded that circularity measurements can be used as an approximation of sphericity. They concluded that Riley circularity is better suited for non-vesicular particles and Cox circularity is better suited for vesicular particles. It should be noted that their research did not take for example roundness to consideration. Holmgren et al. (2017) stated that Cox circularity was found more suitable than Riley circularity to describe the fuel deformation on 2 different biomasses.

Table 3. *Some shape factors and their definitions.*

Shape factor	Definition	Equation	Reference
Sphericity	Area of sphere with same volume as particle divided by the actual particle area	$\varphi = \frac{A_{sph,eq\,V}}{A_{part}}$	Wadell (1933)
Roundness, Pentland	Ratio of projected area of the particle and smallest circumscribed circle	$R_P = \frac{4A_p}{\pi d_{max}^2}$	Nikku et al. (2014)
Circularity, Cox	Ratio of area and perimeter	$C_{Cox} = 4\pi\frac{A_p}{P^2}$	Cox (1927)
Circularity, Riley	Ratio of largest inscribed circle and smallest circumscribed circle	$C_{Riley} = \sqrt{\frac{d_i}{d_c}}$	Riley (1941)
Aspect ratio	Ratio of maximum and minimum dimensional distances	$AR = \frac{\mathrm{d}_{max}}{d_{min}}$	Nikku et al. (2014)
Corey shape factor	Three dimensional. Ratio of the smallest principal length axis of the particle to the square root of the intermediate and longest principle length axis.	$\Psi_C = \frac{\mathrm{d}_{min}}{\sqrt{d_{mean}d_{max}}}$	Mandø & Rosendahl (2010); Nikku et al. (2014)

3.2 Single Particle behaviour in flow

Single particle in an upward flow has 3 forces which affect it: gravitational force, buoyancy and drag force. Gravitational force depends on the mass of the particle and buoyancy on the volume of the particle and density of the surrounding fluid if gravitational acceleration is considered constant. Drag force is typically divided into 2 separate phenomena: pressure drag and frictional drag. Latter one derives from the shear stress that particle causes to the flow's boundary layer. Pressure drag is caused by the particle's shape and the flow separation that occurs because of particle's shape. For example, for a cylindrical object the flow detaches from the surface at some point because of the adverse pressure gradient at the surface of the body. This flow separation creates a low-pressure wake behind the object which adds to the frictional drag. Share of which these 2 drag types affect the object depends on the object's shape and surface. (White 2016, p. 476)

For a streamlined cylinder with zero thickness the frictional drag has 100% share of the total drag (White 2016, p. 476). When thickness equals the chord length of the cylinder frictional drag only has 3% share of the total drag force (White 2016, p. 476). For practical reasons frictional and pressure drag's effects are often combined to a common drag coefficient C_D (Nikku 2015). For a specific shape, drag coefficients are typically determined experimentally (Mandø & Rosendahl 2010; Nasa).

Single particle's velocity in the upward flow can be considered to equal the slip velocity of the particle (Pallarès & Johnsson 2006a; Basu 2015, p. 31). Thus, in order to properly evaluate the particle's axial velocity, one must be able to evaluate the particle's terminal velocity properly. Particle's terminal velocity can be solved from the force balance in equation (4)

$$F_D = F_G - F_B \tag{4}$$

where F_G is gravitational force, F_B is buoyancy and F_D is the drag force (Basu 2006 p. 31). Drag force can be defined as in equation (5).

$$F_D = \frac{1}{2}\rho_f A_p C_D \left(u_f - u_p\right)^2 \tag{5}$$

where ρ_f is density of the fluid, A_p is the particle's projected area and u_p is velocity of the particle (Nikku 2015 p. 35). When fluid's velocity equals the particle's terminal velocity, particle's velocity equals 0. Thus, particle's terminal velocity can be defined as

$$u_t = \sqrt{\frac{2V_p g(\rho_p - \rho_f)}{\rho_f A_p C_D}} \tag{6}$$

where V_p is the volume of the particle, ρ_p is particle's density and g is the acceleration due to gravity. For spherical particle equation (6) contracts to equation (7)

$$u_t = \sqrt{\frac{4d_p g(\rho_p - \rho_f)}{3\rho_f C_D}} \tag{7}$$

where d_p is particle's diameter (Kunii & Levenspiel 1991, p. 80).

There are numerous researches made for determining drag coefficients and terminal velocities for different kinds of shapes and particles (Haider & Levenspiel 1989; Briens 1991; Ganser 1993; Yow et al. 2005; Hölzer & Sommerfeld 2008; Loth 2008; Song et al. 2017; Breakey et al. 2018). These models often use some characteristic dimensions to identify the particle shape and the most used one is sphericity. For example, Haider & Levenspiel (1989) presented following model (equations (8)–(10)) for particle's terminal velocity. Other models for drag coefficient are presented later in the chapter.

$$u_t = u_t^* \left(\frac{\rho_f^2}{\mu_f (\rho_p - \rho_f) g} \right)^{-\frac{1}{3}} \tag{8}$$

where μ_f is dynamic viscosity of the fluid and

$$u_t^* = \frac{1}{\frac{18}{d_p^{*2}} + \frac{2.335 - 1.744\varphi}{d_p^{*0.5}}} \tag{9}$$

$$d_p^* = d_p \left(\frac{\rho_f (\rho_p - \rho_f) g}{\mu_f^2} \right)^{\frac{1}{3}} \tag{10}$$

where φ is sphericity.

Drag coefficient is not always a constant for certain particle but depends on the fluid's properties and velocity. Drag coefficients are usually presented as a function of Reynolds number (Re) which is defined for a particle according to equation (11)

$$Re = \frac{|u_f - u_t| L_p}{\nu_f} \tag{11}$$

where L_p is characteristic length of the particle and ν_f is kinematic viscosity of the fluid. Figure 11a presents drag coefficient of a sphere with smooth and rough surface. It is noticeable that there are numerous of different flow areas included in the Figure 11a. At very low Reynolds numbers the drag coefficient is high for sphere and there exists no

(Figure 11b) or steady flow separation (Figure 11c) from the sphere's surface. When the Reynolds number increases drag coefficient decreases. While this happens, the downstream vortices become unstable behind the sphere (Figure 11d). The wake is very wide and still creates lots of drag. Vortices created are not stable but periodic. This kind of a phenomenon is called Karman vortex street. While the flow velocity and therefore Reynolds number is still increased the periodic flow breaks down into a chaotic wake (Figure 11e). Wake's diameter decreases so the drag coefficient is also a bit smaller than the one from the periodic wake. While the Reynolds number is still increased, the boundary layer transitions into turbulent flow (Figure 11f). While this happens flow separation point moves slightly downstream which causes drag to reduce. This phenomenon also known as drag crisis is not permanent but when Reynolds number is still increased the drag coefficient increases and exceeds the drag of laminar case. Figure 11a also presents the effect of surface roughness to the drag coefficient of the sphere. At certain range the drag of rough sphere is smaller than smooth one's. This happens since the rough surface transitions the flow to turbulent with smaller Reynolds numbers. Thus, the drag crisis occurs in smaller Reynolds numbers for sphere with rough surface. (Nasa)

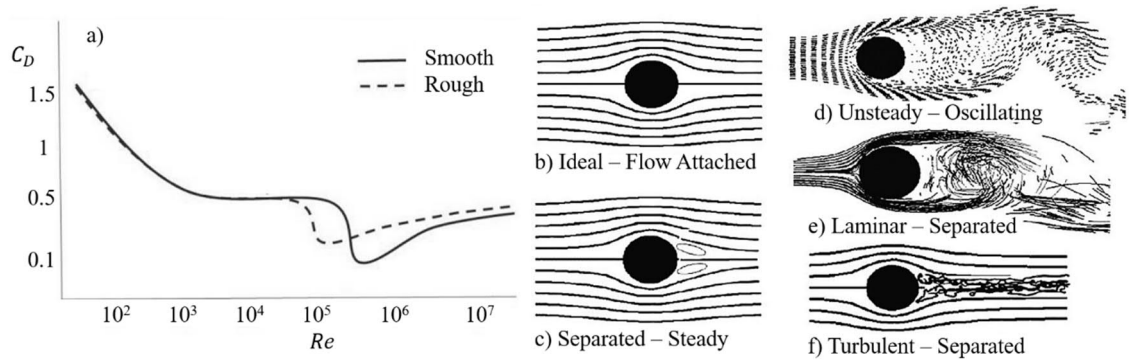

Figure 11. *Drag coefficient of a sphere with smooth and rough surface as a function of Reynolds number (a) and flow patterns around cylinder with different Reynolds numbers. No flow separation (b), steady flow separation (c), periodic vortices in the wake i.e. Karman vortex street (d), chaotic wake (e), turbulent boundary layer and chaotic wake (f). Figure is adapted from Nasa.*

Particles in CFB boiler are not perfect spheres and fuel particles especially could be very non-spherical. Thus, particles can have multiple different drag coefficients depending on their orientation against the flow. Non-spherical particles are associated with characteristic secondary motion which depends on particle shape and Reynolds number regime. For very low Reynolds numbers ($Re < 0.1$) particles with uniform mass distribution will move in slow Jeffrey's orbits. This phenomenon is only valid for certain symmetry conditions and thus excludes all irregular particles. For higher Reynolds numbers ($0.1 < Re < 100$) inertial effects become more important. In the wake of a particle a steady recirculation zone starts to build up and this causes a pressure distribution which forces particle to align itself with maximum cross-sectional area normal to flow (Figure 12a). (Mandø & Rosendahl 2010)

At higher Reynolds numbers ($Re > 100$) significant secondary motion is superimposed on the particle's steady fall or rise. Secondary motion is caused by the onset of wake instability and means the beginning of vortex shedding from the particle's wake. There exist different kinds of forms of secondary motion and besides Reynolds number they have been shown to correlate well with non-dimensional moment of inertia. For smaller amounts of dimensionless moment of inertia particles will fall in periodic oscillations and not perform full rotations (Figure 12b). Dimensionless moment of inertia indicates the inertial resistance of particle to rotation. Thus, particles with low dimensionless moment of inertia are more prone to change rotation direction and thus will not perform full rotations. Figure 13 presents the forces to particle with an angle to flow more precisely. Particles with higher dimensionless moment of inertia undergo full rotation and fall in so called tumbling motion (Figure 12e). An intermediate regime between these two is called glide-tumble regime where particles switch between periodic oscillations and tumbling motion (Figure 12c & Figure 12d). (Mandø & Rosendahl 2010)

Previous chapter included considerations for disks but there are different motion patterns for different shapes. For example, cylinders assume either steady falling or periodic oscillations falling pattern depending on the Reynolds number. Similarly than disks, also cylinders assume orientation where their maximum cross-section is normal to the flow direction. (Mandø & Rosendahl 2010)

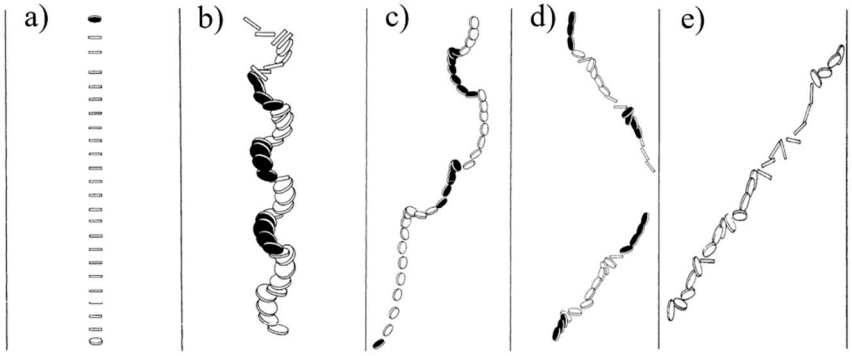

Figure 12. *Regimes of motion for a disk. Steady fall (a), periodic oscillations (b), disk that has just entered glide-tumble pattern (c), motion pattern just before leaving glide-tumble pattern (d), tumbling motion (e). Figure is adapted from Stringham et al. (1969).*

Natural particles rarely have uniform mass distribution which is assumed above. Typically, the movement of centre of mass influences the particle so that it falls with its heaviest side downwards. This can cause considerable changes into terminal velocity since the particle might be in very different orientation that argued above (Shellard & Macmillan 1978). Centre of mass is not only aspect that influences flow characteristics since even if two particles would have coincident centre of mass, they could have different flow patterns in same flow if their moment of inertia differs from one another. Particles with aspect ratio close to unity falls without preferential orientation and in a motion pattern best described as tumbling. It is reported that the resistance towards tumbling increases with increasing aspect ratio. (Mandø & Rosendahl 2010)

If turbulence is not considered the wake instability is the only source which causes secondary motion. According to Mandø & Rosendahl (2010) turbulence significantly affects the motion of a particle but there exists large uncertainty concerning the interaction between non-spherical particles and turbulence. It is reported that non-spherical particles, like spherical particles, can either enhance or attenuate turbulence depending on the shape of the particle and ratio between the particle diameter and the length scale of the turbulence (Mandø 2009). Comparing spherical and non-spherical particles it can be concluded that non-spherical particles have greater effect on turbulence than the volume equivalent spheres and thus secondary motion pattern can change from what is stated above (Sun et al. 2004). (Mandø & Rosendahl 2010)

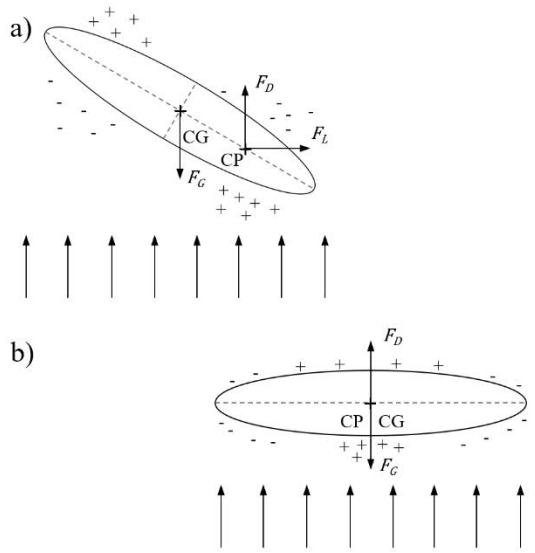

Figure 13. *Forces to a particle in a flow with Re > 100. If particle is tilted (a) centre of pressure (CP) differs from centre of gravity (CG). Thus, pressure distribution around particle causes moment to particle which causes rotational motion. Pressure distribution can also cause sideward force here denoted as F_L. If particle is not tilted (b) particle's CP and CG are located in same place and thus there is no turning moment on the particle. Plus signs indicate higher local pressure and minus lower local pressure. Buoyancy is neglected here. Figure is adapted from Mandø & Rosendahl (2010).*

As stated earlier there are numerous models for drag coefficients for different particles. One of the most used models is the model from Haider & Levenspiel (1989) presented in equation (12). In the same paper Haider & Levenspiel presented a simpler model (equation (13)) which would give almost as precise results as equation (12). Swamee & Ojha (1991) developed 2 correlations based on a data of Schulz et al. (1954). These correlations (equations (14)–(15)) are based on Corey shape factor. Ganser (1993) presented a new model for the drag coefficient of non-spherical particles based on shape factors in Stoke's (k_S) and Newton's (k_N) regimes (equations (16)–(19)). In Stoke's regime inertial terms are negligible compared to viscous terms and thus flow remains attached to sphere and in Newton's regime wake is fully turbulent while boundary layer at the front of the sphere

remains laminar (Bagheri & Bonadonna 2016). Chien (1994) introduced a simple expression (equation (20)) for the drag coefficient based on sphericity which is according to Chhabra et al. (1999) and Elfasakhany & Bai (2019) applicable for the range of $0.2 \leq \varphi \leq 1$ and $Re < 5000$. Yow et al. (2005) introduced new model which uses sphericity to characterize particles (equation (21)–(24)). Model is applicable for the range of $0.006 \leq \varphi \leq 1$ and $10^{-2} \leq Re \leq 10^{5}$. Newer model which has been mentioned as one of the most used models is the Hölzer & Sommerfeld model (2008) presented in equation (25) where $\varphi_{\parallel}$ is lengthwise sphericity which is the ratio between the cross-sectional area of the volume equivalent sphere and the difference between half the surface area and the mean projected longitudinal cross-sectional area of the considered particle. Crosswise sphericity is marked as $\varphi_{\perp}$ which means the ratio between the cross-sectional area of the volume equivalent sphere and the projected cross-sectional area of the considered particle. Table 4 illustrates these models presented above collectively.

Neglecting models presented after 1999, Chhabra et al. (1999) evaluated drag models presented above. They reported that the model by Ganser yielded smallest average error of 16.3% while maximum error was 180.9%. Numbers for Haider & Levenspiel (1989) were 21.5% and 275.8% respectively. Chien (1994) had average error of 23.5% and maximum error of 152.5% while Swamee & Ojha (1991) had numbers of 42.6% and 199.0% respectively. Chhabra et al. (1999) argued that further improvement in accuracy of models would be only achieved by introducing additional shape parameters. Hölzer & Sommerfeld model (2008) took orientation into account and reportedly achieved better results than previous models. Bagheri & Bonadonna (2016) published a new drag coefficient model based on 3D shape information of particles. They reported an average error of 10% which is lower than other existing correlations. Some other new models are the model by Song et al. (2017) which reportedly achieved good results. This model is applicable for the range of $0.471 \leq \varphi \leq 1$, $0.001 \leq Re \leq 100$ and particle shapes of sphere, cube and cylinder. Breakey et al. (2018) reported about technique in which they predicted the drag coefficient and settling velocity of non-spherical particles based on single side view of the particle. They reported that for irregular volcanic particles 74% of predictions were within 25% error margin.

Table 4. *Different drag models for non-spherical particles.*

Reference	Formula	Equation
Haider & Levenspiel (1989)	$C_D = \frac{24}{Re}\left(1 + e^{2.3288-6.4581\varphi+2.4486\varphi^2} Re^{0.0964+0.5565\varphi}\right) + \frac{Re * e^{4.905-13.8944\varphi+18.4222\varphi^2-10.2599\varphi^3}}{Re + e^{1.4681+12.2584\varphi-20.7322\varphi^2+15.8855\varphi^3}}$	(12)
Haider & Levenspiel (1989)	$C_D = \frac{24}{Re}(1 + 8.1716e^{-4.0655\varphi}\ Re^{0.0964+0.5565\varphi}) + \frac{73.69Re * e^{-5.0748\varphi}}{Re + 5.378e^{6.2122\varphi}}$	(13)
Swamee & Ojha (1991)	$C_D = \left(\frac{48.5}{\left(1 + 4.5{\Psi_C}^{0.35}\right)^{0.8} Re^{0.64}} + \left(\frac{Re}{Re + 100 + 100\Psi_C}\right)^{0.32} \frac{1}{{\Psi_C}^{18} + 1.05{\Psi_C}^{0.8}}\right)^{1.25}$	(14)
Swamee & Ojha (1991)	$C_D = 0.84\left(\frac{33.78}{\left(1 + 4.5{\Psi_C}^{0.35}\right)^{0.7} Re^{0.56}} + \left(\frac{Re}{Re + 700 + 1000\Psi_C}\right)^{0.28} \frac{1}{\left({\Psi_C}^4 + 20{\Psi_C}^{20}\right)^{0.175}}\right)^{1.428}$	(15)
Ganser (1993)	$C_D = \frac{24}{Re * k_S}(1 + 0.1118(Re * k_S * k_N)^{0.6567}) + \frac{0.4305k_N}{1 + \frac{3305}{Re * k_S * k_N}}$	(16)
	where	
	$k_N = 10^{1.8148(-\log\varphi)^{0.5743}}$	(17)
	for isometric particles	
	$k_S = \left(\frac{1}{3} + \frac{2}{3\sqrt{\varphi}}\right)^{-1} - 2.25\frac{d_{sph,eq\,V}}{D}$	(18)
	for nonisometric particles	
	$k_S = \left(\frac{1}{3}\frac{d_{sph,eq\,A_p}}{d_{sph,eq\,V}} + \frac{2}{3\sqrt{\varphi}}\right)^{-1} - 2.25\frac{d_{sph,eq\,V}}{D}$	(19)
Chien 1994	$C_D = \frac{30}{Re} + \frac{67.289}{e^{5.030\varphi}}$	(20)
Yow et al. (2005)	$C_D = \frac{a_1}{Re} + \frac{b_1}{\sqrt{Re}} + c_1$	(21)
	where	
	$a_1 = 15.21 + \frac{10.82}{\varphi} - \frac{0.14}{\varphi^2}$	(22)
	$b_1 = 13.41 - \frac{10.64}{\varphi} - \frac{0.06}{\varphi^2}$	(23)
	$c_1 = -8.82 + \frac{5.70}{\varphi} + \frac{0.23}{\varphi^2}$	(24)
Hölzer & Sommerfeld (2008)	$C_D = \frac{8}{Re}\frac{1}{\sqrt{\varphi_\parallel}} + \frac{16}{Re}\frac{1}{\sqrt{\varphi}} + \frac{3}{\sqrt{Re}}\frac{1}{\varphi^{\frac{3}{4}}} + 0.4210^{0.4(-\log\varphi)^{0.2}}\frac{1}{\varphi_\perp}$	(25)

3.3 Particle-particle interactions in flow

In a CFB boiler there are lots of particle-particle interactions with wide particle size distribution. Thus particle-particle interactions also affect the flow of particles. Particles can have different velocities and different sizes and through collisions they exchange momentum with each other's. In theory smaller particles have smaller terminal velocity and therefore they move faster upward in an upward flow. Thus, it can be stated that if single

particle is surrounded by a suspension of smaller particles the single particle will move with greater velocity since the smaller particles collide into it and "carry" it upwards and vice versa (Na et al. 1997, according to Gómez-Barea & Leckner 2010; Pallarès & Johnsson 2006a). This is typically the case in CFB boilers when considering fuel mixing since inert solids form typically around 99% of the bed material (Palchonok et al. 1997; Pallarès 2008a). Win et al. (1995) measured transport velocities of coarse particles in fluidized bed with acoustic technic. They reported that transport velocities of coarse particles decreased with more than 75% with big enough coarse particles and big enough solid circulation of fine particles.

As stated in Chapter 2.2 particles do not flow at constant distance from each other's but tend to form particle clusters in CFB boiler. In the wake of a particle exists an area of lower drag force. When another particle ends up in a wake of other particle the particle in the wake experiences a reduce in drag and therefore falls on top of the other particle. Thus, the effective surface area of the pair is reduced, and the drag force will be lower than gravitational force caused by the combined mass. Thus, particle agglomeration will experience change in velocity and thus fall on top of other particles. This way particles form clusters which are continuously torn apart by the up-flowing gas. Figure 14 presents an illustration from this phenomenon. (Basu 2015, p. 30)

Particle collisions can be roughly divided into two different categories: elastic and inelastic collisions. In the latter one kinetic energy is lost during collision and in elastic collision total kinetic energy of the system is same before and after collision (Young & Freedman 2012, p. 252). In particle collisions in CFB boilers contact can be tangential, act on the normal direction of particle surface or anything in between. However, in all cases forces in collisions depend on the mechanical properties of the particles, relative velocities and angle of contact (Nikku 2015). On the impact of collisions to the flow structure Li & Kuipers (2003) concluded that particle collisional dissipation can dramatically intensify the formation of heterogenous flow structures.

It is not very clear when solid-fluid suspension should be considered dilute and when dense. Dilute phase can be considered to be phase where particle motion is controlled by the fluid forces and dense flow to be controlled by collisions or continuous contact. Based on particle volume fraction the flow can be considered to be dilute when volume fraction is smaller than 0.001, collision dominated if volume fraction is greater than 0.001 but smaller than 0.1 and contact dominated when volume fraction is greater than 0.1. An industrial CFB boiler can have all of the fluid dynamical regions mentioned above. (Crowe et al. 2012, p. 26–29)

Particles do not only affect each other's but dense suspension also alters the flow field significantly. Thus, when modelling particle flows one must consider to what extent different phenomena should be considered. Simplest way is to consider that flow affects particles but not vice versa. However, this one-way coupling is not enough in every cases

and other aspects like how particles affect the flow or how particles interact with each other's should also be noted in some cases.

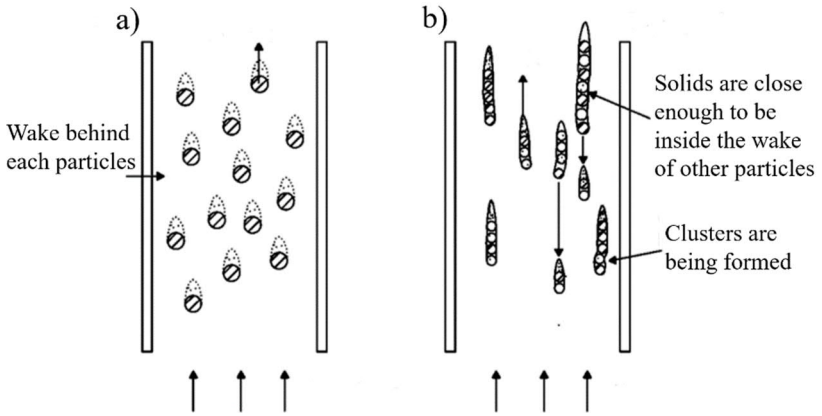

Figure 14. *Pneumatic transport (a) and cluster formation in the wake of particles (b). Adapted from Basu (2015, p. 31)*

Particles can experience also other interparticle forces than what comes from collisions and friction. Other forces include: van der Waals, electrostatic, capillary, sintering and magnetic forces (Wang & Fan 2013; Nikku 2015). Van der Waals forces are result of electric dipole moments between atoms or molecules (Young & Freedman 2012, p. 1407). They are relevant only for very small distances in order of 10^{-10} m (Nikku 2015). Thus, their significance in larger particles with rough surfaces are very small.

Electrostatic forces are found between electrically charged particles and atoms. Their strength is directly proportional to the strength of the charge and force decreases with distance. Thus, their effect decreases with larger particle sizes. Particles can become charged through collisions and friction with other particles and through thermionic emission in high temperatures. Electrostatic forces can have significant role in fluidized bed with fine particles (Geldart classification group C) and their strength depends on chemical composition, surface properties, size and shape of particles, fluidization velocity and relative humidity of air. Greater amounts of relative humidity have been shown to reduce the amount of electrostatic forces in fluidized beds since water molecules appear to discharge the particles. (Nikku 2015)

At high humidity there may exist capillary condensation between particles. If moisture increases, there are more and more liquid bridges between particles (Li & Kato 2001). Thus, their significance grows with greater humidity. Capillary forces are stronger with small particles (Group C) but can also affect group A and B particles (Nikku 2015).

At high temperatures particles can form bridges and neck between each other's even before reaching the melting point. Sintering is a complicated process were particles are combined through surface diffusion, volume diffusion, grain boundary diffusion, viscous flow, plastic flow, vaporization and condensation. In CFB boilers bed agglomeration is related to high content of alkali metals in fuels (Kovács 2003; Steenari et al. 2019). Thus,

for biomass combustion annual plants are more problematic since they have higher contents of potassium than wood-based biomass (Kovács 2003; Alakangas 2016). CFB boilers do not typically use magnetic particles so their significance in industrial scale units is negligible.

There is not a great number of models for particle-particle momentum exchange in open literature. Nowak et al. (1996) presented a model for quasi-steady state motion of a coarse active particle in an upward flow of dilute uniform suspension. Based on work by Novak et al. (1996), Palchonok et al. (1997) presented a model for calculation of effective velocity of a fuel particle which is presented in equations (26)–(27).

$$\frac{2}{1+\frac{m_b}{m_a}}\frac{(d_a+d_b)^2}{4}\rho_{s,core}\frac{(u_{t,a}-u_{t,b})|u_{t,a}-u_{t,b}|}{2} + C_D\frac{\pi d_a^2}{4}\rho_f\frac{u_{t,a}|u_{t,a}|}{2} - gm_a = 0 \tag{26}$$

where m_b is mass of inert bed particle, m_a is mass of active fuel particle, d_a is diameter of active fuel particle, d_b is diameter of inert bed particle, $\rho_{s,core}$ is solids concentration at core region, $u_{t,a}$ is terminal velocity of active fuel particle, $u_{t,i}$ is terminal velocity of inert bed particle and

$$C_D = \frac{\frac{24}{Re_a}+0.44}{\varepsilon_{core}^{4.75}} \tag{27}$$

where Re_a is Reynolds number of active fuel particle and ϵ_{core} is voidage at core region. According to Nikku (2015) Syamlal et al. (1993) presented a model for the solid-fuel drag force which is based on Syamlal (1985) and Lebowitz (1964). Latter model is also used in LUT model (Nikku 2015) while model by Palchonok et al. (1997) was used in work by Pallarès & Johnsson (2006a). Soriano Sánchez (2019) concluded that model by Palchonok et al. (1997) gave higher values for effective terminal velocity of fuel particles compared to test results with bed material in laboratory scale CFB riser.

4. MODELLING OF CFB BOILERS

4.1 CFB Modelling overview

Objectives of modelling in general are to obtain information for reliable design, scale-up, process optimization, reduced costs and lead times. Industrial scale CFB boilers offer a challenging measurement environment and thus accurate model could offer valuable information from the different processes in the boiler. Over a several decades the development of CFB boilers trusted on empirical experience (Pallarès & Johnsson 2013). During 21st century the interest towards more comprehensive models have grown but still there is work to be done to accomplish accurate holistic model of the process in CFB boiler.

Modelling efforts in fluidized bed combustion can be categorized to three main types: empirical correlations, semi-empirical modelling and CFD. Empirical correlations have been typically used for specific processes e.g. axial solids concentration. They are purely based on experimental results and have drawbacks in extrapolating far outside their derived conditions. Semi-empirical modelling consists of expressions that combine a theoretical basis with certain empirical content. Models are typically based on the closure of mass and heat balances while momentum balance is not considered. Degree of empirical content varies greatly in different models. Semi-empirical models consist of numerous sub-models which content vary from empirical relations to transport equations. Main advantage of the semi-empirical model is the lesser calculation time compared to CFD. Semi-empirical modelling allows a holistic model to offer results in relatively short calculation time. Main drawback is that they rely to some empirical correlations which limit the usage in different conditions and scaling-up. Computational fluid dynamics solves also momentum balance of the gas-solid flow. CFD modelling of an industrial scale boiler requires very long calculation times. In the finest scale of CFD calculation known as direct numerical simulation, Navier-Stokes equations are solved at such small scales that resolve Kolmogorov scales fully in turbulence. However, this requires even more computational time and thus cannot be used in CFB modelling. Thus, coarser resolutions are needed, and this requires again empirical expressions to account for phenomena inside the computational cell. These expressions limit the accuracy of the model and thus CFD models have in most cases shown only limited agreement with measurements. Benefits of CFD modelling are the derivation from first principles and capability to offer transient results for strongly fluctuating circulating fluidized bed boilers. (Pallarès & Johnsson 2013)

CFB models can also be divided based on dimensions in their calculation. The simplest model is a zero-dimensional (0D) model which is correlation-based model which fulfils the basic continuity equations for the basic model. Benefits of 0D models are fast and simple usage while drawbacks are low flexibility, they cannot take into account spatial

effects, they do not provide details of the in-furnace phenomena and they are not usually capable of predicting the effects of changing geometry and boundary conditions. A more detailed description of the in-furnace process is provided with one-dimensional models (1D) where furnace is divided into vertical sections. Drawback of this model is that it does not take into consideration the core-annulus flow structure inside the furnace. (Myöhänen 2011)

More sophisticated and more popular method is the 1.5-dimensional (1.5D) model where furnace is divided into up-flowing core region and down-flowing annulus region. Dense bed is typically considered as separate section and flow behaviour and the mixing between these three regions are determined with empirical correlations. These different flow characteristic zones can also be divided to several control volumes. Some models with core-annulus approach are presented in Adánez et al. (1995), Kruse & Werther (1995), Wang et al. (1999), Huilin et al. (2000), Hua et al. (2004), Gungor (2009), and Kaikko et al. (2017). (Myöhänen 2011)

Models which can take into account the three-dimensional nature of CFB boilers are known as 3D models. Benefit of these models is the capability to predict also horizontal differences in the furnace e.g. oxygen and temperature changes in different spots of the cross-section of the boiler. Number of 3D semi-empirical comprehensive models in the literature is very small. Only three different models have been presented and these are shortly introduced in Table 5 with selected references. Validation of models requires validation data from industrial scale boilers and more validation data allows more useful models. Thus, all of the 3D models are developed with industrial partners which however means that dissemination of specific correlation data is often limited. (Myöhänen 2011)

Table 5. *Comprehensive 3D semi-empirical models. Table is adapted from Pallarès & Johnsson (2013).*

Model name	University	Industrial partner	References
CUT	Chalmers University of Technology	Valmet	Pallarès (2008a) Pallarès & Johnsson (2009) Palonen et al. (2011) Pallarès et al. (2012)
LUT	Lappeenranta University of Technology	Sumitomo SHI FW	Hyppänen et al. (1991) Vepsäläinen et al. (2009) Myöhänen (2011) Nikku (2015) Nikku et al. (2016)
TUHH	Hamburg University of Technology	Stadtwerke Duisburg	Knoebig et al. (1999) Luecke et al. (2004) Wischnewski (2008) Ratschow (2009)

This thesis focuses on CUT model most notably presented in Pallarès (2008a). Model consists of sub-models which are combined to a comprehensive process model. Model

can be divided into 3 main sub-models which consists of fluid dynamics, combustion chemistry and heat transfer all of which interact with each other (Pallarès & Johnsson 2013). Figure 15 illustrates this interaction with 3 main sub-models. Thickness of the arrow indicates the impact of particular process to the following process. Comprehensive model takes geometry information and operating parameters as an input and provides information e.g. about distributions and fluxes of solids, gases and heat (Pallarès & Johnsson 2013). Model presented in literature is presented as 3D, but model user also has capability to use 1.5D calculation method which differs in some regions from the 3D version and offers more limited information about the in-furnace process.

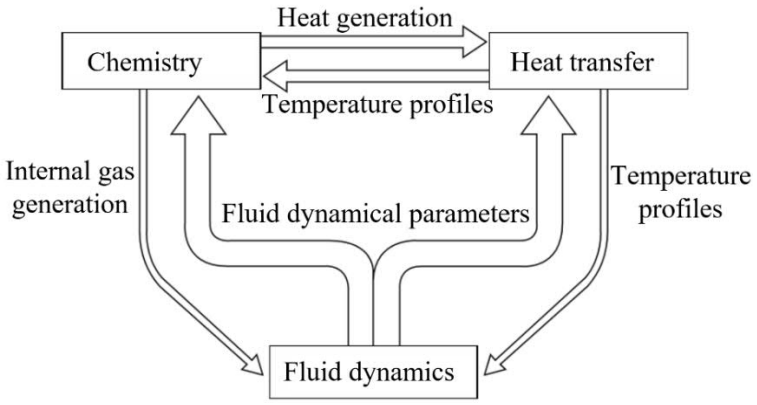

Figure 15. *Input-output data exchange between different sub-models. Thickness of the arrow indicates the impact of that output to following sub-model. Figure is adapted from Pallarès & Johnsson (2013).*

As presented in Figure 4 fluid dynamical model can be divided into three different zones: dense bed, splash zone and transport zone (Pallarès 2008a). Dense bed is considered as a region with constant pressure gradient i.e. solids concentration is considered constant there on a time-averaged basis. Solids concentration in the core of the freeboard is calculated according to equations (1)–(3). Solids inventory is divided to certain amount of calculation batches according to PSD and solids concentration is calculated separately for every size class. Zhang et al. (1995) measured velocities of solids in the down flowing layer and the results indicate that particles will fall there with their terminal velocity (Pallarès & Johnsson 2006). Thus, it can be considered that there is no upward gas flow in the layer.

Heat transfer in CFB operation can be related to heat transfer in fuel particles during combustion process or overall distribution of temperature and heat fluxes inside the furnace. This section deals with the latter one. Most notably this topic is addressed in Pallarès (2008a) and Pallarès et al. (2012). Heat transfer is considered as two separate phenomena: convection and radiation. Basu & Nag (1996) gave a formulation to the overall heat transfer coefficient (h) to the walls according to equation (28)

$$h = c\rho_s^b \tag{28}$$

where c and b are coefficients. Breitholtz et al. (2001) suggested that convective heat transfer could be modelled with same equation while values of c and b would be different. CUT model uses the formulation by Breitholtz et al. (2001) for convective heat transfer. Radiative heat transfer is modelled with emitted and absorbed radiation from every cell in the mesh. Radiation in the model is considered as grey and model allows radiation heat transfer also to non-neighbouring cells which gives more realistic image of the radiation phenomenon than diffusion approach (Pallarès et al. 2012). Radiation originates mostly from solids in CFB boiler, so effects of gas radiation are neglected (Pallarès et al. 2012). Particles and gas are also considered to have same temperature since individual solid particles have low thermal inertia due to their small size.

Main chemical process in CFB boiler is the combustion process. As presented in Chapter 2.3 fuel conversion can be divided into 3 mechanisms: drying, devolatilization and char combustion. These 3 mechanisms can be modelled with different sub-models. In Pallarès (2008a) model for drying and devolatilization is based on the description of the evolution of the temperature profile within the particle published by Thunman et al. (2004) and model for char combustion is based on Field et al. (1967). Fuel fragmentation is modelled with given fragmentation pattern e.g. after certain time fuel particle disintegrates to certain number of fragments (Pallarès & Johnsson 2008b).

4.2 Axial fuel mixing modelling

Fuel particles are injected from lower parts of the furnace and are likely to occupy the bottom part of the furnace after their injection (Pallarès & Johnsson 2008b). During their conversion fuel particles lose mass as stated in Chapter 2.3. Thus, larger particles which fall to the dense bed of a CFB boiler become lighter during their combustion and may be elutriated from the dense bed to the upper area of the boiler or even to the cyclone and loop seal. This affects where the combustion happens in the boiler and thus may have significant impact on boiler operation. Thus, fuel mixing modelling is a vital part of operation of a comprehensive CFB boiler model.

Fuel mixing can be divided into axial i.e. vertical and horizontal mixing. In the bottom bed axial mixing has been shown to be a lot greater than horizontal since lateral dispersion is at least 1 order of magnitude smaller than axial (Niklasson et al. 2002). In the transport zone fuel particles are expected to flow upwards in the core region as inert solids. Similarly as for inert particles, back mixing of fuel is expected to happen due to particles net flow from core region to wall layer.

There are not many fuel mixing models described in open literature but most noticeable to author's knowledge are presented here. Pallarès & Johnsson (2008b) presented a semi-empirical fuel mixing model for the CUT model which is also basis for this thesis. Köhler et al. (2017) presented a model for the axial fuel mixing of char in bottom bed of a CFB boiler. Model divided the bottom bed to bubble phase and emulsion phase and its results

were compared to results from tracer particle measurements. Nikku (2015) described a new fuel flow model for the LUT model which uses momentum equation -based approach. Modelling results were validated to large-scale measurements and it was shown that the modelling efforts improved significantly.

As stated earlier there is possibility to use 1.5D or 3D model in CUT model. Rest of this chapter focuses on axial fuel mixing in 1.5D model which reminds the 3D model. Most notable difference being that the 3D model notices horizontal mixing also inside core region. Due to fuel particle's change in size and shape during combustion process, must fuel mixing calculation notice these changes. Thus, burn out time of fuel particles is discretized to several time steps for which the fuel particles correspond to correct size and shape. Fuel concentration of these individual batches is calculated separately, and the total fuel concentration is based on sum of these individual batches' fuel concentration as presented in Table 6. Grey areas in table present total fuel concentration in the furnace.

Table 6. *Calculation scheme for calculating fuel concentration in the boiler. Table is adapted from Pallarès (2008a).*

Fuel batch	$t = t_0$	$t = t_1$	$t = t_2$	$t = t_3$	...	$t = t_{burnout}$	$t = t_{burnout} + 1$
1	C_0	C_1	C_2	C_3	...	$C_{burnout}$	0
2		C_0	C_1	C_2	...	$C_{burnout}$ -1	$C_{burnout}$
3			C_0	C_1	...	$C_{burnout}$ -2	$C_{burnout}$ -1
4				C_0	...	$C_{burnout}$ -3	$C_{burnout}$ -2
...	...	...	...	...	...	...	...
n						C_0	C_1
n+1							C_0

Fuel concentration of single batch is calculated similarly than concentration of inert solids. Figure 16 illustrates this calculation loop which is presented more precisely below. First particle flow to furnace is calculated. All of the particles are expected to first go into dense bed where a constant axial fuel concentration is assumed. Dense bed is given an initial fuel concentration in which fuel concentration of other cells is compared. After this entrainability of fuel particles is examined and for fuel particles which have greater slip velocity than zero a variable called $c2d$ is calculated according to equation (29)

$$c2d = \max(1 - X * u_{slip}, 0) \tag{29}$$

where X is a coefficient and u_{slip} is slip velocity. If slip velocity is not greater than 0 variable $c2d$ is given a value of 1. Terminal velocity of particles is calculated with the model by Haider & Levenspiel (1989) which is presented in equations (8)–(10). Variable $c2d$ describes the portion of particles which behave according to ballistic decay. Thus, if $c2d$ equals 1 all of the particles behave according to ballistic decay and vice versa. For

particles which are affected by the ballistic decay, ballistic fuel concentration (C_{bal}) is calculated according to equation (30)

$$C_{bal} = C_{H_b} * e^{-a*(z-H_b)} \tag{30}$$

where C_{H_b} is fuel concentration at dense bed surface. Similarly, for particles which are affected by the dispersive decay, dispersive fuel concentration (C_{disp}) is calculated according to equation (31).

$$C_{disp} = C_{H_b} * e^{-K*(z-H_b)} \tag{31}$$

Both concentrations are then updated to the cumulative fuel concentration and one time step is taken forward. Again, number of particles are calculated in the furnace and fuel concentration is calculated. This loop is continued until burnout time is reached and after that total fuel concentration can be evaluated.

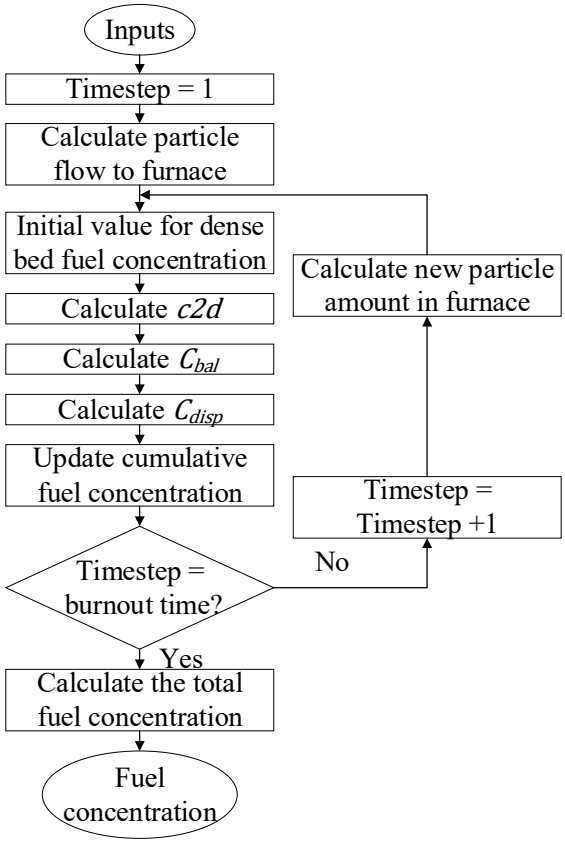

Figure 16. *Calculation of fuel concentration in 1.5D model.*

Fuel related inputs which affect the calculation results are fuel particle dimensions, density, conversion pattern and the fuel flow into the furnace. Other inputs which affect the results are fluidization gas properties, boiler geometry, inert bed material properties and the length of the time step in calculation.

5. RESEARCH MATERIALS AND METHODS

5.1 Research structure

This thesis consists of literature survey, experimental and modelling work. Figure 17 presents structure of this thesis compactly. Literature survey was used to find information on fluid dynamical behaviour of CFB boiler which has great effect on fuel particle flow in CFB boiler. Information was also searched for particle behaviour in flow and fuel particle behaviour during combustion. Focus was also used for finding information on existing CFB models and drag models used to evaluate drag coefficient and terminal velocity of non-spherical particles. This information was used as a basis for the work and analysis of results found later in the thesis.

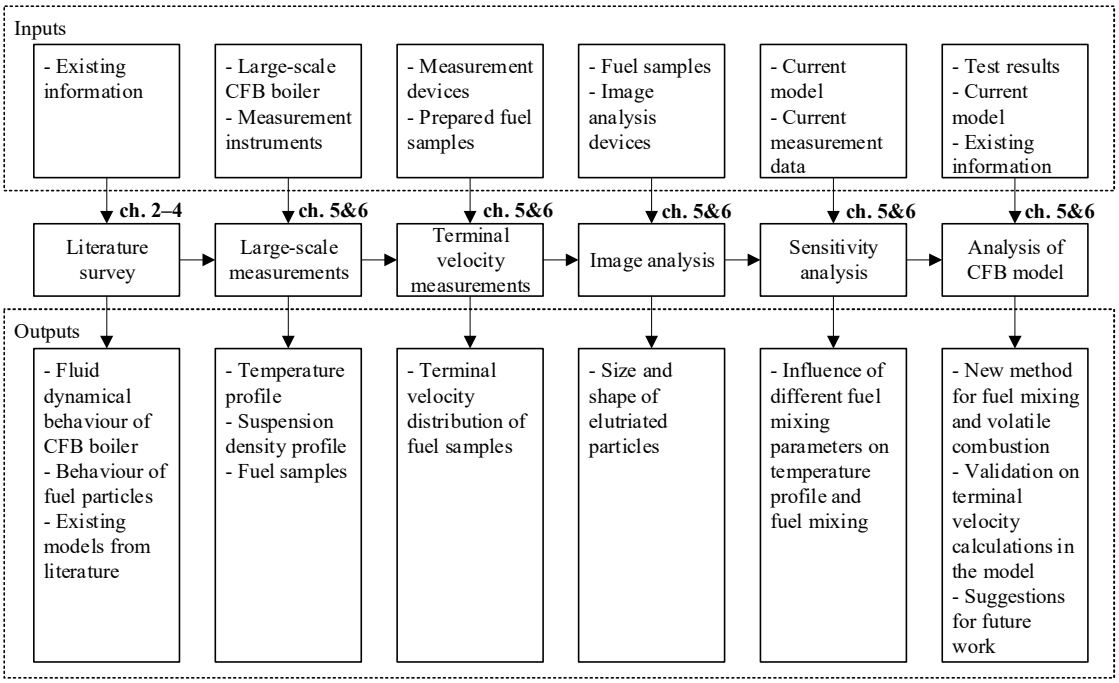

Figure 17. *Structure of this thesis. Numeric notations indicate in which chapter part in question is discussed.*

Temperature measurements were done in large-scale CFB boiler to get validation data for the modelling part of the work and to obtain knowledge on temperature distributions with different fuels. Fuels used in the large-scale measurements were used in terminal velocity measurements. In terminal velocity measurements focus was on finding terminal velocity distributions for fuel samples which were then analysed with image analysis equipment. Focus in image analysis was to find size and shape information on the fuel particles which had certain terminal velocity. These measurement results were used to validate terminal velocity model of the comprehensive CFB model, fuel mixing model and temperature distribution from the comprehensive CFB model.

Influence of different fuel mixing parameters in comprehensive CFB model on temperature distribution and fuel mixing was studied in sensitivity analysis. Information from sensitivity analysis and measurements were used in an analysis of CFB model to evaluate the model's capability to predict the axial temperature distribution. Based on new knowledge on fuel mixing, new method for calculating temperature profile is presented in Chapter 6.4. In addition, some suggestions are done for future work on comprehensive CFB model and its development.

5.2 Large-scale temperature measurements

For the validation of the comprehensive model large-scale temperature measurements were executed in 400 MW_{th} scale CFB boiler. Temperature was measured from 7 different heights around the boiler at 27 different measurement ports. Measurement ports excluding bottom bed and cyclone outlet temperature measurement ports are presented in Figure 18 with red and yellow colour. Same figure also illustrates an example of the measurement signal from one measurement port. Boiler has internal heat transfer surfaces as division wall and as wing walls. In addition, flue gas can be recirculated back to the bottom part of the furnace. Boiler has two cyclones and thus two different loop seals in which there exist a heat exchanger. Boiler was operated in steady state for the duration of measurements. Temperature profile was measured with only coal as fuel and with fuel being 80% biomass and 20% coal by the energy content. Boiler load was similar for both cases: 92% and 94% respectively. Ideally the other fuel mix would have been 100% biomass, but in this case, it was not possible, so biomass-coal mixture was used instead. Coal was fed to the boiler from the front wall while biomass was fed from front and rear wall. Recirculated flue gas was injected to the furnace in both cases, but significantly more recirculated flue gas was used with the coal case.

Temperature was measured with non-cooled and cooled probes. Probes were approximately 1,5 m and 2,3 m inside the boiler respectively. Longer probes were used to measure temperature from the front wall where longer probes were needed to avoid cooler area between wing walls. Longer probes were also used to validate necessary length of the shorter probes to reach the core of the boiler below wing walls. Temperature was measured every 10 seconds using these probes. Bottom bed and cyclone exit temperatures were not measured separately but their values are based on measurements from plants automation system. In total 8 measurement ports were used for bottom bed temperature and 4 for cyclone exit temperatures.

Gas injections to the boiler caused some differences to the operating conditions between two measurements. Amounts of primary air was similar in both measurement cases but the amounts of secondary air and recirculated flue gas varied. For coal the amount of recirculated flue gas was over 10 times greater than for biomass-coal mixture while biomass-coal case used more secondary air compared to coal case. For information about fuel's impact to axial temperature profile it would have been optimal to use similar gas

feeds to the boiler for both cases. However, boiler is in commercial use, so commercial aspects had to be noticed during tests and thus plant's automation system adjusted the process depending on the fuel mixture used.

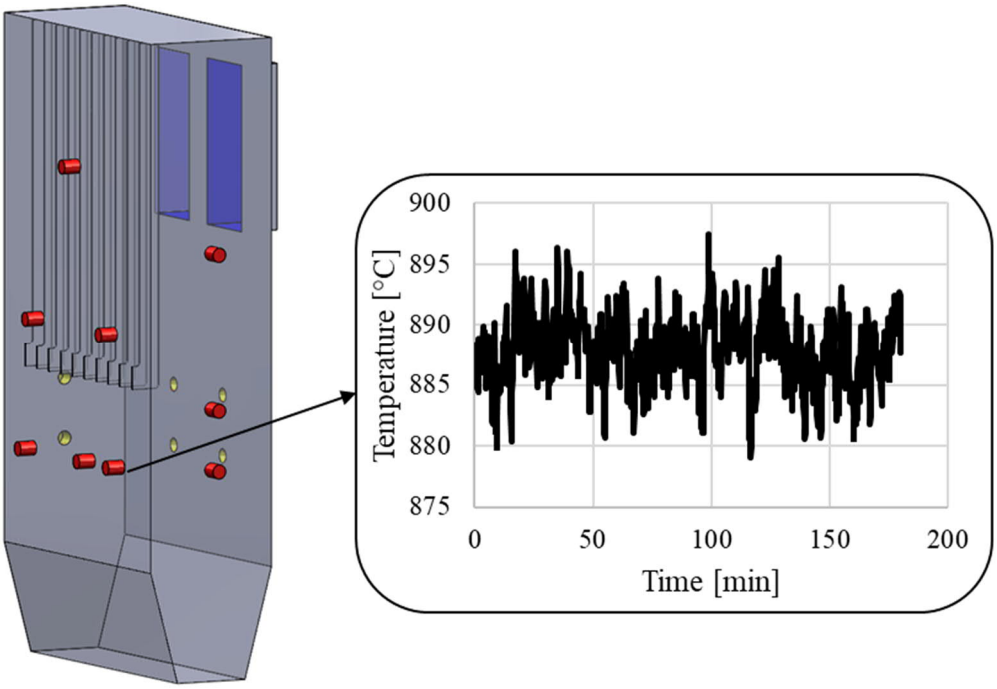

Figure 18. *Temperature measurement ports in used CFB boiler and typical measurement signal as a function of time. Red ports illustrate measurement ports at front and right wall and yellow ports illustrate measurement ports at left and rear walls. Blue colour indicates exit ducts to cyclones. Notice that division wall is not shown here.*

In addition to temperature measurements a pressure profile was measured from the boiler to validate solids concentration in the calculated cases in the model. Pressure was measured from 5 different heights: 5.5 m, 11.8 m, 15.2 m, 19.2 m and 24.0 m. Table 7 presents information from the boiler and the fuels used. There is sieving results of fuels, dry composition and lower heating value (LHV), bulk density and moisture as as received (A.R.).

Table 7. *Fuel analysis results.*

		Coal	Biomass			Coal	Biomass
A.R.				Dry			
	Bulk density [kg/m^3]	650	322		Volatile [%]	35.4	77.1
	LHV [MJ/kg]	24.37	8.81		Ash content (550 °C) [%]	12.0	3.6
	Moisture [%]	13.9	47.2		O [%]	3.6	39.6
Sieve	(under certain percentage)				S [%]	0.35	0.04
	X10 [mm]	0.219	0.72		C [%]	71.6	50.3
	X50 [mm]	1.372	6.851		H [%]	4.9	5.9
	X90 [mm]	6.123	20.401		N [%]	2.46	0.57

5.3 Fuel terminal velocity measurements

Terminal velocity distribution was measured for the fuel samples that were collected from the conveyor belts during large-scale temperature measurements. Terminal velocities were measured for 3 different conversion stages for both biomass and coal: as received, dry and devolatilized. Fuel samples were dried in an oven for 2 days in 105 °C and devolatilization was done in an oven in 900 °C. Heating rate was fairly low since heating time from ambient temperature to 900 °C was on average 70 minutes. After reaching 900 °C fuel samples were kept at constant temperature for 30 min and after this cooled to ambient temperature in the oven. In addition to just measuring terminal velocity of the fuel particles themselves, effective terminal velocities were measured for fuel particles with bed material. Figure 19 illustrates images from biomass sample used in terminal velocity measurements as A.R. and as devolatilized. Respectively Figure 20 illustrates same conversion stages for coal.

Figure 19. *Biomass used in large-scale temperature measurements and terminal velocity measurements. a) represents as received fuel and b) represents devolatilized fuel. Units in the ruler are centimetres.*

Terminal velocity measurements were executed with and without bed material. Measurements without bed material were done in a 1 m tall plastic tube with a diameter of 75 mm. Fuel particles were dropped to the bottom of the tube from which air was blown to the tube. Fuel particles that flew out of the tube at certain velocity were weighed and thus a terminal velocity distribution was formed to certain fuel and conversion stage. For devo-

latilized biomass and coal samples downcomer was equipped with filter bag which collected fuel particles and at every velocity filter was weighed. Flow was adjusted by adjusting valve opening and velocity steps used in measurements varied between 0.4 m/s and 1.7 m/s depending on fuel and conversion stage. Larger velocity steps were used for larger particles which had significantly greater terminal velocities than the smaller particles. Figure 21a illustrates the measurement device used. Three upward arrows indicate the air blown into the riser and 1 downward arrow indicates the exiting fuel particles and air.

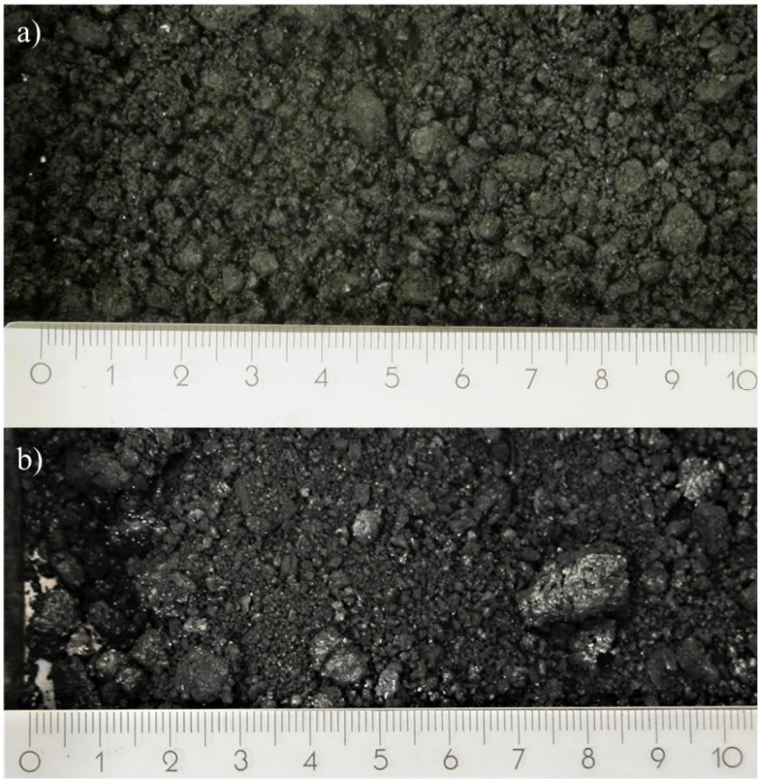

Figure 20. *Coal used in large-scale temperature measurements and terminal velocity measurements. a) represents as received conversion stage and b) represents devolatilized fuel. Units in the ruler are centimetres.*

Due to relatively small diameter of the riser tube wall effects were clearly visible. Some particles circulated the riser next to walls at constant height and if they were transported to the centre of the tube, they were immediately elutriated higher in the riser. Thus, relatively long run times were used for each sample so that the significance of wall effects would be smaller. Tube was also shaken by hand from time to time to get particles to the core of the flow from the wall or from the bottom. At some velocities, especially biomass particles attached to riser wall due to electric forces. This was most visibly at velocities from 4 m/s to 6 m/s. At higher velocities particles were not attached to walls anymore.

Terminal velocity measurements with bed material were done in a 1.9 m tall riser with diameter of 190 mm. At the top of the riser was the exit duct to cyclone and on the bottom of the cyclone was sieve with 3.35 mm openings which collected elutriated fuel particles.

Collected fuel particles were weighed similarly as in measurements without the bed material. Bed material was circulated back to the riser through 2 bubbling fluidized beds. Figure 21b illustrates the measurement device. Fuel samples that were tested in this device were dry biomass and devolatilized biomass. Since the sieve openings were larger than some fuel particles, fuel was first sieved through same size sieve and only larger particles were tested in the riser. Since some of the fuel particles were very elongated, sieve after cyclone may not have collected all of the particles which were elutriated. Riser had 14 pressure measurement ports which were used to obtain solids concentration profile in the riser. Velocities that were used in the measurements varied from 1 m/s to 1.4 m/s. Measurement device is presented also in Johansson et al. (2003) and Soriano Sánchez (2019) who used the device in similar measurements with wood pellets and wood chips.

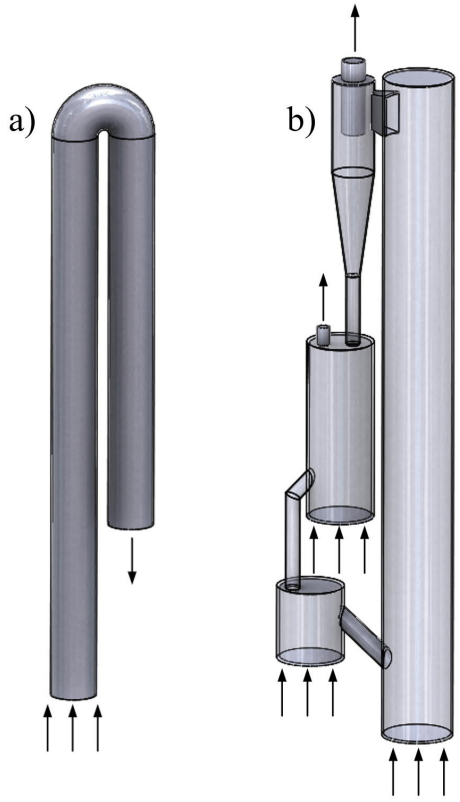

Figure 21. *Measurement devices used in terminal velocity measurements. Three upward arrows illustrate fluidization air and single arrow illustrates exiting air. Figure a) illustrates measurement device for tests without bed material and b) for measurements with bed material. In b) right hand side tall riser is the fuel riser which was fluidized with variating velocities.*

Bed material which was used in measurements was ballotini which consists of spherical glass beads which density is 2600 kg/m^3. Half of the bed material was in the size range of 75–120 µm and half in range of 180–300 µm. Smaller ballotini was added to the riser since larger beads had troubles in lifting fuel from the riser. This helped the cause but also caused some plugging in the pressure measurement ports. Thus, some of the pressure measurements had to be discarded.

There was also some bed material accumulation in the cyclone downcomer. Thus, air was led to the downcomer which helped the issue but caused also bed material loss through the cyclone air exit. Thus, solids concentration varied significantly with same velocities. Approximately 20–30% of the bed material could have been lost through cyclone in 15 minutes of operation. Regularly bed material from the filter was returned to the riser to keep PSD and amount of bed material relatively similar.

Some fuel attrition from devolatilized biomass happened during tests since bed clearly changed its colour from white to darker. It is difficult to evaluate how much attrition happened but collected fuel particles seemed relatively intact, so it can be assumed that attrition was not the largest source of uncertainty in the tests. Static electricity caused some issues also in tests with bed material. It could be observed that the transparent plastic riser caused some particles to attach themselves to the walls and thus they were not elutriated so easily.

5.4 Image analysis

Fuel particles which had been used in terminal velocity measurements were analysed with image analysis program to obtain shape and size information about the particles which were elutriated at certain velocity. Two fuel samples were analysed in total: A.R. biomass which was used in tests without bed material and devolatilized biomass which was used with bed material. These fuels were chosen since only biomass with A.R. and dry conversion stages were elutriated without filter in tests without bed material and dry sample had been used later with bed material. Devolatilized biomass was chosen to be the other sample since it had produced best results from measurements with bed material. Images were taken with system camera while fuel samples were on a light diffuser. Image analysis program identified particles based on lighter and darker pixels in which fuel samples represented the darker particles. Size of 1 pixel varied from 7.6 µm to 68 µm based on used photographic objective and distance from the table. Larger particles were analysed with coarser resolution while smaller particles were analysed with finer resolution. Figure 22 illustrates the setup for particle imaging.

It was presumed that particles would lay on the light diffuser at their maximum projection surface. For smaller particles it was visible that this was not necessarily true since they may have aligned differently due to static electricity. These particles were placed again to the diffuser and usually this helped. Since some particles were very small it is possible that all of the wrongly aligned particles were not detected and thus their maximum projection was not analysed. From the images: area, perimeter and length of major and minor axis was detected. From this information a diameter of a circle with equivalent area as the particle was calculated with aspect ratio, Cox circularity and Pentland roundness.

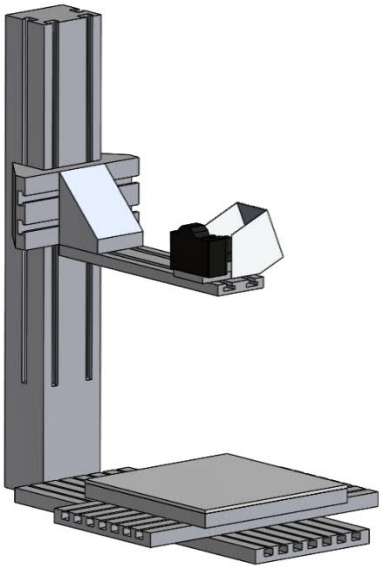

Figure 22. *Setup for particle imaging. Plate under the camera worked as a light diffuser on which fuel particles were laid out.*

5.5 Identifying the most impactful variables in fuel mixing model

Sensitivity analysis where the influence of main axial fuel mixing parameters to the comprehensive CFB model outputs was performed. Sensitivity analysis was performed with the 1.5D model and results from them were compared to 3D model. Different boiler model was used in sensitivity analysis compared to rest of this thesis to save time since measurements in large-scale boiler were not executed immediately after the start of this thesis project.

Evaluation of the length of time steps for fuel conversion model and fuel mixing model was performed. Values in which fuel concentration, temperature profile and so-called release profiles stayed constant were used in actual sensitivity analysis for fuel mixing model. Release profiles represent mass loss as a function of boiler height in which moisture, volatiles and char is lost from the fuel particle. Basis in the evaluation of the time steps were the initial values used for fuel conversion model and fuel mixing model in the comprehensive model. Length of these time steps were manipulated until convergence was reached.

Actual sensitivity analysis was performed as partial sensitivity analysis and variables which were chosen for it were terminal velocity u_t, transport zone decay constant K, splash zone decay constant a, and variable $c2d$. These values were multiplied with numbers ranging from 0.01–100 while keeping other variables at their default value. In addition, this evaluation was performed also to other formulation of K which is not presented in this thesis. Thus, 64 different scenarios were evaluated in the sensitivity analysis in addition to time step evaluation. Benchmark result had been calculated with the default

values and new results were compared to it. Length of time steps used for fuel conversion and mixing models were based on results from the time step evaluation.

Calculation domain inside the furnace is divided to calculation cells and at every height the difference between new and benchmark result was calculated. Result from every height was squared to increase the impact of large differences and the sum of these squares was calculated. Thus, the effect of value change of different variables was evaluated to all of the 5 evaluation profiles presented earlier.

5.6 Analysis of measurements and CFB model

With results from terminal velocity measurements without bed material and image analysis, terminal velocity model by Haider & Levenspiel (1989) was evaluated. Results from terminal velocity measurements were compared to ones from the Haider & Levenspiel (equations (8)–(10)) model. Cox circularity was used as an approximation of the sphericity based on results from Bagheri et al. (2015). As received biomass was used in this analysis and its material density was approximated to be double the bulk density which results in typical biomass material density value (Baxter 2005). Drag coefficient for A.R. biomass was determined with method by Nikku et al. (2014). Only difference for the method used in this thesis and work by Nikku et. al (2014) is that while Nikku et al. (2014) used average diameter of the particle this thesis uses the length of major axis. This was due to software used in image analysis. Also, the difference in mean and maximum diameter of a forest residue is relatively small in work by Nikku et al. (2014). Thus, it is assumed a reasonable approximation to use the length of major axis in the method.

Terminal velocity measurements were done in cold conditions and thus do not represent boiler conditions even if fluidization gas would be considered same in measurements and boiler. Dynamic viscosity of air increases as temperature increases while values of density decreases. Thus, terminal velocity of particles changes from cold conditions to hot conditions and thus A.R. biomass results were correlated to hot conditions based on information from terminal velocity measurements and image analysis. Air was assumed to be the fluidization gas in both cold and hot conditions since the gas properties are relatively similar for both air and flue gas.

If the effects of buoyancy are neglected drag force remains constant in both hot and cold conditions when particles drop at their terminal velocity. Thus, terminal velocity of particles at hot conditions can be solved by stating that the drag force is constant in both cases while terminal velocity changes. Nikku (2015) presented a method to compare drag forces in cold and hot conditions by integrating equations (5) and (32).

$$C_D = \frac{24}{Re}(1 + 0.15Re^{0.687}) \tag{32}$$

Thus, Nikku (2105) presented that drag force can be written according to equation (33).

$$F_D = 3\mu_f + \frac{9}{20}\left(\rho_f d_p \left(u_f - u_p\right)\right)^{0.687} \mu_f^{0.313} \tag{33}$$

When equation (33) is written for hot and cold conditions and marked equal, terminal velocity of a fuel particle at hot conditions can be solved from equation (34)

$$1 = \frac{3\mu_{f,h} + \frac{9}{20}\left(\rho_{f,h} d_p u_{t,h}\right)^{0.687} \mu_{f,h}^{0.313}}{3\mu_{f,c} + \frac{9}{20}\left(\rho_{f,c} d_p u_{t,c}\right)^{0.687} \mu_{f,c}^{0.313}} \tag{34}$$

where subscript h refers to hot conditions and c to cold conditions. Thus, terminal velocity for hot conditions can be written according to equation (35).

$$u_{t,h} = \frac{\left(\frac{3\mu_{f,c} + \frac{9}{20}\left(\rho_{f,c} d_p u_{t,c}\right)^{0.687} \mu_{f,c}^{0.313}}{\frac{9}{20}\mu_{f,h}^{0.313}}\right)^{1.4556}}{\rho_{f,h} d_p} \tag{35}$$

In addition to equation (35) terminal velocity in hot conditions was evaluated with equations (8)–(10), with integrating equations (5) and (12) together and using drag coefficients which were obtained from the Nikku et al. (2014) method. When evaluating the terminal velocity in hot conditions with equations (8)–(10), length of major axis was used as particle diameter because of results presented in Chapter 6.2. When drag coefficients from Nikku et al. (2014) method was used, a fitting curve was used based on measurements to estimate drag coefficients between and outside of measurements results.

In the analysis of the comprehensive CFB model 1.5D and 3D models were used. Principally analysis was performed with 3D model since it was shown to correlate better to measurement data. Large-scale temperature measurements were used as a validation data in this thesis. As presented in Figure 15 fluid dynamical parameters have major impact on heat transfer and chemistry models. Thus, fluid dynamics model for inert particles was validated with suspension density measurements. These validated fluid dynamics solutions were used as a basis for the rest of the work.

After having validated results for inert fluid dynamics model a benchmark result for temperature profile was calculated for both validation cases with default parameters. Heat transfer coefficients for water wall and internal heat transfer surfaces were determined based on previous research and measurements from same boiler used in the validation cases. Benchmark results were analysed and based on these results fuel mixing parameters presented in Chapters 4.2 and 5.5 were manipulated so that the results would correlate better with the measurements from large-scale boiler. Based on findings from these experiments the best method for improving temperature profile was chosen based on new results. These methods are presented in Chapter 6.4.

6. RESULTS AND DISCUSSION

6.1 Results of large-scale temperature measurements

To get validation data for the modelling efforts, temperature profiles were measured from one boiler with 2 different fuel mixtures. Figure 23 illustrates the average temperatures from every measurement height used. Vertical bars represent the variation between maximum and minimum temperature between measurement values at same height. At 100% coal case there is significantly more variation between maximum and minimum temperatures at certain heights compared to biomass-coal mixture. This is explicable with the fact that coal was fed to the boiler only through the fuel feeders at the front wall. Thus, the core area is hotter near the front wall than it is near the rear wall. This is clearly visible in the Figure 24 which compares temperature profiles from every wall. Front and rear wall temperatures are presented as averages since there were multiple measurement ports at those walls excluding the highest point at the front wall. Right and left walls had only one measurement port at certain height, so the results indicate those values. Temperature variation is significantly lower in 3 highest measurement ports. This is because there was only one measurement port at 24 m and 28 m height and measurements from 19 m are based only on results from front wall.

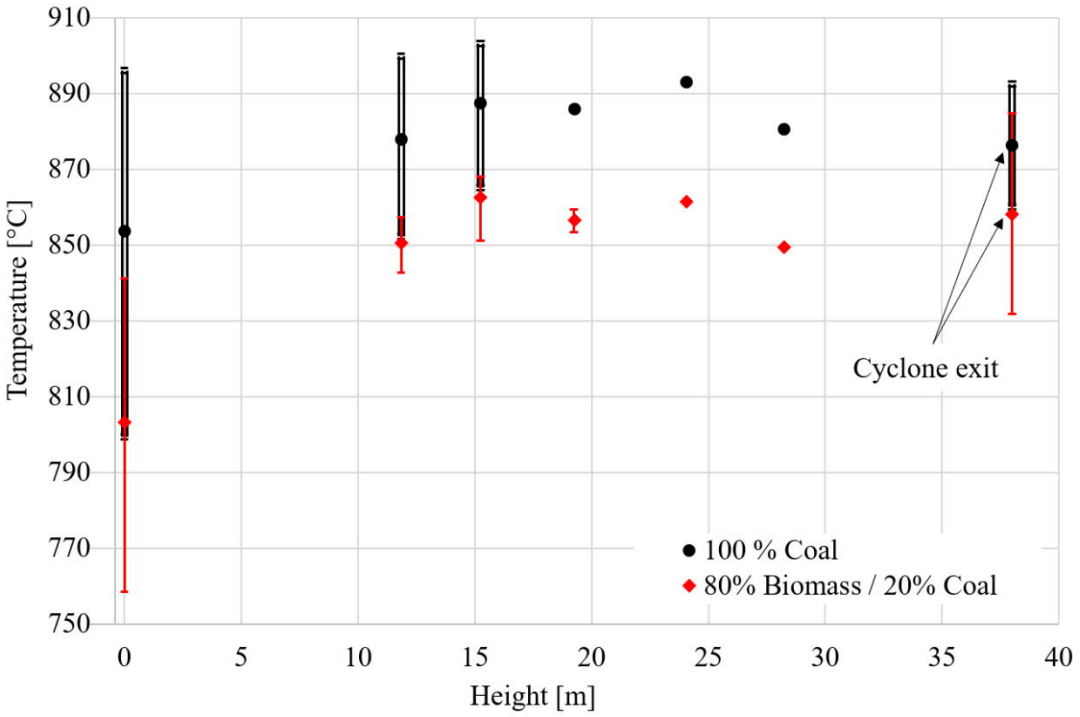

Figure 23. *Average temperatures at different heights. Vertical bars represent the maximum and minimum measurement temperature at every height while the markers indicate the average temperature.*

As stated earlier, when coal is used as fuel in CFB boiler axial temperature profile is expected to be quite even, while biomass is expected to have lot more variation in temperatures. In these measurements the temperature profiles in Figure 23 are however quite similar by their shape. Biomass-coal mixture still has more temperature rise from the bottom bed to the mid-parts of the riser, but difference is not as visible as presented by La Nauze (1987, according to Nikku 2015). This could be explained by the large amount of recirculation gas used in coal test compared to biomass-coal mixture. Boiler regularly runs on biomass-coal mixture and when the fuel mix started to turn towards coal, the bed temperature started to rise. Thus, control system started to increase the amount of recirculation gas which started to cool down the bed. Most significant difference in the measurements is the temperature difference between 2 fuel mixtures. Biomass-coal mixture has significantly lower temperatures at every measurement height.

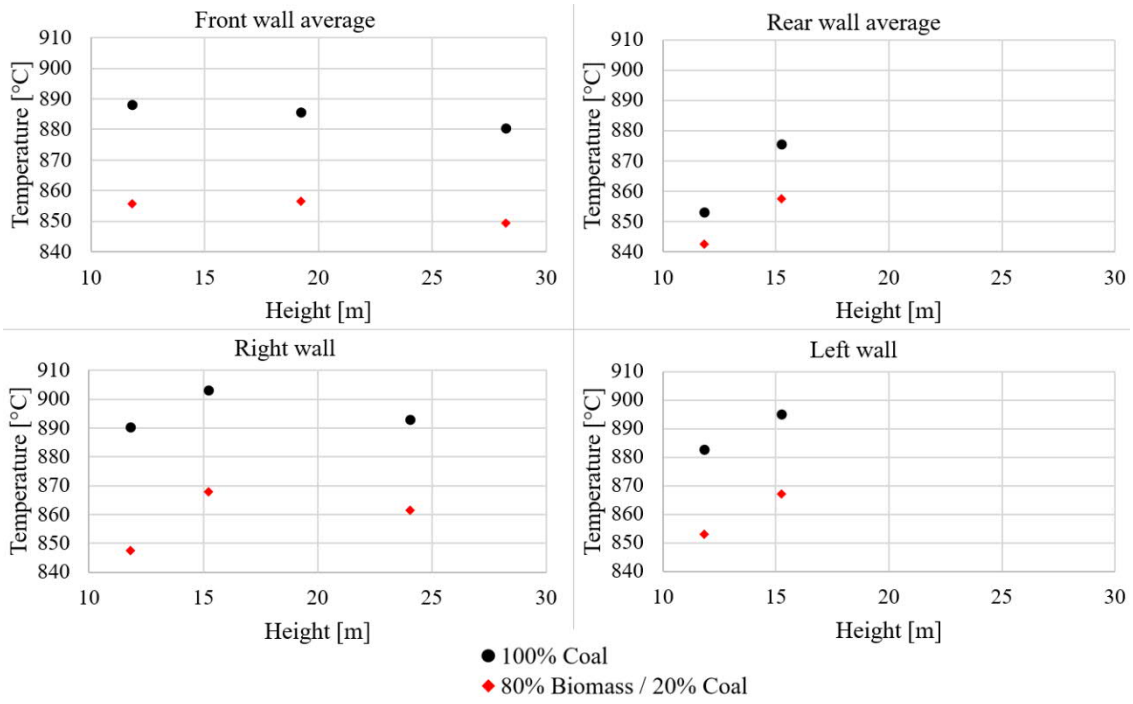

Figure 24. *Temperature profiles at different walls.*

At height of 19 m there is a small decrease in temperature compared to measurements below and above. These values are based on 2 measurement ports located at front wall. Wing walls are already used at that height, so they are probably the reason for cooler temperature compared to value from 24 m which was measured from right wall. Longer measurement probes which reach past wing walls were used at wing wall area. Thus, this result is not caused by measurement probes being between the wing walls. Comparison between shorter and longer probes indicated that there is sharp temperature gradient near wing walls. Shorter probes gave at height of 19 m over 30 °C lower temperature than the longer probes. Thus, it can be stated that wing walls have a significant cooling effect at front wall and the temperatures at 19 m height were probably higher at other walls than

at front wall. At 28 m height the difference between longer and shorter probes was not very significant.

Usage of shorter measurement probes away from wing walls was validated by comparing measurement results from different probes from same measurement port. This test was done at 12 m height, so the wing walls did not affect the results. These measurements gave similar results, so it can be assumed that shorter probes were long enough to reach the core of the flow where temperature gradients are not very steep even though core temperature cannot be assumed even at every operating condition as seen with coal measurements.

During measurements, temperature stayed relatively constant excluding approximately 1-hour time period for biomass-coal mixture while temperatures were approximately 10 °C lower than for the rest of the 4-hour test run. This is probably due to variations in fuel quality and plant's control system backs up this assumption since it shows small decrease in fuel power during same time period. Figure 25 illustrates temperature measurements which are averaged for 1 minute as a function of measurement time. There are data from front wall measurement port at 12 m height and from right wall measurement port at 24 m height. The drop of temperature between minutes 90–150 for biomass mixture can be seen from the figure. It should also be noted that for coal front wall temperature is hotter than upper right wall temperature. This is vice versa for biomass rich mixture which indicates that combustion occurs higher in the furnace for biomass and with 100% coal mixture more combustion occurred at front wall due to fuel feeding.

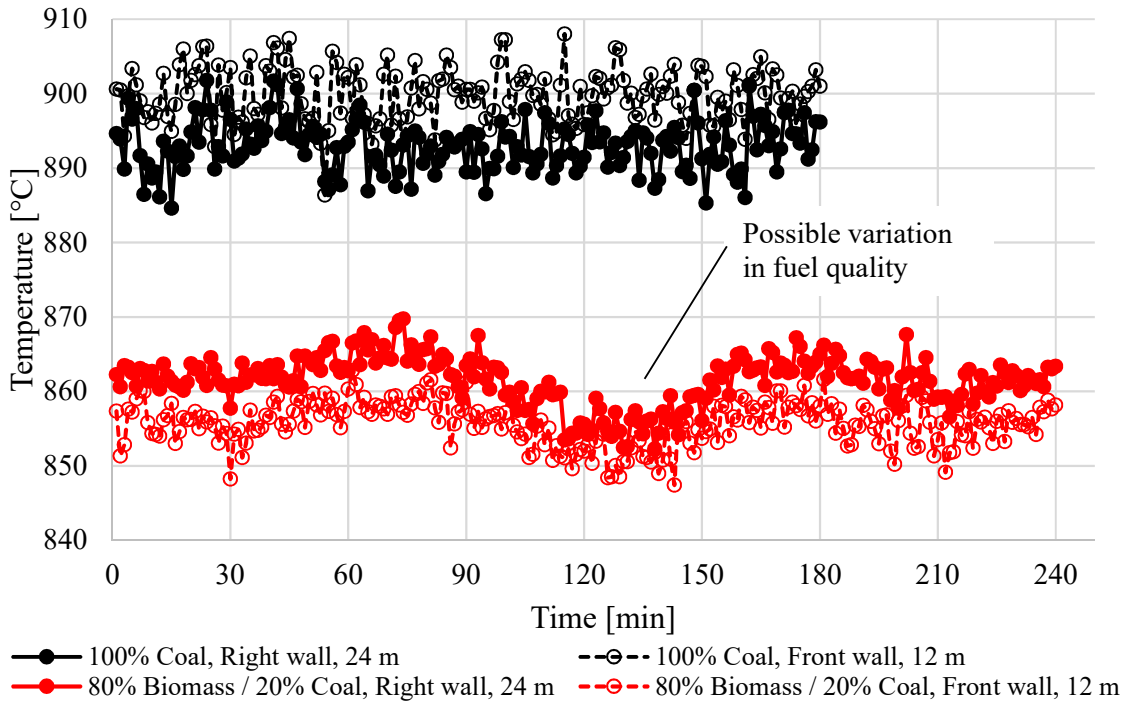

Figure 25. *Temperature variation during test runs for two different locations. Temperatures are averaged for one minute.*

For the validation of fluid dynamics model in the comprehensive model also pressure measurements were executed. From the pressure measurements an average suspension density was calculated between every measurement port based on hydrostatic pressure. This average suspension density is assumed to locate in the middle of measurement ports. Figure 26 illustrates this suspension density profile for both measurements. Noticeably suspension densities are almost identical for both cases.

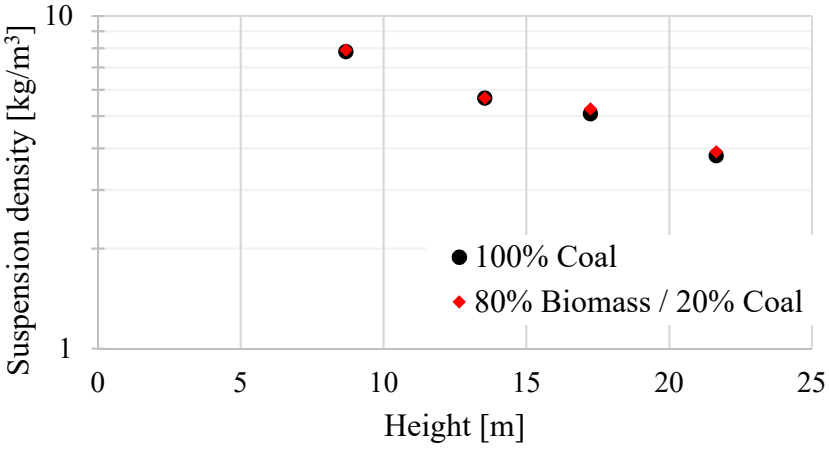

Figure 26. *Averaged suspension density during measurements.*

6.2 Terminal velocity of fuel particles

6.2.1 Measurements and image analysis without bed material

Terminal velocity of fuels from large-scale temperature measurements were measured to obtain knowledge on fuel behaviour without the bed material. Cumulative terminal velocity distributions for two different fuels and three different conversion stages are presented in Figure 27. Due to limited time with the test device some results are based on small sample size which consists of only one test run. Fuels that were tested with more than one time were devolatilized biomass and coal and A.R. biomass. Figure 27 illustrates the results of these tests so that the point indicates the mass share which had been elutriated from the riser with corresponding velocity. Curve of A.R. biomass does not reach unity since some of the particles in the fuel were too large for the test device. Thus, it can be only stated that their terminal velocity is higher than 12 m/s. Results indicate that devolatilized fuel samples have smaller terminal velocities than dried samples and dried samples have smaller terminal velocity than A.R. fuel samples. Results also indicate that biomass sample has smaller terminal velocity than coal if A.R. samples are excluded. Similar terminal velocities for A.R. samples resulted from the larger particle size of biomass. Since the coal had smaller moisture and volatile content the terminal velocities of coal particles did not change as much during fuel conversion as it does for biomass particles.

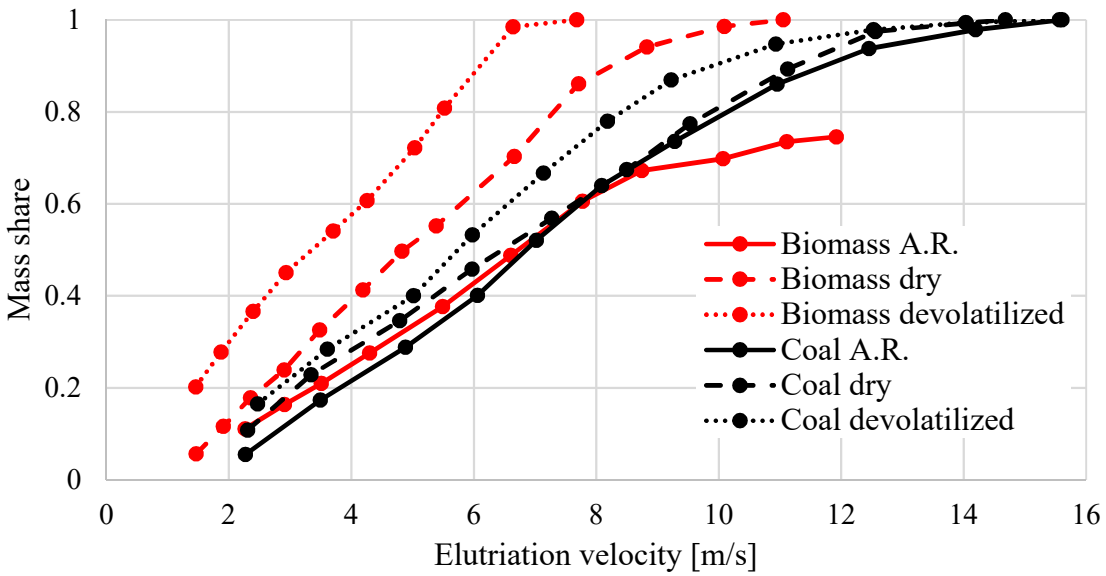

Figure 27. *Cumulative terminal velocity distributions of tested fuels.*

Due to small diameter of the riser tube significant wall effects where noticed during the tests. Reynolds number for the tube during measurements varied from 6 000 to 60 000. Thus, flow at the tube can be assumed to be turbulent. However, the length of the riser tube was not very long compared to diameter of the tube. Thus, the velocity profile cannot be estimated precisely for example with power law profiles. It can be stated that the velocity profile was not even and thus particles may have experienced higher velocity than the average in the centre area of the tube and vice versa near the walls. Since the significance of wall effects is difficult to estimate precisely, this thesis assumes that the terminal velocity of the particles was the average of the mass flow out of the tube. Figure 28 illustrates A.R. biomass particles that were elutriated with varying velocities. Numbers on the ruler indicate centimetres and one gap between the lines indicates 1 mm.

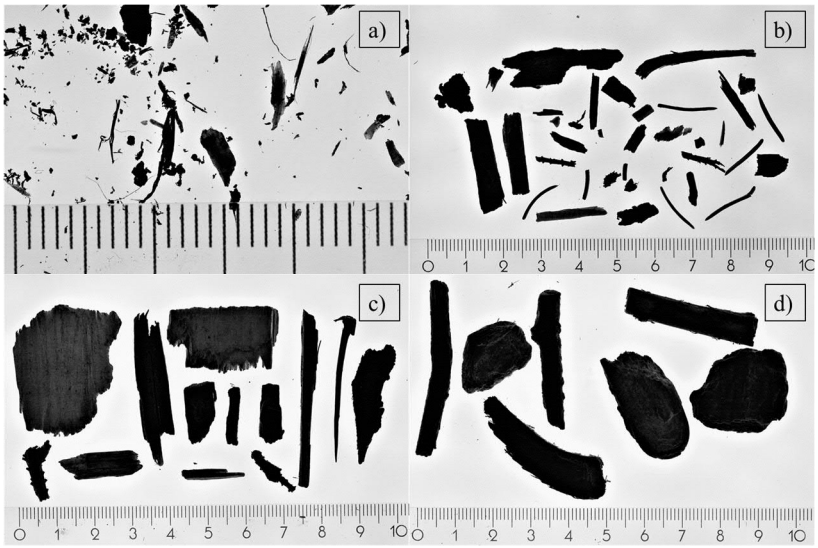

Figure 28. *As received biomass particles that were elutriated with a) 2.3 m/s, b) 5.5 m/s, c) 7.8, d) 11.1 m/s gas velocity.*

Due to measurement techniques used in terminal velocity measurements only A.R. biomass was used in image analysis from the fuels used in measurements without bed material. Size and shape of particles which had same terminal velocities were analysed as one batch. Figure 29 illustrates the average particle diameter of a circle with equivalent area than the imaged particle as a function of the velocity in which particles were elutriated from the riser tube. Figure also illustrates the 10th, 25th, 75th and 90th percentile (PCTL) of the particle size and values for Pentland roundness. The average diameter of particles increases as a function of fluidization velocity while the shape of particles does not seem to have any significant trend. Same observation can be made from Figure 30 where roundness of the particles is plotted as a function of particle diameter. Nikku et al. (2014) reported that in forest residue which they had analysed smallest particles did not have small values for roundness. Results from this thesis indicate that at least with this fuel sample this kind of a conclusion cannot be done. Image analysis used in this thesis does not produce exact values for the smallest particle sizes, but indication is that even though smaller particles may have larger roundness on average they also have particles with small values of roundness. Based on Figure 30 it can also be stated that particles with same terminal velocity were possibly elutriated at different velocities. There are particles with same size and shape and different elutriation velocities. Thus, results from measurements cannot be used to estimate terminal velocity of single particle precisely but as an indication of the terminal velocity distribution of the whole fuel sample.

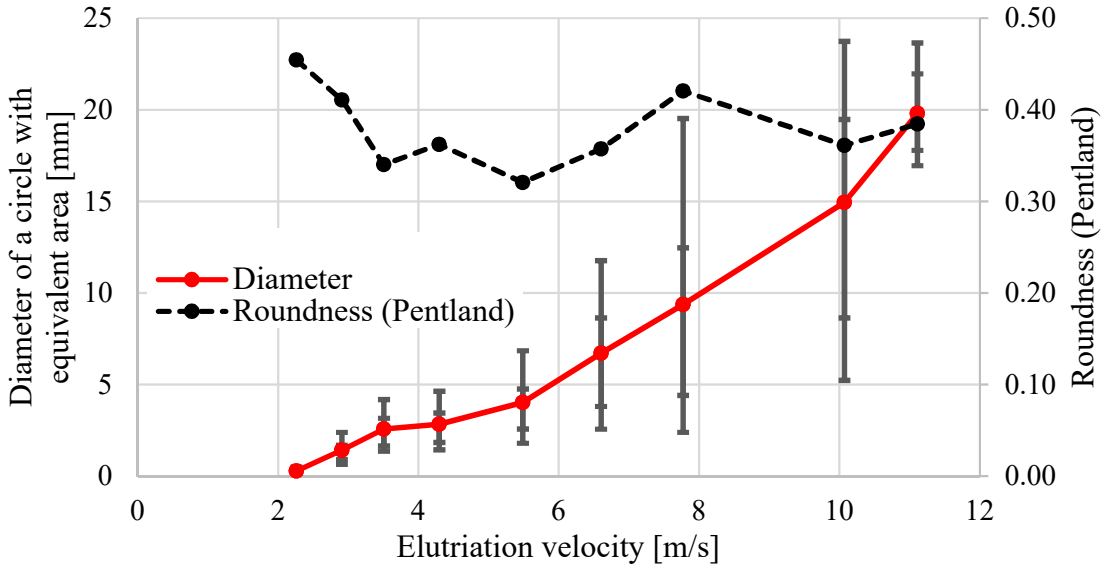

Figure 29. *Shape and size of as received biomass as a function of elutriation velocity.*

Figure 29 illustrates how particle groups with larger terminal velocity have larger variation in size. However, this is true when considering the dimensions of the particles but the ratio between the value of the certain percentile and the average value remained relatively constant between different batches of elutriated fuel. It should be noted that the greatest velocity of 11.1 m/s had small number of particles to be analysed and thus the

size variations are much smaller than for previous terminal velocity classes. Table 8 illustrates more comprehensive information on size and shape of the selected velocity batches. As can be seen in the table, different shape factors used in analysis gave different values. Cox circularity gave largest values while reciprocal of aspect ratio gave smallest values. However, all of the used shape factors gave similar classification on particle sphericity between different batches. Thus, it can be stated that all of the 3 used shape factors identify these fuel particles similarly even though they give different values. However, based on these results particle sphericity cannot be evaluated with all of these shape factors. Since measuring of sphericity is challenging this thesis does not include measurements of particle sphericity. Thus, there are no tools to estimate which shape factor gives most precise information on sphericity.

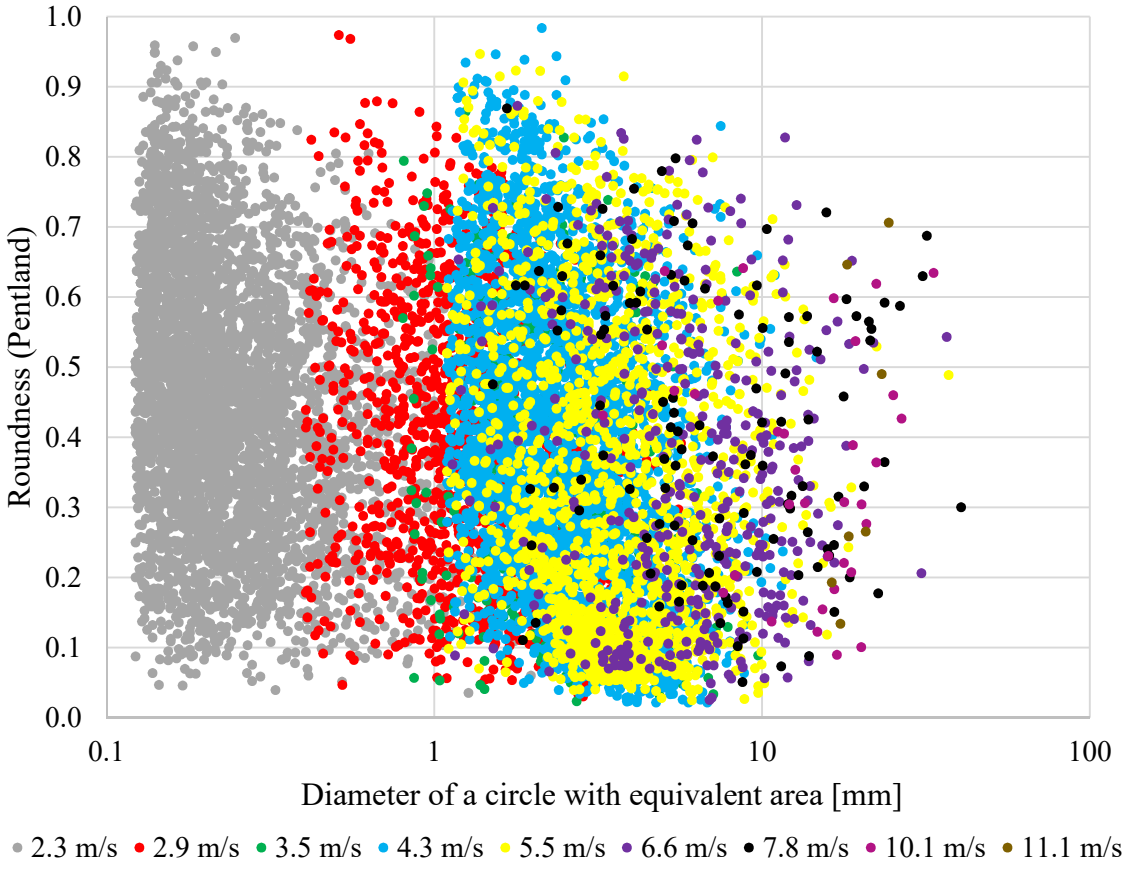

Figure 30. *Shape of particles as a function of particle size. Different colours illustrate different elutriation velocities.*

Results from terminal velocity measurements without the bed material indicate that the terminal velocity distribution is wide for fuels used in commercial CFB boiler. These results are measured in cold conditions and do not represent terminal velocity of hot conditions which is evaluated in Chapter 6.2.3. It should also be noted that due to slow heating rate in the devolatilization, fuel particles may experience more deformation in CFB boiler and coal may experience some fragmentation during devolatilization. This may cause for example biomass to reach more spherical shape which may cause increase in

terminal velocity while for coal swelling or fragmentation may decrease it. However, according to great difference in terminal velocities between devolatilized biomass and coal in these experiments, biomass is lot more likely to be elutriated to the upper parts of the boiler. However, if smallest biomass particles end up in the bottom bed at the beginning of combustion they may burn out at the bottom region before they can be elutriated. Thus, elutriated particles would be char from larger particles which means that most of the volatiles would be released in bottom region similarly as for coal.

Table 8. *Size and shape information based on image analysis for as received biomass.*

Terminal velocity [m/s]	Number of analysed particles	PCTL	$d_{sph,eq\ A_p}$	Major axis [mm]	Minor axis [mm]	Roundness, Pentland	Circularity, Cox	Aspect ratio^{-1}
0-2.3	3934	10th PCTL	0.14	0.19	0.05	0.20	0.24	0.14
		25th PCTL	0.16	0.24	0.09	0.31	0.35	0.25
		Average	0.28	0.48	0.18	0.45	0.53	0.42
		75th PCTL	0.32	0.54	0.21	0.59	0.71	0.58
		90th PCTL	0.49	0.89	0.34	0.71	0.82	0.72
2.3-2.9	1376	10th PCTL	0.65	0.97	0.23	0.16	0.22	0.10
		25th PCTL	0.90	1.39	0.38	0.25	0.33	0.19
		Average	1.42	2.59	0.82	0.41	0.50	0.37
		75th PCTL	1.69	3.10	1.03	0.54	0.65	0.53
		90th PCTL	2.39	4.87	1.54	0.66	0.74	0.69
3.5-4.3	3619	10th PCTL	1.44	2.07	0.43	0.10	0.17	0.06
		25th PCTL	1.83	2.83	0.68	0.17	0.29	0.12
		Average	2.83	6.05	1.37	0.36	0.51	0.30
		75th PCTL	3.44	7.84	1.72	0.51	0.68	0.45
		90th PCTL	4.63	12.26	2.64	0.66	0.80	0.65
4.3-5.5	1734	10th PCTL	1.79	2.75	0.43	0.08	0.15	0.05
		25th PCTL	2.57	4.25	0.73	0.12	0.21	0.08
		Average	4.03	9.07	1.82	0.32	0.45	0.27
		75th PCTL	4.76	12.50	2.37	0.48	0.63	0.42
		90th PCTL	6.84	16.36	3.79	0.65	0.77	0.64
6.6-7.8	120	10th PCTL	2.39	3.80	0.96	0.16	0.28	0.08
		25th PCTL	4.41	5.90	1.58	0.25	0.39	0.13
		Average	9.37	16.37	4.95	0.42	0.53	0.36
		75th PCTL	12.46	22.71	5.56	0.59	0.71	0.56
		90th PCTL	19.53	34.53	10.32	0.68	0.78	0.78
7.8-10.1	34	10th PCTL	5.20	7.36	1.03	0.13	0.13	0.04
		25th PCTL	8.60	17.93	2.23	0.21	0.28	0.12
		Average	14.95	27.90	6.87	0.36	0.44	0.27
		75th PCTL	19.48	38.91	9.16	0.48	0.60	0.37
		90th PCTL	23.74	40.10	14.00	0.63	0.70	0.57

6.2.2 Measurements and image analysis with bed material

Effective terminal velocity of dry and devolatilized biomass was measured by using the measurement set-up presented in Chapter 5.3. Results for effective terminal velocity distribution is presented in Figure 31a. Since part of the fuel sample was too small to be captured with the sieve under the cyclone smallest particles had to be excluded from the measurements. Thus, it is assumed in Figure 31a that these smaller particles would be entrained at the same velocity than first larger particles are entrained. From the devolatilized sample 51% was too small to be collected with the sieve and for dry biomass 32% were too small and 4% were too large to be entrained through the cyclone. With dry biomass elutriation of particles was not very significant and due to limited time focus was put more into devolatilized sample. Thus, the following analysis is focused on results from devolatilized biomass. The results show that in these experiments very large share of the particles was elutriated with small gas velocities compared to tests without the bed material. As stated in Chapter 5.3 the bed material loss through the cyclone to filter caused issues with the suspension density. Ideal situation would have been to keep constant suspension density through the tests so that the gas velocity would have been the only variable. However, this was not reached in the tests and Figure 32 illustrates maximum and minimum solids concentration profiles for 3 different gas velocities. Results in Figure 32 are presented as an average during one measurement period so the real momentary maximum and minimum values are bit higher and lower for the maximum and minimum curves respectively. During the measurements there were some blocking up of pressure measurement ports and thus some results from the measurements had to be excluded. However, results indicate that the solids concentration was not nearly a constant during measurements even with same velocities. This was also observed visually.

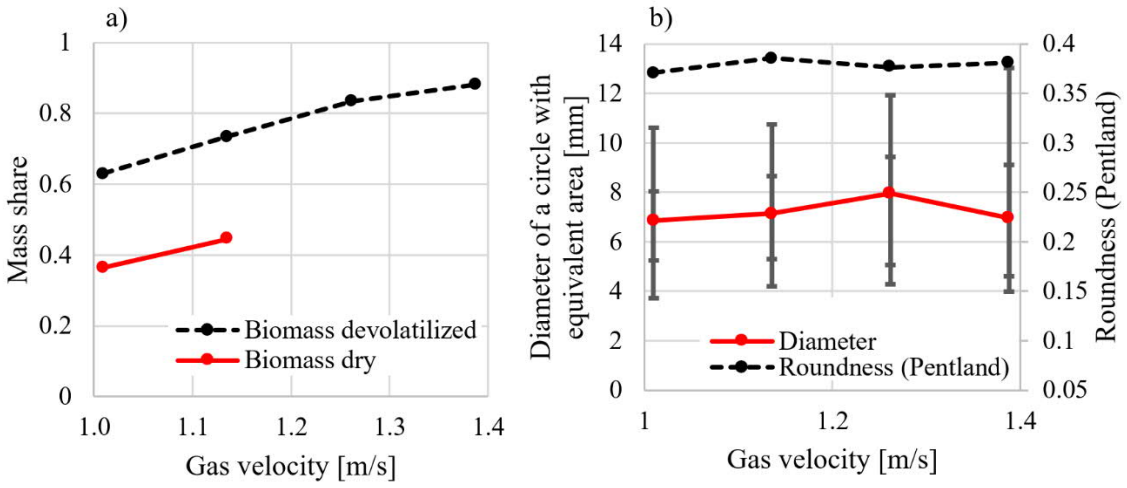

Figure 31. *Cumulative terminal velocity distribution of two fuels with bed material a) and size and shape of devolatilized biomass particles as a function of elutriation velocity with bed material b).*

Similarly, as with A.R. biomass from the tests without the bed material, image analysis was done for the particles elutriated from the riser with the bed material. Figure 31b illustrates results from the image analysis. Similarly, as in Figure 29: 10th, 25th, 75th and 90th percentile is plotted with the average value of diameter of a circle with equivalent area than the analysed particles. Results indicate that there was no major difference in average elutriated particle size during different gas velocities. Similarly, the average roundness of elutriated particles is similar through the tests. Figure 33 illustrates particles that were elutriated at 2 different velocities. Visually it can be observed that there are larger particles with 1.26 m/s velocity than with 1.01 m/s velocity. However, with the 1.26 m/s velocity there are also significantly smaller elutriated particles than the maximum particle size was with the smaller velocity. It is probable that the larger particles with small velocities were elutriated at moments of high solids concentration.

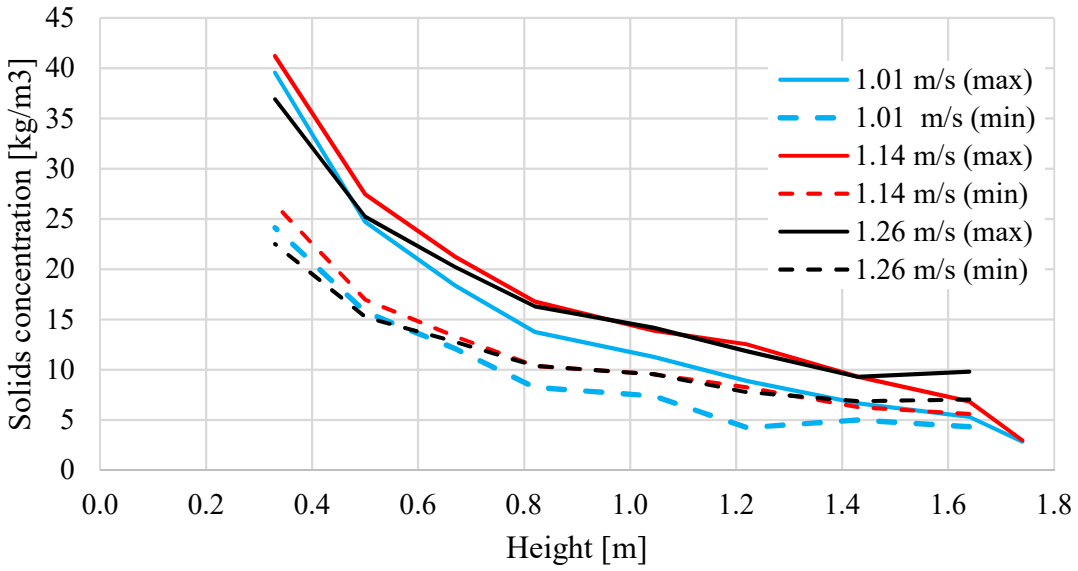

Figure 32. *Minimum and maximum solids concentration from 3 different gas velocities.*

Figure 31b illustrates the averaged roundness of elutriated devolatilized biomass particles. When compared to Figure 29 it is clear that the average roundness is not increased through devolatilization. It was stated in Chapter 2.3 that biomass particles become more spherical through devolatilization. This difference between previous results and results of this thesis are explained mostly with low heating rate used in devolatilization of fuel particles. When biomass particles are heated slowly volatile gases are able to flow from the particle freely due to natural porosity of biomass particles. Thus, major deformation is not achieved. However, biomass had some shrinkage during devolatilization. It can be argued that measurement results might change if higher heating rate would have been used. It should also be noted that with large particles temperature rise in CFB boiler is not as rapid as for small particles. Thus, larger particles may not experience as much deformation in CFB boiler as smaller particles. One future research possibility is to focus on more realistic heating rate compared to heating rate in CFB boiler and study effect of

deformation on drag coefficient and terminal velocity of particles with and without bed material.

Some attrition was observed during tests. Transparent bed material turned significantly darker due to attrition. Thus, all of the devolatilized fuel was not possible to be collected after the cyclone since the particles from attrition were smaller than the sieve size. Thus, it can be stated that even higher amount of devolatilized biomass could be elutriated from the riser than what Figure 31a indicates.

It was noticed that with small solids concentrations near the cyclone exit the fuel entrainment was small. Thus, it obvious that higher the solids concentration higher the momentum transfer from inert bed material to the fuel. Visually it was also observed that fuel particles bounced above the bed even though they were not elutriated to the higher parts of the test riser. Compared to tests without bed material where fuel particles were elutriated relatively fast when gas velocity was increased, in tests with bed material fuel particles needed more time to be elutriated. Variating amount of bed material affected the amount of fuel elutriated but it was also clear that all of the fuel particles which can be elutriated at certain velocity and certain solids concentration were not collected by the sieve under the cyclone immediately. Not all of the particles which end up in the top of the riser enter cyclone and not all fuel particles can flow immediately out of the denser suspension when air flow is increased.

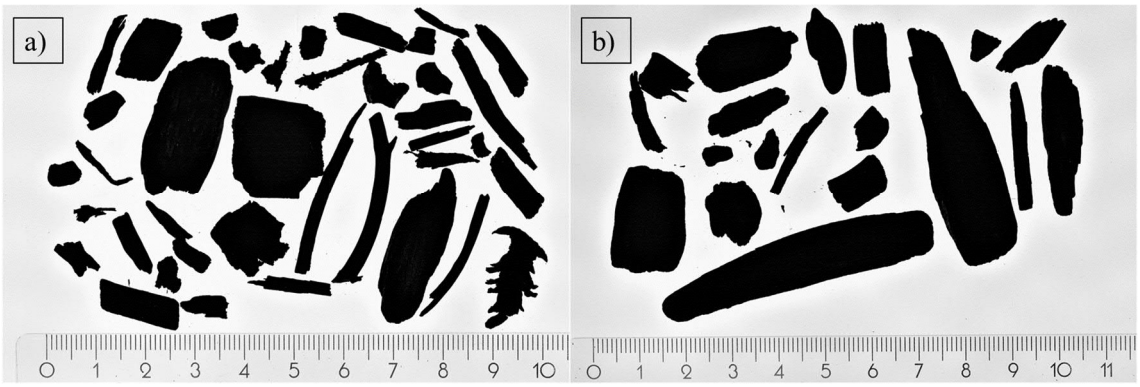

Figure 33. *Devolatilized biomass particles elutriated at velocities of a) 1.01 m/s and b) 1.26 m/s.*

Height and width of the test riser was small compared to CFB boilers, so it can be argued that exploding bubbles had significant impact on the test results and local gas velocities exceeded the average gas velocity significantly. Thus, there are some uncertainties in estimating the real gas velocity in which particles were elutriated. However industrial scale CFB boiler also has inhomogeneous flow field and thus the averaged results offer reasonably accurate comparison with different situations. Tests did not provide information about fuel concentration on different heights of the riser, but they provided information that char particles can flow lot above the bottom bed even if the average gas velocity is

smaller than the terminal velocity of the particles. Thus, it can be stated that char combustion can occur at regions of relatively low solids concentrations compared to bottom bed even though terminal velocity of fuel particles is much higher than the average gas velocity.

During measurements, values for solids concentration were relatively high when compared to values in boiler at transport zone. Solids concentration at cyclone height was in some runs 10 kg/m^3 while in large-scale measurements the highest measured suspension density value was 8 kg/m^3 at 8 m height. Thus, the measurement data does not provide reliable data on fuel elutriation at low solid concentrations.

Based on measurement results it can be stated that bed material has major effect on the axial fuel mixing in the CFB boiler at least at lower parts of the boiler where solids concentration has greater values. Thus, it can be stated that the axial fuel mixing has different behaviour compared to the axial fuel mixing model presented in Chapter 4.2. Fuel particles are not trapped in the bottom bed and splash zone until there terminal velocity is low enough to reach the cyclone entrance without momentum transfer from bed material. They may fly above the splash zone due to momentum transfer from the bed material even though gas velocity is much smaller than their terminal velocity. When solids concentration decreases higher in the boiler the influence of momentum transfer from bed material decreases and fuel entrainment depends more on the fuel particle properties.

6.2.3 Analysis of the terminal velocity and drag coefficient models

Results from the terminal velocity measurements without bed material and image analysis were compared to the terminal velocity model by Haider & Levenspiel (1989) which is presented in equations (8)–(10). Same model is also used in the comprehensive CFB model. Terminal velocity of a certain batch was assumed to be the average of that specific velocity measurement gap since there was also data from average size of elutriated fuel particles. Results are presented in Figure 34. Figure presents the measured terminal velocity as a function of diameter of a circle with equivalent area as the particle. There are also plus and minus 10 percent values for measurements presented with grey lines. Dotted black line indicates the terminal velocity from the model while diameter of a circle with equivalent projected area as particle is used in model. Solid black line indicates the results from the model while length of major axis is used as a diameter in the model. Green line indicates the Cox circularity values for certain size batch. Results indicate that model gives reasonably accurate results when the length of the major axis is used as particle diameter in the model. All of the results for A.R. biomass are within 10% margin lines.

Drag coefficient of A.R. biomass batches were calculated as presented in Chapter 5.6. Results for the drag coefficient are presented in Figure 35. Figure also illustrates drag coefficients of a sphere and a non-spherical particle according to different models. Value

of sphericity used in the models is 0.5. Results indicate that drag coefficient of used biomass is relatively constant in calculation area. Maximum and minimum values being 2.4 and 1.5 respectively. Results are in line with drag models for non-spherical particles since the models also predict relatively even drag coefficient at the specific values of Reynolds number. However, all of the drag coefficient models predict drag coefficient to be higher than the ones from Nikku et al. (2014) method. Nikku et al. (2014) concluded that method described by them cannot be considered as absolutely accurate. This same conclusion can be said for the drag coefficients calculated here based on accuracy of the measurement methods and differences to the drag coefficients from the different drag coefficient models. They can be thought more of as a basis when estimating a drag coefficient of a fuel particle. If drag coefficient of fuel particles is considered as interesting value and results from this thesis need to be validated in the future, a simple way to estimate drag coefficient of a single particle could be performed by measuring the terminal velocity and projected area of particle as presented in this thesis. In addition, mass of particle should be measured and then drag coefficient of a single particle could be calculated with equation (5). This method assumes that fuel particle would drop with its largest projection normal to the flow. This can be used as a rough approximation of the situation based on theory presented in Chapter 3.2 even though Reynolds number indicates that there might occur significant secondary motion.

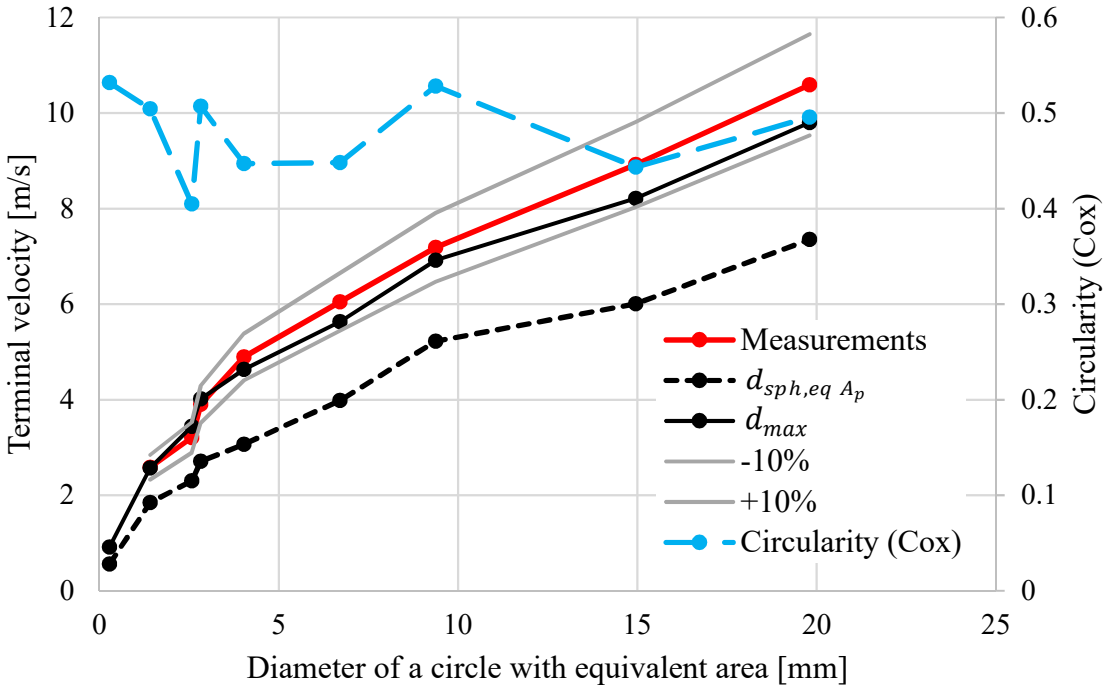

Figure 34. *Comparison of terminal velocity from measurements and model by Haider & Levenspiel (1989) with two different particle diameters. Particle circularity is presented with the blue line and 10% difference to measurements with grey lines.*

Terminal velocity of a particle varies depending on gas properties. For small particles (in order of 100 microns) terminal velocity decreases when temperature is increased. This is

due to increase in gas viscosity. When particle size is increased the inertial forces become dominant over viscous forces which leads to increase in terminal velocity due to decrease in gas density (Yates 1996, Nikku 2015). Terminal velocity of A.R. biomass from measurements without bed material was adjusted to hot conditions (850 °C) according to methods presented in Chapter 5.6. Results are presented in Figure 36. Results show that all models excluding equation (35) estimate the terminal velocity to increase from cold conditions to hot conditions by a factor of 1.7–2.0 depending on particle size and used drag model. Equation (35) estimates the terminal velocity in hot conditions to be significantly larger than other models. Model uses drag coefficient by Schiller & Naumann (1935) (equation 32) which is not suitable for non-spherical particles on relatively wide Reynolds number scale. Thus, the drag coefficient decreases significantly between Reynolds number values of 100–10 000 while in other models drag coefficient remains relatively constant in that gap as presented in Figure 35. Thus, the relation between terminal velocities does not remain constant but changes from 1.7 to 2.3. Based on drag models for non-spherical particles and results from Nikku et al. (2014) method the drag coefficient remains relatively constant in particular range of Reynolds numbers. Thus, results from other models than equation (35) can be stated to be more accurate in predicting the terminal velocity in hot conditions.

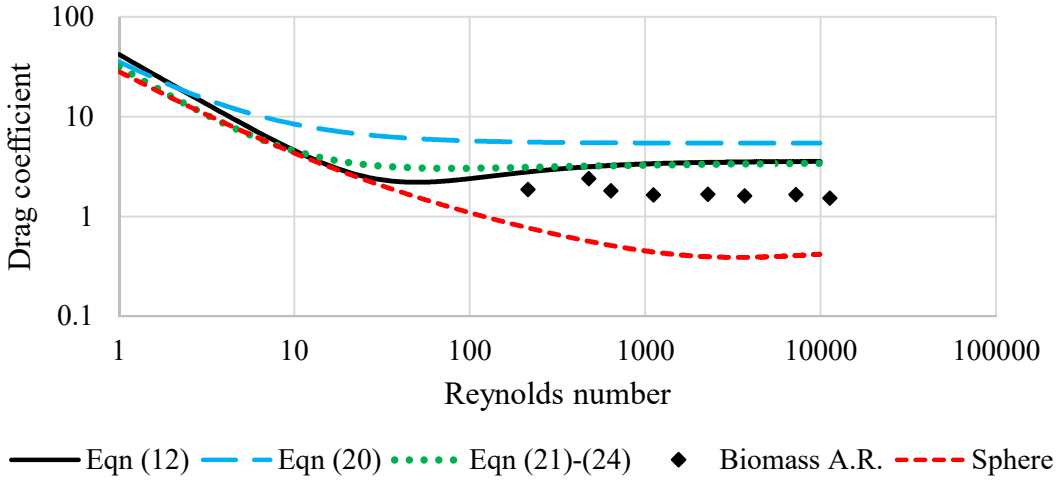

Figure 35. *Drag coefficient of as received biomass and drag coefficient curves for non-spherical particles with sphericity value of 0.5 with different models. Red line indicates drag coefficient of a sphere.*

Terminal velocity of the devolatilized biomass particles with then bed material was also examined with the Palchonok et al. (1997) model presented in equations (26)–(27). Results are rough since the solids concentration varied during tests and there was no information about the mass of the particles. However, results give similar indications as the results from Soriano Sánchez (2019). The model predicts higher terminal velocity for the fuel particles with the bed material than was measured. These results can be explained by false inputs to the model or with the assumption that model gives too high values for effective terminal velocity or with the assumption that flow field inside the test riser was

inhomogeneous and thus particles were elutriated with higher velocity than the average velocity indicates. The truth is probably combination of all of these 3 aspects. Therefore, accurate statements about the accuracy of the Palchonok et al. (1997) model cannot be made based on results from this thesis. However, it can be stated that the Palchonok et al. (1997) model predicts the terminal velocity of the particles in suspension much better than the Haider & Levenspiel (1989) model presented in equations (8)–(10).

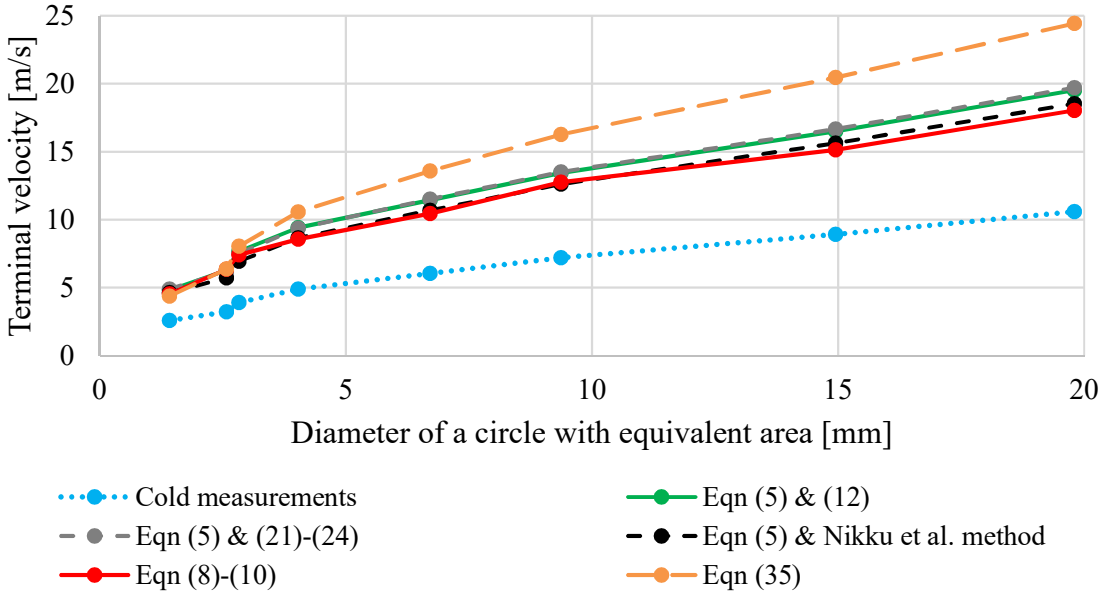

Figure 36. *Terminal velocity of as received biomass in cold measurements and hot conditions according to different models.*

Results indicate that in both biomass and coal there are fuel particles that can be elutriated to the upper parts of the boiler immediately after injection to the boiler even if terminal velocity of the particles is increased in hot conditions as presented above. However, even if terminal velocity indicates that fuel particles may be elutriated, this may not be the case in reality. Fuel is injected from the wall where small particles may fall directly to the bed with larger particles or due to down flowing solid particles in wall layer. Results for devolatilized fuels in Chapter 6.2.1. indicate that there can be relatively large share of char particles that are capable of being elutriated to the cyclone entrance height in the furnace, especially with biomass. Even if it would be estimated that terminal velocity of devolatilized particles in hot conditions is 2 times greater than the one measured in cold conditions there is still approximately one third of particles which could be elutriated without the momentum transfer from bed material with the biomass sample.

Due to differences in solids concentration it is not meaningful to try to make correlations for the momentum transfer from bed material to the fuel particles based on results in this thesis. However, there are only few models for momentum transfer in literature and they have not been validated extensively. Thus, terminal velocity measurements with and without bed material could be used in validating old models or developing new models

for momentum transfer to the fuel particles from bed material. This could be a possible research topic related to axial fuel mixing in fluidized beds in the future.

6.3 Results of identifying the most impactful variables in fuel mixing model

6.3.1 Time step evaluation

Sensitivity analysis was performed to get information about the importance of different variables which affect fuel mixing. Before actual sensitivity analysis an evaluation of the length of time steps was executed for the fuel conversion and fuel mixing model. Length of time step in fuel conversion model affects how long is the time step between points when for example fuel particle size, density and thus terminal velocity is evaluated. The less frequently this is evaluated the larger the steps are between different conversion stages. Length of time step in fuel mixing model affects how long is the time step in calculating 1 fuel size class as presented in Chapter 4.2.

Time steps of fuel conversion and fuel mixing models are not totally separated and thus their influence on convergence should be studied together. Thus, benchmark result was calculated with default values and then results for fuel concentration, temperature profile and release profiles were compared to benchmark result. Originally time step for fuel conversion model was 0.1 s and time steps in fuel mixing model were divided to 2 parts. Mixing during first second of conversion was calculated every 0.02 seconds while after first second time step increased directly to 5 s. Length of time steps was shortened for both fuel conversion and fuel mixing models. For fuel mixing model time steps were at first shortened only from the end so that original 5 s time span shortened until time steps were equal throughout calculation. After this time steps were shortened so that the length remained equal through calculation. For fuel conversion model the length of time step was shortened every time by a tenfold. Table 9 presents time steps used in the fuel mixing model.

Table 9. *Used timesteps for fuel mixing model.*

Number	Length of time steps during 1st second [s]	Length of time steps after 1st second [s]	Number	Length of time steps during 1st second [s]	Length of time steps after 1st second [s]
1	0.02	5	7	0.01	0.01
2	0.02	3	8	0.005	0.005
3	0.02	1	9	0.001	0.001
4	0.02	0.2	10	0.0005	0.0005
5	0.02	0.05	11	0.0001	0.0001
6	0.02	0.02	12	0.00005	0.00005

Results for time step evaluation are shown in Figure 37 excluding moisture release which behaved similarly to volatiles release. Results are shown so that y-axis values show the ratio between the difference of concurrent value and benchmark result and maximum difference to benchmark result from all of the time step evaluations. Thus, the values on y-axis are not very interesting but the time step when the results seem to converge. Numbers on the x-axis indicate the time step used in the fuel mixing model as presented in Table 9. Different lines illustrate the different time steps for fuel conversion model.

Clear indication from the results is that convergence was not achieved with default values for time steps in fuel conversion and fuel mixing models. Regarding time steps in fuel mixing results seem to converge on different time steps depending on which output was considered. For fuel concentration results converge relatively early but for temperature clear convergence cannot be identified from these results. When considering the time steps in fuel conversion model it is clear that the default values do not result in same values as shorter time steps. Fuel concentration and release profiles start to remind each other's when time step is shortened to 10 ms but convergence of the results happens while time step equals 1 ms.

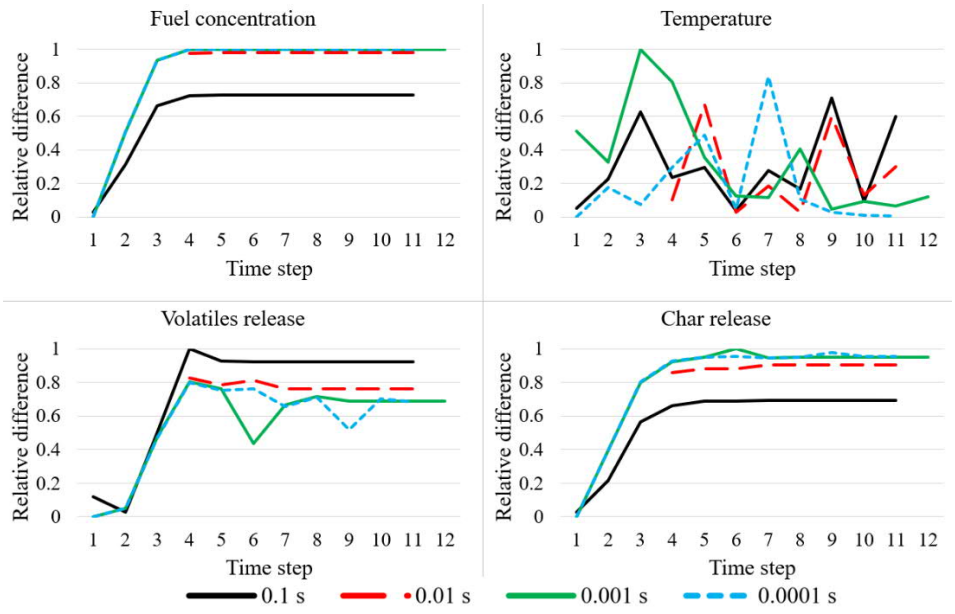

Figure 37. *Convergence of different values in time step evaluation. Different lines illustrate different time steps in the fuel conversion model.*

This time step evaluation was done by using 1 size class for fuel. Fuel was bio based and had small particle size on average. Thus, burnout time of particles was relatively small. Thus, even very small time steps did not increase calculation time dramatically. However, for 2 smallest fuel mixing time steps used the calculation time of combustion and heat transfer model started to increase significantly. When time step of 0.001 s was used for fuel conversion model, the ratio between shortest (0.05/0.05 ms) and the third shortest (0.5/0.5 ms) time steps in fuel mixing model for calculation time of combustion and heat transfer model was 18 while for longer time steps calculation time remained relatively

constant. Thus, it can be assumed that the calculation times for multiple size classes in fuel would increase significantly if shortest time steps were used in addition to 3D model. Thus, time steps of 1 ms for fuel conversion and 0.5 ms for fuel mixing were chosen for partial sensitivity analysis. The non-convergence of temperature may be because of iterative nature of heat transfer model calculation. The results are iterated until they reach certain values and thus there may be small variations between temperature values. Convergence criteria for heat transfer model was kept constant during time step evaluation. However, the differences in temperature profiles were not major during time step evaluation so the relevance of non-convergence can be assumed relatively small since the results are starting to remain relatively constant for very small time steps.

If fuel conversion model uses longer time steps than fuel mixing model the values for fuel mixing model are interpolated from the data of the fuel conversion model. On default, the model uses cubic spline interpolation. However, this was noticed to result in negative or large values in some cases if data had big differences between contiguous cells. Thus, this sensitivity analysis uses linear interpolation in selected parameters since the length of time steps is very small and thus does not lead to major errors. However, it should be noted that the difference in values for large and small time steps could decrease if cubic spline interpolation would be used.

In this time step evaluation, the size of step between different time steps was quite coarse. Thus, it should be stated that these time steps are not probably optimal but rather close enough when considering the convergence of the results. More research could be done to find optimal time steps in relation to result accuracy and calculation capacity. For example, the optimal time step allocation could consist of more than just 2 different time steps lengths. In addition, it should be noted that different fuels have different combustion times and thus longer time steps could be used for example for coal or for larger particles. Thus, main indication from the time step analysis is that different fuels need different lengths of time steps in fuel conversion and fuel mixing modelling.

6.3.2 Partial sensitivity analysis for fuel mixing model

In partial sensitivity analysis values of K, a, $c2d$ and u_t were multiplied by values from 0.01 to 100. As a default value K had formulation which has not been published. Thus, benchmark result is calculated with that formulation and this benchmark result is also compared to K which is defined according to equation (3). Results for original formulation of K are presented in Figure 38 excluding moisture release which resembled results from volatiles release. Similarly, as in time step evaluation, results are shown so that y-axis values show the ratio between the difference of concurrent value and benchmark result and maximum difference to benchmark result. Thus, the bigger the value on y-axis the bigger the difference to benchmark results and thus the bigger the influence to result of that specific output.

Results show that the terminal velocity of the fuel particles was relatively small already at the benchmark result since the results do not change a lot after u_t is multiplied by values under 1. However, while coefficient for u_t is greater than 1 difference between new results and benchmark result grows fast regarding fuel concentration and release profiles. However, these large differences in fuel concentration and release profiles do not result in large differences in temperature profile. This is partly since when terminal velocity is increased the moisture and volatiles are released at the bottom bed, but char conversion happens mostly after couple of meters of height. This could be since the combustion is staged with air feeding. Thus, all of the energy cannot be released in the bottom bed and thus part of the conversion must happen above secondary air injections. Clear indication from the Figure 38 is that K and $c2d$ are the most influential parameters to the temperature distribution in this analysis. With the manipulation of K the maximum temperature was achieved near secondary air injections or at the top of the furnace. These peak values were achieved with very large and very small values of K respectively. Thus, it can be stated that variable K has very big influence on the shape of the temperature profile.

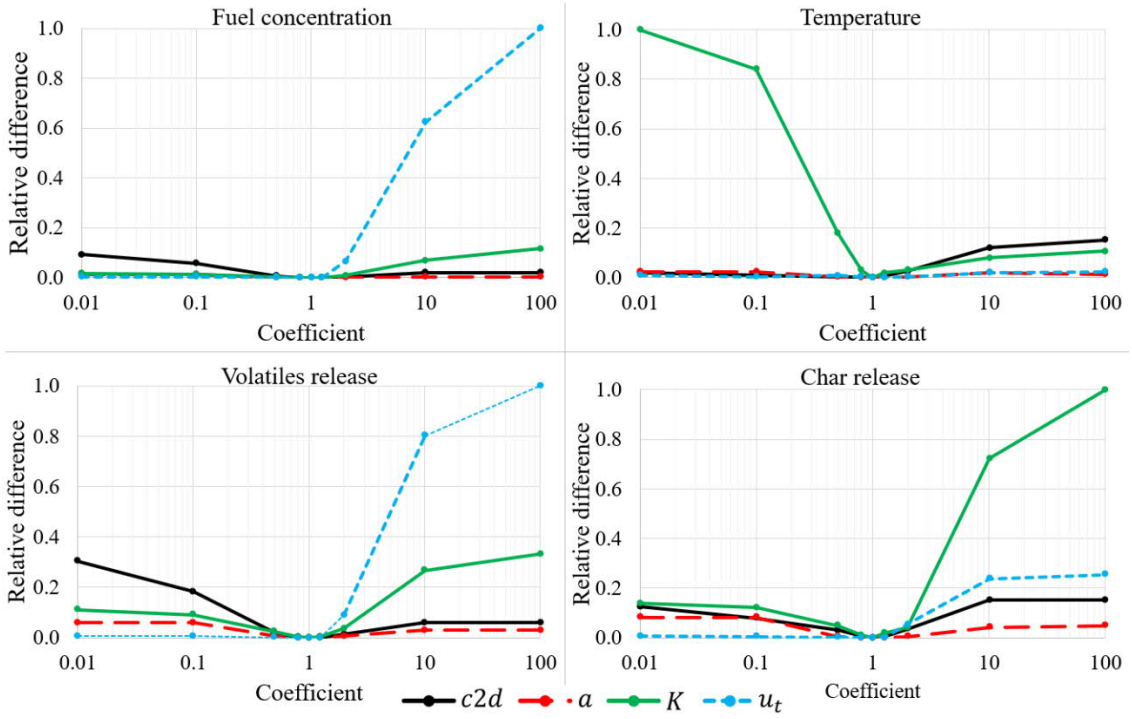

Figure 38. *Difference of fuel concentration, temperature profile, volatiles release and char release to benchmark result with the default formulation of K.*

Variable $c2d$ had also big influence on the temperature profile but the differences in profile shapes were not so dramatical as with manipulation of K. In all cases maximum temperature was reached at similar heights but there were differences in the value of maximum temperature and the gradient of the temperature rise in different heights of the boiler. Variable a influences the ballistic decay of particles in the lower zone of the furnace. Thus, the manipulation of a influences the temperature profile mostly in the lower part

of the boiler. Thus, the temperature gradient is greater in the bottom part when a has small values and vice versa.

Figure 39 illustrates the same sensitivity analysis results while K was defined as in equation (3). Notice that the results are compared to the original result of the model. Similarly, as with the original formulation of K the increase of u_t has significant impact on the fuel concentration and release profiles. However, the differences in temperature profile are small when terminal velocity is multiplied by a large number. Significant differences to temperature profiles come when coefficient for u_t is smaller than 2. When equation (3) is used for K, terminal velocity of the particle affects also the values of K. Thus, the shape of temperature profile is affected more in this scenario when values of u_t are changed. Temperature gradient in the lower parts of the boiler is smaller when u_t is smaller since K gets smaller values and thus more fuel is concentrated to the upper parts of the furnace which leads to more heat release at the upper parts.

Similarly, as with the original formulation of K, equation (3) causes large variations to temperature profile with different coefficients. Largest and smallest difference to temperature profile is achieved by manipulating values of K. While coefficient is smaller than 1, highest temperature is achieved near the top of the boiler. When coefficient for K is 10 or 100 highest value is reached near secondary air injections. Thus, the temperature gradient is steep at the bottom part of the furnace.

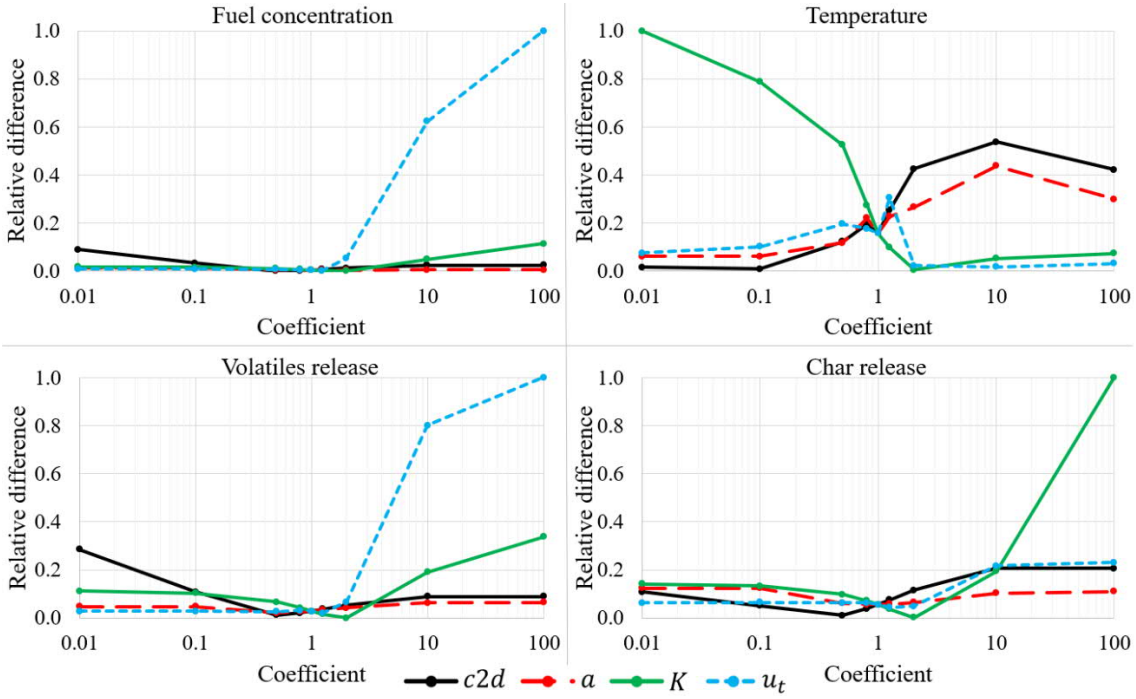

Figure 39. *Difference of fuel concentration, temperature profile, volatiles release and char release to benchmark result when K is defined as in equation (3).*

When K is calculated through equation (3) variable $c2d$ has lot greater influence on temperature profile. While coefficient for $c2d$ gets small values the temperature profile does

not vary a great deal from the benchmark result. However, when coefficient in $c2d$ calculation gets large values and thus more particles behave according to transport zone decay the temperature profile changes a lot towards profiles in which K gets small values. Also, variable a has lot more importance on the temperature profile when K is defined according to equation (3). With small coefficients profiles remind each other's but with great coefficients the profile becomes again relatively smoothly ascending.

Overall it can be stated that when using the default formulation of K the temperature profile is much more dependent on K and $c2d$ than terminal velocity. Based on this result it could be argued that it is questionable how much of a positive impact better knowledge of terminal velocity of particles has to the temperature profile modelling if other variables are not correct. However, when defining K based on equation (3) u_t has lot greater effect on the temperature profile since then it affects the values of K also. Thus, it can be stated that variable K has great influence on temperature profile since it affects the fuel mixing strongly in transport zone which consists a large part of the non-refractory lined area of the boiler. However, depending on the case and formulation of different variables the fuel mixing is not dominated only by 1 variable in the model. Thus, this kind of a partial sensitivity analysis does not offer perfect answers since it does not show the dependence of variables on other variables. It can however be stated, that it offers reasonable answers to the influence of different variables on fuel mixing.

After sensitivity analysis was completed temperature profile was fitted to measurement results based on observations from the sensitivity analysis. Since sensitivity analysis was performed with the 1.5D model these found coefficients were used for the same case in 3D model to see if the changes in temperature profile would be similar compared to default profile. Results were similar in 3D model and temperature profile resembled the one from measurements better with the new coefficients which were used in 1.5D model. Thus, based on this observation it can be stated that results from sensitivity analysis in 1.5D model are applicable also to 3D model at least in some extent.

6.4 Modelling

As a starting point a benchmark results were calculated for both validation cases obtained during this thesis. Temperature profiles for these benchmark results are presented in Figure 41 and Figure 42 with new modelled results. It was noticed that in the benchmark results fuel concentration was very low at the upper parts of the boiler compared to the bottom bed values. This could be expected also in real life since inert solids concentration at the transport zone can be less than 1% from that of dense bed. However, this low fuel concentration at the upper parts of the boiler lead to a relatively even temperature distribution opposite to rising temperature profile from measurements. Thus, larger share of the combustion process must occur in the upper parts of the furnace than model predicts. There are two ways to increase the share of combustion in the upper parts of the furnace:

increase fuel concentration in the upper parts of the boiler or modify the model so that more volatile combustion occurs higher in the boiler. As presented in Chapter 4.2. the fuel mixing model predicts entrainability based on terminal velocity of a single particle without noticing the effects of bed material. However, terminal velocity measurements with bed material proved that bed material has great effect on fuel entrainability. Thus, it can be stated that larger fuel particles than the model predicts, can be entrained above the splash zone. However, altering the calculation code to notice momentum transfer from the bed particles is beyond the scope of this thesis so alternate ways have been developed to better notice the effects of bed material.

Methods to increase fuel concentration in the upper parts of the boiler were to decrease terminal velocity of the fuel particles, change the definition of entrainability and alter the definition of other fuel mixing parameters. This way temperature profiles reached agreement with measurements. However, these solutions lack the basis from the physics and thus leads to some unrealistic results in different evaluation criteria. Methods presented above leads to a relatively even fuel concentration profile compared to the one from inert solids. Measurements in this thesis provided information about entrainability of the fuel particles and not about fuel concentration in the riser. However, it can be stated that it is very unlikely that fuel concentration would be significantly more even than the one from inert solids. In addition, methods presented above leads to relatively high amounts of moisture release in the upper parts of the boiler which seems unlikely since the fuel is injected in the refractory lined area. Thus, other methods were evaluated.

It was stated in Chapter 2.4. that according to la Nauze (1987, according to Nikku 2015) the difference in shape of axial temperature profiles for coal and biomass in CFB boiler resulted from different share of volatile gases in the fuels. Thus, volatile combustion was examined for these two different scenarios. It was found that in both benchmark results oxygen consumption for volatile combustion was concentrated heavily to the dense bed and secondary air injection heights. Even though lots of volatile combustion surely happens near the air injections it could be argued that gas mixing may not be as fast as model predicts. Thus, a limiter for the oxygen consumption was set to the volatile combustion model to limit oxygen usage. This clearly improved modelling efforts in comparison to the benchmark results. Even though volatile combustion was limited from the benchmark results the share of oxygen did not increase in the flue gas exiting the furnace. Thus, it can be stated that the limiter does limit the combustion in reasonable amounts when considering the furnace as a whole.

Based on results presented above, the limiting of gas mixing in computational cells for volatile combustion was chosen as a basis for the new method in calculating fuel mixing and combustion. In addition to just altering the gas combustion also fuel mixing was decided to change based on measurement results. It was decided to change the value of coefficient X in equation (29) to a large value so that all of the entrainable particles would behave according to dispersive decay. Even if this does not fulfil physics completely it

does increase the fuel concentration in the upper parts of the boiler from the benchmark results which is likely to be the case in reality. In addition, this way one experimental coefficient can be eliminated from the fuel mixing model. Regarding other fuel mixing parameters, the temperature profile was found to correlate best when transport zone decay constant K was formulated similarly as it is for bulk solids in equation (3). Splash zone decay constant a was kept at its original formulation with particle terminal velocity model. Sphericity values used for fuels in coal case and biomass case were 0.75 and 0.5 respectively.

Method presented above was validated by using one or six different fuel size classes in the model. If one size class was used the size was evaluated based on d_{50} size from sieving results. Particle size distribution for both fuels was also determined based on sieving results. These two methods did produce similar results for temperature profiles especially when regarding the shape of temperature profile. Thus, it can be stated that if fast calculation results are needed then only one size class can be utilized. However, results for temperature profiles were depended on fuel size input. Thus, it is important to have accurate knowledge on fuel PSD while modelling temperature profiles. For example if fuel PSD was calculated based on terminal velocity measurements and equations (8)–(10) average dimeter of fuel particles was significantly larger than in sieving results. Thus, the bottom bed temperature was higher than with smaller fuel particles.

Even though differences in temperature profiles were small with and without PSD for coal, fuel concentrations had significant differences. When PSD was used the amount of fuel in dense bed was significantly higher since the larger particles have longer burnout times and thus greater amount of fuel accumulates to the dense bed. However, the difference in fuel concentration was not that significant anymore in the transport zone even though the case without PSD for fuel had higher fuel concentration in the transport zone. For biomass-coal mixture, the fuel concentrations were similar with and without PSD. However, the effect was similar to coal since dense bed had more fuel with PSD and less fuel in the transport zone. It should be noted that the coal fragmentation was not noticed in the calculations. As presented in Chapter 2.3, larger particles are more prone to fragmentation and thus the model may produce too great fuel concentrations for the coal in the dense bed if fuel PSD is used and fragmentation is not noticed.

Terminal velocity behaviour of the fuel particles during conversion process was examined in the model. Both fuels were divided into 6 different size classes based on terminal velocity measurements for A.R. samples. After this an average terminal velocity was determined for each batch and diameter for average fuel particle in that batch was determined from equations (8)–(10). These diameters were then used as an input for fuel size in the model. Based on terminal velocity measurements without bed material, terminal velocity for devolatilized samples was determined by evaluating the terminal velocity of the devolatilized sample with same cumulative mass share as the A.R. sample. Terminal velocity of fuel particles in the model during conversion process was then plotted as a function

of time. These curves were compared to relating terminal velocities of devolatilized samples and these results are presented in Figure 40. Three different size classes are presented for both coal and biomass. If devolatilization is assumed to end for coal when the gradient of terminal velocity sharply changes, it can be stated that the terminal velocity of a char is in relatively good agreement with the measurements. Moisture release and devolatilization are thought as rapid process in CFB boiler. Thus, terminal velocity of a fuel particle should reach the terminal velocity of a devolatilized particle from measurements in short time compared to overall burnout time. This does not seem to be the case for biomass particles since the terminal velocity of a particle reaches the one from measurements near the burnout time. In the Figure 27 the A.R. sample with same mass share as devolatilized sample had around twice the terminal velocity of a devolatilized sample. As stated in earlier chapter the deformation of biomass particles during devolatilization in measurements may not have been completely realistic compared to one in CFB boiler. However, based on measurements done during this thesis it can be stated that the fuel deformation and thus terminal velocity behaviour during combustion for the biomass may not be completely realistic in the comprehensive model. However, to get more validation for this statement more experiments should be done with fuel particles that have been devolatilized with high heating rate. It can be estimated that this slow drop in terminal velocity for biomass compared to measurements can lead to a hotter bottom bed in the model if larger biomass particles are used. If particles are not elutriated from the bottom bed they will combust in the bottom bed and thus release their energy there. There was more difference between modelled temperature profiles with biomass-coal mixture when using and not using a PSD for fuel, than there was for coal case. This terminal velocity behaviour of fuel particles in the model during conversion may have been at least partly the reason but since the combustion model of the particle is outside the scope of this thesis it was not examined more.

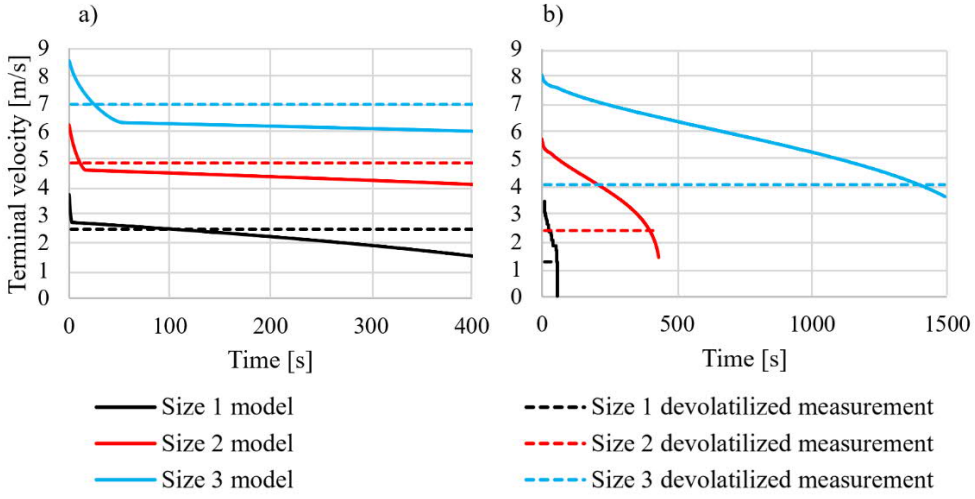

Figure 40. *Terminal velocities of different sizes of coal (a) and biomass (b) in the model during conversion. Dashed line indicates the terminal velocity of devolatilized sample from measurements. Dashed line had approximately the same terminal velocity before devolatilization than the modelled particle when time is zero.*

Results for modelled temperature profiles in the core of the boiler are presented in Figure 41 and Figure 42. Results are achieved with the method presented above which is based on height dependent volatile combustion limiter. Figures also illustrates the benchmark results and the results achieved by using the default setups for the fuel mixing model and the new limiter for volatile combustion. Following results are presented when one fuel size is used in the modelling. Time step for fuel conversion and fuel mixing were kept at default values since the results did not vary significantly when time steps were shortened. Difference to the results in Chapter 6.3 are probably caused by the much longer burnout times in these 2 validation cases which were caused by larger fuel particle size and different fuel. Improvement in modelling results with the new method from benchmark results is significant, especially at the lower part of the furnace. However, with the biomass-coal mixture bed temperature is higher than the measured one and cyclone outlet temperatures are in both cases lower than the one from measurements. The higher bed temperature for biomass case may be because of higher dense bed which increases the volatile combustion in the dense bed. Since the limiter is dependent on the meshing and dense bed uses the most accurate meshing, the biomass case may consume more volatiles in the lower part of the boiler and thus the bottom area may be hotter than in measurements. This phenomenon can be seen also in Figure 44 where oxygen concentration after the dense bed is smaller in biomass-coal case compared to coal case. Figure 41 and Figure 42 illustrate how the most significant improvement in the temperature profile modelling comes from the limiter for volatile combustion. In the coal case the new method produces significantly lower bottom bed temperature than just the usage of volatile combustion limiter. However, for the biomass-coal case the difference is almost negligible. This is because of larger particle size which causes fuel entrainment to be smaller for biomass. Thus, much larger share of a fuel particle combusts in the bottom bed as argued earlier.

With the new calculation method, fuel concentration increased in the upper parts of the boiler. Figure 43 illustrates fuel concentration for both validation cases with the new method and the default method. While the new method produces constantly greater fuel concentration for coal above the dense bed (Figure 43a) the biggest difference for biomass-coal mixture (Figure 43b) is in the transport zone. Fuel concentration in the dense bed for the biomass-coal case is similar with the new method and the default method. This is because of the long combustion time of the biomass particle before it becomes entrainable. In the sensitivity analysis it was shown that manipulating values of K and $c2d$ resulted in differences in fuel concentration. Thus, new method produces more even fuel concentration profile compared to the benchmark results. This increased fuel concentration in the upper parts of the boiler also resulted to the higher temperature difference between dense bed and maximum temperature compared to the benchmark values. In the Figure 43 coal has higher fuel concentration in the transport zone than the biomass-coal mixture. This can be explained with a longer burnout time of the coal particles which leads to a higher amounts of fuel particles in the riser. In addition, the average coal particle was also entrainable sooner than the average biomass particle. Based on terminal velocity

measurements, average devolatilized biomass particle has significantly smaller terminal velocity than average devolatilized coal particle. If devolatilization is assumed to happen rapidly in CFB boiler, the biomass particle should not be entrainable significantly later than the coal particle as presented earlier. However, there is not a lot of research on axial fuel concentration in CFB riser. Thus, these fuel concentration values presented here cannot be validated with measurement results at the moment. Measurements relating to fuel concentration are recommended for example with tracer particles in laboratory-scale CFB riser to obtain more knowledge on fuel concentration in CFB riser with varying particle shapes and sizes.

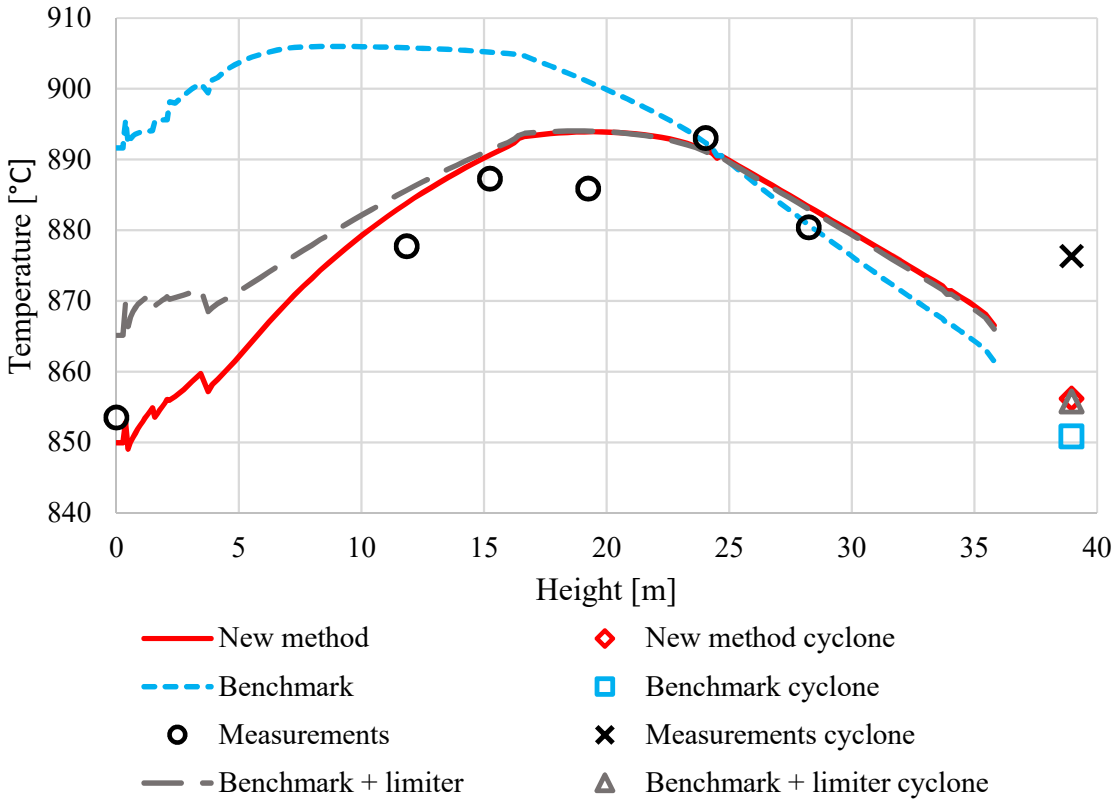

Figure 41. *Modelled and measured temperature profiles with coal as fuel.*

Since volatile combustion was limited in the new method, oxygen concentration increases in the lower parts of the furnace. Figure 44 illustrates oxygen concentrations for coal (a) and biomass-coal mixture (b). Oxygen concentration with the new method is significantly higher in the splash zone and lower parts of the transport zone compared to benchmark results. However, there are no measurements from the boiler to use in validation. Thus, other results for oxygen concentration and gas mixing are presented below.

Myöhänen (2011) published gas concentration measurements from a 15 MW_e CFB boiler. In those measurements, oxygen concentration increased in the centreline of the boiler from measurements below. This was explained by slow gas mixing between secondary air jets and main gas stream. De & Nag (2000) published oxygen concentration profile from their measurements in laboratory-scale riser. In those results it is shown that oxygen

decreases constantly through the height of a 5 m tall riser. Adánez et al. (2003) presented results for oxygen concentration in a 12 MW_{th} CFB boiler. Also, in there results the average oxygen concentration decreases as a function of the boiler height even at the transport zone. Wang et al. (1999), Tourunen et al. (2003) and Pallarès & Johnsson (2015) reported similar results from their measurements. In the benchmark results the oxygen concentration decreases as a function of the boiler height even in the transport zone, but the decrease is very small as can be seen in Figure 44. With the new method presented here the oxygen concentration decrease is lot more significant in the transport zone.

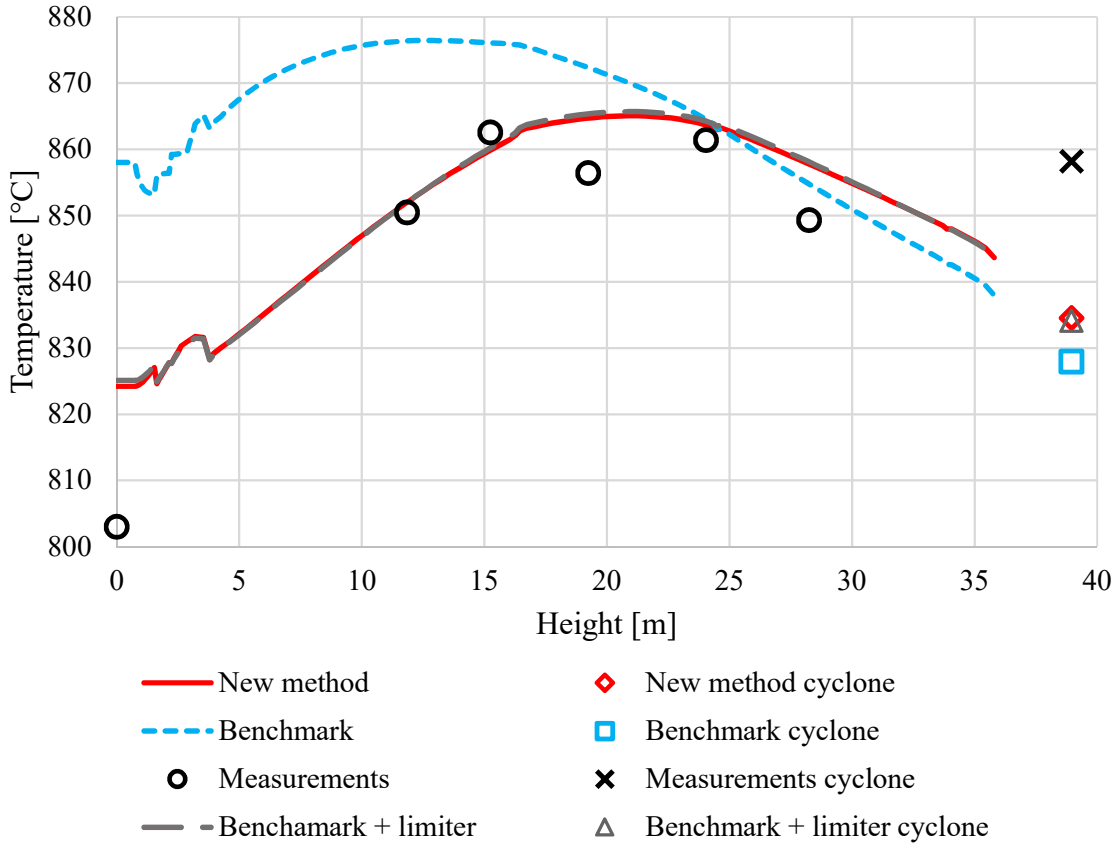

Figure 42. *Modelled and measured temperature profile with 80% biomass and 20% coal as fuel.*

Pallarès & Johnsson (2015) stated that assuming infinitely fast gas combustion kinetics is a valid assumption when modelling gas combustion in CFB furnace. Raiko (2002) stated that combustion temperature is usually so high that kinetics does not significantly reduce the speed of reaction. Thus, it can be assumed that gas mixing is the limiting factor in volatile combustion. Sternéus et al. (2000a) and Sternéus et al. (2002) studied the gas mixing in CFB boiler. They concluded that in their tests the maximum mixing level was found in the splash zone close to the surface of the dense bed. This was caused by large velocity fluctuations caused by eruption and collapse of bubbles. More focussed studies made for the bottom zone conditions were made in Wiesendorf et al. (1999) and Sternéus et al (2000b). They reported that while in 12 MW_{th} CFB boiler at Chalmers University of

Technology conditions varied between oxidising and reducing, in 600 MW_{th} pant-leg design CFB boiler conditions were strongly oxidising. This was explained by the fact that the measurement port in large-scale measurements was far away from the fuel injection ports. Thus, insufficient lateral fuel mixing occurred, and oxygen passed the bottom bed without being totally consumed.

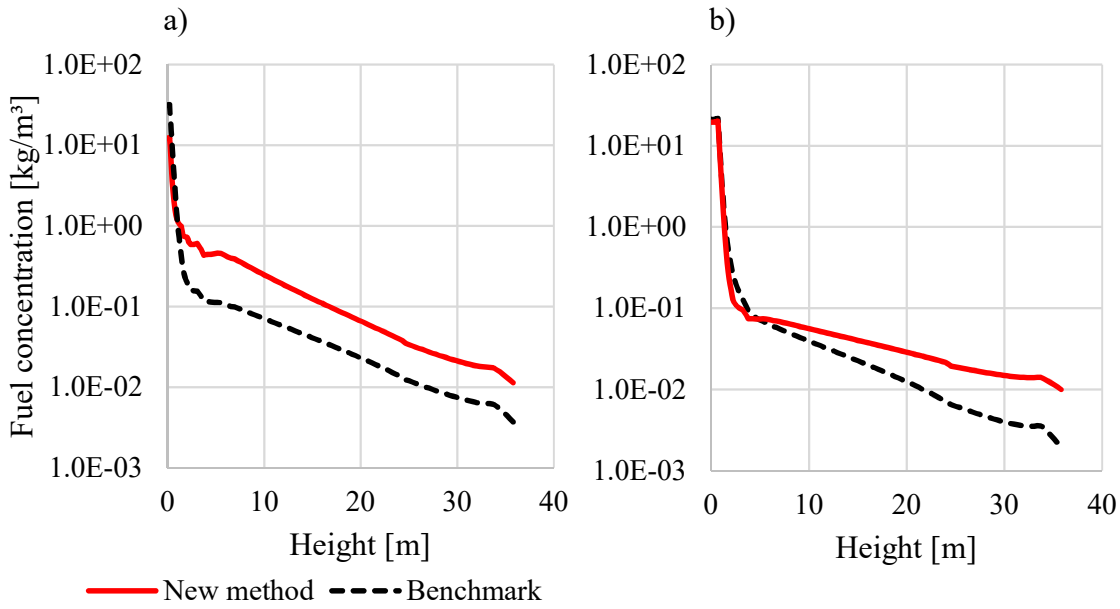

Figure 43. *Fuel concentration as a function of height for coal case (a) and biomass-coal mixture (b).*

Based on results presented above it can be argued that more oxygen in total can pass dense bed, as through flow or through an emulsion where fuel concentration is low, than it is presented in benchmark results in Figure 44. Thus, more of the volatile combustion could occur above the splash zone. Thus, limiting volatile combustion can be thought of as a valid method to improve modelling of temperature profile. However, arguments can also be made that volatiles are released lower in the model compared to real boiler because of approach used in the fuel mixing model. As stated earlier in this thesis, it is likely that major part of the fuel particles ends up in the dense bed after injection to the boiler. In addition, noticing the fast nature of devolatilization it can be argued that large share of the volatiles is released in the bottom part of the boiler. Thus, volatile release can be considered to be relatively accurate in the model. Considering gas mixing, the horizontal gas dispersion coefficient and gas species diffusion coefficient were changed to small values but this did not produce lower bottom bed temperatures. In addition, horizontal fuel dispersion coefficient was changed to a small value compared to original and this did not reduce the bottom bed temperature significantly. Thus, limiting volatile combustion can be thought of as a valid method to improve modelling of temperature profile. However, based on the measurements in this thesis it is not possible to say for sure if the real-life mechanism is because of gas or fuel mixing but it can be argued that the main cause is the gas mixing. However, results from literature are mostly from smaller boilers and

thus measurements should be done in large-scale boilers to validate conclusions of this thesis and to develop the gas combustion model further.

Horizontal temperature distributions were not the focus of this thesis and thus they were not examined thoroughly. However, it can be stated that horizontal temperature distributions were also in agreement with the measurements while using the new method. These distributions are presented in Figure 45 for height of 11.8 m with the measurement results. Especially with the biomass-coal mixture (Figure 45b) the results from modelling are in good agreement with the measurements. For coal case (Figure 45a) the horizontal temperature distribution is more even than the one from the measurements but still modelling results are within reasonable accuracy. Colder area in the middle of the core is due to cooling effect of the division wall.

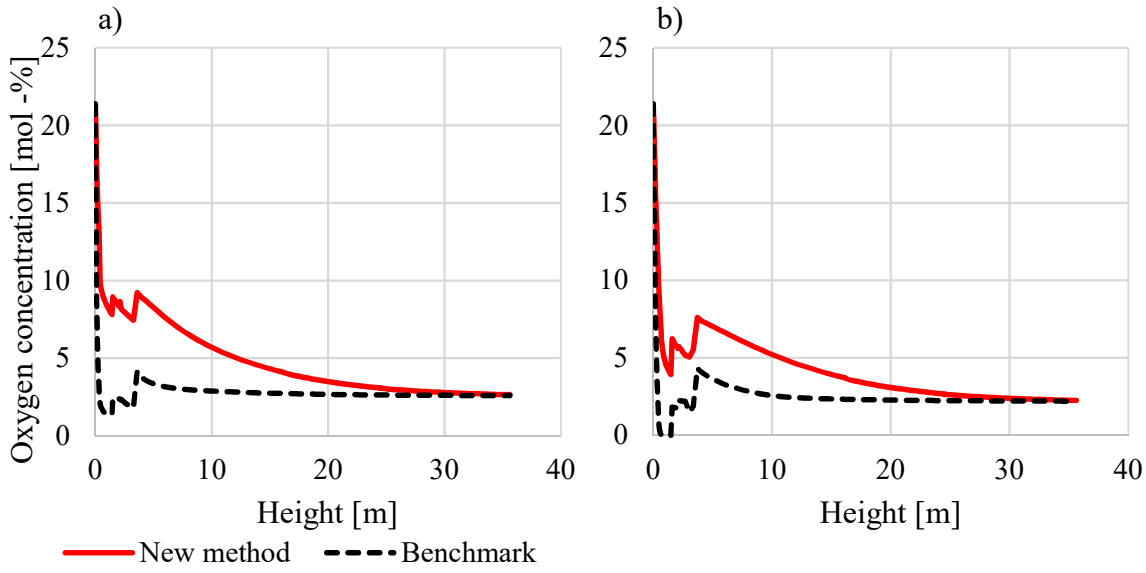

Figure 44. *Average oxygen concentration as function of height for coal case (a) and biomass-coal mixture (b).*

In addition to the two validation cases presented here this new calculation method was validated with one measurement case from coal boiler with small temperature rise in the boiler. These results corresponded well with the measurements. Thus, it can be stated that the new method can accurately model also situations with relatively even temperature profiles in the furnace. However, more validation should be done to confirm the findings of this thesis including experiments with varying loads. The method presented here is not a result of extensive optimization and thus should be considered more as an indication of pathways to improve the model still. Useful information for the modelling efforts related to topic of this thesis would be fuel concentration measurements in a CFB riser possibly with tracer particles, oxygen concentration measurements in a large-scale CFB furnace and terminal velocity behaviour of fuel particles during conversion.

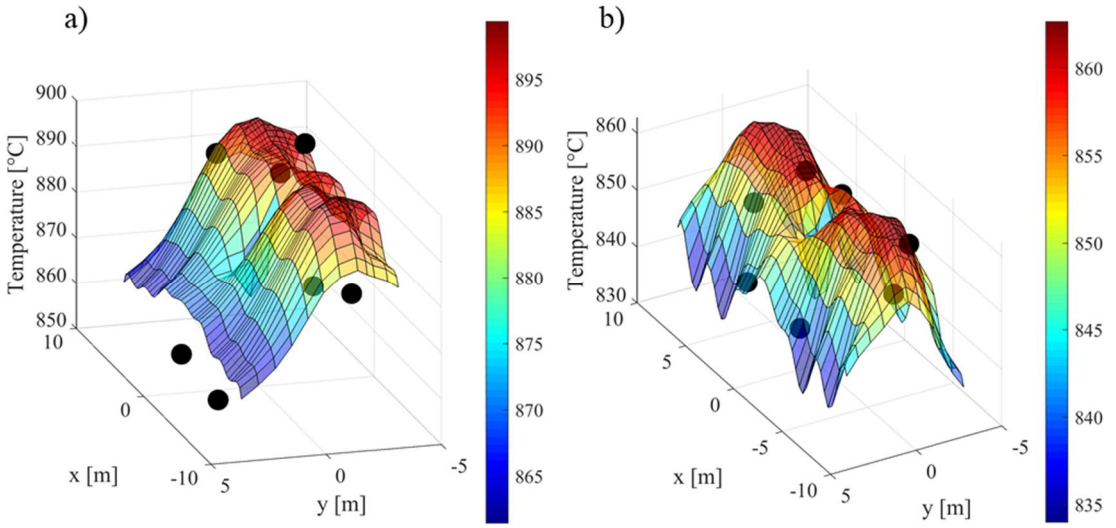

Figure 45. *Modelled and measured temperatures at 11.8 m height at the core region for coal (a) and biomass-coal mixture (b).*

The greatest improvement in modelling of temperature profile is due to limiter implemented to volatile combustion model. There was no method found for fuel mixing model which would alone improve significantly temperature profile modelling efforts and still have some physical basis since the calculation code was not modified to compensate for the effects of bed material. For more realistic fuel mixing model, the effects of the bed material should be noticed based on measurement results presented in this thesis. If this change in calculation method is implemented, a simplified momentum equation should also be considered instead of current method. Usage of momentum equation would probably increase calculation times and big change like this would possibly require changes to other sub-models also. Thus, this thesis does not recommend an implementation of momentum equation for the fuel mixing model but states that its usage should be considered in the future. Future best solutions could be to notice the effects of bed material to the axial fuel mixing with closer inspection of the gas mixing model. If the effects of the bed material would be noticed the volatiles release could increase in the upper parts of the boiler which could lead to a more realistic temperature profile without such a big limitation to the volatile combustion as is done in this thesis.

7. SUMMARY AND CONCLUSIONS

Accurate modelling of the CFB process can improve the design, performance, reliability and safety of a boiler. Thus, there is interest in accurate models of the boiler operation. The goal of this thesis was to analyse and improve the axial fuel mixing modelling in a comprehensive CFB model and through that improve the modelling of the average axial temperature profile. The secondary goals were to increase the knowledge on axial fuel mixing and fuel particle elutriation. Fuel elutriation was studied with defining terminal velocities for biomass and coal samples with three different conversion stages without bed material in laboratory-scale measurements. The terminal velocity of biomass was also studied with bed material. The fuels used in the tests were the same fuels that were used in large-scale temperature measurements. These temperature measurements were used in the validation of the comprehensive CFB model.

It was shown with the large-scale temperature measurements that a fuel mixture which had 80% biomass, based on energy content, and 20% coal produces significantly higher temperatures in the transport zone compared to the temperatures in the bottom bed. It was also shown that the operating conditions influence the temperature profile since similar phenomenon was observed with pure coal as fuel. In coal case this was mostly due to cooling effect of recirculated flue gas, which was injected to the bottom part of the boiler.

Terminal velocity measurements of the fuels showed that the terminal velocity distribution of commercially used fuels is wide, at least in this particular case. The results from image analysis showed that there are also significant differences in particle size and shape within the same terminal velocity. The results also showed that terminal velocity of biomass changes more during the conversion from as received to devolatilized compared to coal sample. The terminal velocity model from Haider & Levenspiel (1989) was validated with as received biomass and it was shown to be in agreement with measurements when the average length of the major axis of the fuel particle is used as particle diameter and the average Cox circularity is used as sphericity. Based on the method from Nikku et al. (2014), the drag coefficient for as received biomass was determined, and it was shown to vary between 2.4 and 1.5 when Re is between 200 and 11 000. The terminal velocity for as received biomass was also adjusted from cold conditions to hot conditions (850 °C) and it was shown that for a particular particle size range, the terminal velocity increases by a factor of 1.7 to 2.0 from cold to hot conditions. The terminal velocity measurements with bed material showed that terminal velocity of fuel particles can decrease significantly because of momentum transfer from bed material. Also, the solids concentration was shown to influence the particle elutriation significantly while the terminal velocity of devolatilized biomass can drop to a quarter from the measurements without bed material.

In the modelling part of this thesis, the default set ups for the fuel mixing model was analysed and the terminal velocity was found not to be the only crucial variable influencing fuel mixing and thus the temperature profile in the model. The terminal velocity of fuel particles did affect the temperature profile, but it can be argued that the terminal velocity measurement results from a certain fuel do not help significantly the modelling efforts of a new boiler case compared to accurate information on size and shape of fuel particles. In the current state of the comprehensive model, the terminal velocity measurements are more informative in the development of the model, and not in the actual modelling of a certain case. Instead, when modelling new boiler cases, the efforts should be put into acquiring accurate information on the size and shape of the fuel particles.

Instead of fuel mixing, volatile combustion was identified as the crucial aspect in formation of the temperature profile. Thus, a new method based on this assumption was built where the combustion of volatiles is limited compared to the original model. In addition, fuel elutriation from the dense bed and splash zone was increased to accommodate for the large fuel particles elutriated to the transport zone, which was observed in the terminal velocity measurements with bed material. With the new method, the modelling efforts were improved regarding the axial average temperature profile. The new method is currently validated with three different cases from which two are presented in this thesis.

However, the new method presented in this thesis is not based on extensive optimization and validation and thus it should be considered more as an indication of the needed focus areas in the future improvement of the model. Suggested actions to further improve the accuracy of the model are to validate the new method with more cases, validate the model which accounts for biomass deformation during conversion, measure gas fields in a commercial CFB furnace and measure the fuel concentration in a CFB riser, for example with tracer particles in a laboratory-scale unit. Based on the measurements and modelling results, the focus should be in validation of the gas combustion and fuel mixing models. As the usage of low-volatile coals is decreasing and the usage of different bio-based fuels is increasing, the future fuels will have large shares of volatiles in them. Thus, the significance of volatile combustion in the modelling can be expected to increase.

To summarise, the main contributions of this thesis are:

- Suggesting a new method to increase the accuracy of average axial temperature profile in a comprehensive CFB model.
- Providing information on terminal velocity of fuel particles.
- Demonstrating the effects of bed material on terminal velocity of fuel particles.
- Suggesting that volatile combustion is the most crucial part in modelling of the temperature profile in the current state of the comprehensive CFB model.
- Suggesting areas for future work related to validation and improvement of the comprehensive CFB model.

REFERENCES

Adánez, J., de Diego, L.F., Gayán, P., Armesto, L. & Cabanillas, A. (1995). A model for prediction of carbon combustion efficiency in circulating fluidized bed combustors, Fuel, Vol. 74, Issue 7, pp. 1049–1056.

Adánez, J., Gayán, P., de Diego, L.F., Garcia-Labiano, F. & Abad, A. (2003). Combustion of wood chips in a CFBC. Modeling and validation, Industrial and Engineering Chemistry Research, Vol. 42, Issue 5, pp. 987–999.

Agbor, E., Zhang, X. & Kumar, A. (2014). A review of biomass co-firing in North America, Renewable and Sustainable Energy Reviews, Vol. 40, pp. 930–943.

Alakangas, E. (2005). Properties of wood fuels used in Finland, Technical Research Centre of Finland, VTT Processes, Project report PRO2/P2030/05 (Project C5SU00800), 90 p. + app. 10 p.

Alakangas, E., Hurskainen, M., Laatikainen-Luntama, J. & Korhonen, J. (2016). Suomessa käytettävien polttoaineiden luokituksia, VTT Technology 258, 229 p. + app. 35 p.

Arce, M.E., Saavedra, Á., Míguez, J.L., Granada, E. & Cacabelos, A. (2013). Biomass Fuel and Combustion Conditions Selection in a Fixed Bed Combustor, Energies, Vol. 6, pp. 5973–5989.

Arrhenius, S. (1896). On the Influence of Carbonic Acid in the Air upon the Temperature of the Ground, Philosophical Magazine and Journal of Science, Series 5, Vol. 41, No. 251, pp. 237–276.

Bagheri, G.H., Bonadonna, C., Manzella, I. & Vonlanthen, P. (2015). On the characterization of size and shape of irregular particles, Powder Technology, Vol. 270, Part A, pp. 141–153.

Bagheri, G. & Bonadonna, C. (2016). On the drag of freely falling non-spherical particles, Powder Technology, Vol. 301, pp. 526–544.

Bartok, W. & Sarofim, A.F. (1991). Fossil fuel combustion, a source book, John Wiley & Sons Inc., 866 p.

Basu, P. & Nag, P.K. (1996). Heat transfer to walls of a circulating fluidized-bed furnace, Chemical Engineering Science, Vol. 51, No. 1, pp. 1–26.

Basu, P. (2006). Combustion and Gasification in Fluidized Beds, CRC Press Taylor & Francis Group, 473 p.

Basu, P. (2015). Circulating Fluidized Bed Boilers: Design, Operation and Maintenance, 1st edition, Springer International Publishing, 366 p.

Baxter, L. (2005). Biomass-coal co-combustion: opportunity for affordable renewable energy, Fuel, Vol. 84, Issue 10, pp. 1295–1302.

Blaszczuk, A., Komorowski, M. & Nowak, W. (2012). Distribution of solids concentration and temperature in the combustion chamber of the SC-OUT CFB boiler, Journal of Power Technologies, Vol. 92, No. 1, pp. 27–33.

Breakey, D.E.S., Vaezi, F.G., Masliyah, J.H. & Sanders, R.S. (2018). Side-view-only determination of drag coefficient and settling velocity for non-spherical particles, Powder Technology, Vol. 339, pp. 182 – 191.

Breitholtz, C., Leckner, B. & Baskakov, A.P. (2001). Wall average heat transfer in CFB boilers, Powder Technology, Vol. 120, pp. 41–48.

Brereton, C.M. & Grace, J.R. (1993). End effects in CFB hydrodynamics, Circulat Fluidiz Bed Technol, 4, pp. 137–144.

Briens, C.L. (1991). Correlation for the direct calculation of the terminal velocity of spherical particles in newtonian and pseudoplastic (power-law) fluids, Powder Technology, Vol. 67, Issue 1, pp. 87–91.

van den Broek, R., Faaji, A. & van Wijk, A. (1996). Biomass combustion for power generation, Biomass and Bioenergy, Vol. 11, Issue 4, pp. 271–281.

Budinis, S., Krevor, S., Mac Dowell, N., Brandon, N. & Hawkes, A. (2018). An assessment of CCS costs, barriers and potential, Energy Strategy Reviews, Vol. 22, pp. 61–81.

Cai, R., Ke, X., Lyu, J., Yang, H., Zhang, M., Yue, G. & Ling, W. (2017). Progress of circulating fluidized bed combustion technology in China: a review, Clean Energy, Vol. 1, No. 1, pp. 36–49.

Carman, P.C. (1937). Trans. Inst. Chem. Eng., 15, 150.

Cavarretta, I., O'Sullivan, C. & Coop, M.R. (2009). Applying 2D shape analysis techniques to granular materials with 3D particle geometries, AIP Conf. Proc. 1145, pp. 833–836.

Cetin, E., Moghtaderi, B., Gupta, R. & Wall, T.F. (2004). Influence of pyrolysis conditions on the structure and gasification reactivity of biomass chars, Fuel, Vol. 83, Issue 16, pp. 2139–2150.

Chhabra, R.P., Agarwal, L. & Sinha, N.K. (1999). Drag on non-spherical particles: an evaluation of available methods, Powder Technology, Vol. 101, Issue 3, pp. 288–295.

Charry, K., Aubin, J., Guindé, L., Sierra, J. & Blazy J.M. (2018). Cultivating biomass locally or importing it? LCA of biomass provision scenarios for cleaner electricity production in a small tropical island, Biomass and Bioenergy, Vol. 110, pp. 1–12.

Chen, W. Jiang, P. (2011). Design and Operation of CFB with Compact Separator, Power-Gen Asia, Kuala Lumpur.

Chien, S.F. (1994). Settling velocity of irregularly shaped particles, SPE Drilling & Completion, Vol. 9, Issue 04, p. 281.

Clift, R. & Grace, J.R. (1985). Continuous Bubbling and Slugging. Fluidization. pp. 73–132.

Climate Action Tracker. web page, Available (accessed 22.10.2018): https://climate-actiontracker.org/

Cox, E.P. (1927). A Method of Assigning Numerical and Percentage Values to the Degree of Roundness of Sand Grains, Journal of Paleontology, Vol. 1, No. 3, pp. 179–183.

Crowe, C.T., Schwarzkopf, J.D., Sommerfeld, M. & Tsuji, Y. (2012). Multiphase Flows with Droplets and Particles, 2nd edition, CRC Press Taylor & Francis Group, 494 p.

Davidson, J.F. (2000). Circulating fluidised bed hydrodynamics, Powder Technology, Vol. 113, pp. 249–260.

De, S. & Nag, P.K. (2000). Temperature and gas concentration profiles in a circulating fluidized-bed combustor burning an Indian coal, Proceedings of the Institution of Mechanical Engineers, Part A: Journal of Power and Energy, Vol. 214, Issue 3, pp. 281–286.

Durmaz, T. (2018). The economics of CCS: Why have CCS technologies not had an international breakthrough?, Renewable and Sustainable Energy Reviews, Vol. 95, pp. 328–340.

Dutta, A. & Basu, P. (2002). An experimental investigation into the heat transfer on wing walls in a circulating fluidized bed boiler, International Journal of Heat and Mass Transfer, Vol. 45, Issue 22, pp. 4479–4491.

Djerf, T., Pallarès, D. & Johnsson, F. (2018). Bottom-bed fluid dynamics – Influence on solids entrainment, Fuel Processing Technology, Vol. 173, pp. 112–118.

Elfasakhany, A. & Bai, X.S. (2019). Numerical and experimental studies of irregular-shape biomass particle motions in turbulent flows, Engineering Science and Technology, an International Journal, Vol. 22, Issue 1, pp. 249–265.

Eriksson, O., Finnveden, G., Ekvall, T. & Björklund, A. (2007). Life cycle assessment of fuels for district heating: A comparison of waste incineration, biomass- and natural gas combustion, Energy Policy, Vol. 35, Issue 2, pp. 1346–1362.

European Commission, Climate strategies & targets, web page, Available (accessed 22.10.2018): https://ec.europa.eu/clima/policies/strategies_en

Field, M.A., Gill, D.W., Morgan, B.B. & Hawksley, P.G.W. (1967). Combustion of pulverized coal, The British Coal Utilization Research Association, Surrey

Fotovat, F., Ansart, R., Hemati, M., Simonin, O. & Chaouki, J. (2015). Sand-assisted fluidization of large cylindrical and spherical biomass particles: Experiments and simulation, Chemical Engineering Science, Vol. 126, pp. 543–559.

Fourier, J. (2013). Mémoire sur les températures du globe terrestre et des espaces planétaires. In J. Darboux (Ed.), Oeuvres de Fourier: Publiées par les soins de Gaston Darboux, Cambridge University Press, pp. 95-126.

Fridahl, M. & Lehtveer, M. (2018). Bioenergy with carbon capture and storage (BECCS): Global potential, investment preferences, and deployment barriers, Energy Research & Social Science, Vol. 42, pp. 155–165.

Ganser, G.H. (1993). A rational approach to drag prediction of spherical and nonspherical particles, Powder Technology, Vol. 77, Issue 2, pp. 143–152.

García-Galindo, D., Cieplik, M., Van de Kamp, W. & Royo, F.J. (2019). Maximization of Co-Firing Biomass in Coal Power Stations: Issues on Fly-Ash Quality, 7 p.

Geldart, D. (1973). Types of gas fluidization, Powder Technology, Vol. 7, Issue 5, pp. 285–292.

Gómez-Barea, A. & Leckner, B. (2010). Modeling of biomass gasification in fluidized bed, Progress in Energy and Combustion Science, Vol. 36, Issue 4, pp. 444–509.

Grace, J.R. & Clift, R. (1974). On the two-phase theory of fluidization, Chemical Engineering Science, Vol. 29, Issue 2, pp. 327–334.

Grace, J.R. (2017). Hydrodynamics of Fluidization, Multiphase Flow Handbook, 2nd edition edited by Michaelides, E.E., Crowe, C.T.& Schwarzkopf, J.D., CRC Press Taylor & Francis Group, 1394 p.

Gungor, A. (2009). One dimensional numerical simulation of small scale CFB combustors, Energy Conversion and Management, pp. 711–722.

Guo, Q., Chen, X. & Liu, H. (2012). Experimental research on shape and size distribution of biomass particle, Fuel, Vol. 94, pp. 551–555.

Gupta, M., Yang, J. & Roy, C. (2002). Density of softwood bark and softwood char: procedural calibration and measurement by water soaking and kerosene immersion method, Fuel, Vol. 81, Issue 10, pp. 1379–1384.

Haider, A. & Levenspiel, O. (1989). Drag Coefficient and Terminal Velocity of Spherical and Nonspherical Particles, Powder Technology, Vol. 58, Issue 1, pp. 63–70.

Hartge, E.U., Budinger, S. & Werther, J. (2005). Spatial effects in the combustion chamber of the 235 MWe CFB boiler Turow No 3, Proceedings of the 8th International Conference on Circulating Fluidized beds, Hangzhou, pp. 675 – 682.

He, J., Liu, Y. & Lin, B. (2018). Should China support the development of biomass power generation?, Energy, Vol. 163, pp. 416–425.

Hilligardt, K. & Werther, J. (1986). Local Bubble Gas Hold-Up and Expansion of Gas/Solid Fluidized Beds, German chemical engineering, 9(4), pp. 215–221.

Hiltunen, M.A., Vilokki, H.A.J. & Holopainen, H.A. (2003). Green energy from wood-based fuels using Foster Wheeler CFB boilers, Proceedings of the 17th International Conference on Fluidized Bed Combustion, Jacksonville, pp. 77–81.

Holmgren, P., Wagner, D.R., Strandberg, A., Molinder, R., Wiinikka, H., Umeki, K. & Broström, M. (2017). Size, shape, and density changes of biomass particles during rapid devolatilization, Fuel, Vol. 206, pp. 342–351.

Hua, Y., Flamant, G., Lu, J. & Gauthier, D. (2004). Modelling of axial and radial solid segregation in a CFB boiler, Chemical Engineering and Processing: Process Intensification, Vol. 43, Issue 8, pp. 971–978.

Huilin, L., Guangbo, Z., Rushan, B., Yongjin, C. & Gidaspow, D. (2000). A coal combustion model for circulating fluidized bed boilers, Fuel, Vol. 79, Issue 2, pp. 165–172.

Hurskainen, M. & Vainikka, P. (2015). Technology options for large-scale solid-fuel combustion, Fuel Flexible Energy Generation edited by Oakey, J., Woodhead Publishing, 334 p.

Hyppänen, T., Lee, Y.Y. & Rainio, A. (1991). A three-dimensional model for circulating fluidized bed combustion, Proceedings of the 3rd International Conference on Circulating Fluidized Beds, Pergamon Press, pp. 563–568.

Hyppänen, T. & Raiko, R. (2002). Leijupoltto, Poltto ja Palaminen, 2nd edition edited by Raiko, R., Saastamoinen, J., Hupa, M. & Kurki-Suonio, I., Internationl Flame Research Foundation – Finnish Flame Research Committee, 750 p.

Hölzer, A. & Sommerfeld, M. (2008). New simple correlation formula for the drag coefficient of non-spherical particles, Powder Technology, Vol. 184, Issue 3, pp. 361–365.

IEA-ETSAP, IRENA (2013). Biomass co-firing, 24p.

Intergovernmental Panel on Climate Change (2014). Climate Change 2014: Mitigation of Climate Change, Available (accessed 23.10.2018): http://www.ipcc.ch/report/ar5/wg3/

Intergovernmental Panel on Climate Change (2018). Global Warming of 1.5 °C, Available (accessed 22.10.2018): http://www.ipcc.ch/report/sr15/

International Energy Agency, web page, Available (accessed 23.10.2018): https://www.iea.org/tcep/

Jiankun, H., Zhiwei, Y. & Da, Z. (2012). China's strategy for energy development and climate change mitigation, Vol. 51, pp. 7–13.

Johansson, E., Lyngfelt, A., Mattisson, T. & Johnsson, F. (2003). Gas leakage measurements in a cold model of an interconnected fluidized bed for chemical-looping combustion, Powder Technology, Vol. 134, Issue 3, pp. 210–217.

Johnsson, F. & Leckner, B. (1995). Vertical distribution of Solids in a CFB-furnace (No. CONF-950522—), American Society of Mechanical Engineers, New York

Johnsson, F., Vrager, A. & Leckner, B. (1999). Solids flow pattern in the exit region of a CFB-furnace - influence of exit geometry, Proceedings of the 15th Int. Conference on Fluidized Bed Combustion, Savannah

Kaikko, J., Mankonen, A., Vakkilainen, E. & Sergeev, V. (2017). Core-annulus model development and simulation of a CFB boiler furnace, Energy Procedia, Vol. 120, pp. 572–579.

Kallio, S., Peltola, J. & Niemi, T. (2015). Analysis of the time-averaged gas–solid drag force based on data from transient 3D CFD simulations of fluidized beds, Powder Technology, Vol. 274, pp. 227–238.

Kastberg, S. & Nilsson, C. (2002). Combustion optimization study of biomass powder, SLU.

Kemper, J. (2015). Biomass and carbon dioxide capture and storage: A review, International Journal of Greenhouse Gas Control, Vol. 40, pp. 401–430.

Kleinhans, U., Halama, S. & Spliethoff, H. (2018). Char particle burning behavior: Experimental investigation of char structure evolution during pulverized fuel conversion, Fuel Processing Technology, Vol. 171, pp. 361–373.

Knoebig, T., Luecke, K. & Werther, J. (1999). Mixing and reaction in the circulating fluidized bed – A three-dimensional combustor model, Chemical Engineering Science, Vol. 54, Issue 13–14, pp. 2151–2160.

Konttinen, J., Orasuo, V. & Vakkilainen, E. (2018). The importance and sustainability of bioenergy in Finland and globally, IX Liekkipäivä, Available (accessed 31.01.2019): http://www.ffrc.fi/Liekkipaiva_2018.html

Koornneef, J., Junginger, M. & Faaij, A. (2007). Development of fluidized bed combustion – An overview of trends, performance and cost, Progress in Energy and Combustion Science, Vol. 33, pp. 19–55.

Koornneef, J, van Breevoort, P., Hamelinck, C., Hendriks, C., Hoogwijk, M., Koop, K., Koper, M., Dixon, T. & Camps, A. (2012). Global potential for biomass and carbon dioxide capture, transport and storage up to 2050, International Journal of Greenhouse Gas Control, Vol. 11, pp. 117–132.

Korhonen, H. (2012). Biopolttoaineiden leijutusominaisuuksien karakterisointi, Master's thesis, Lappeenranta University of Technology, 82 p. + app. 1 p.

Kovács, J. (2003). What is fluidised bed agglomeration?, IFRF Online Combustion Handbook. ISSN 1607-9116, No. 50.

Kruse, M. & Werther, J. (1995). 2D gas and solids flow prediction in circulating fluidized beds based on suction probe and pressure profile measurements, Vol. 34, Issue 3, pp. 185–203.

Kunii, D. & Levenspiel, O. (1991). Fluidization Engineering, 2nd edition, Butterworth–Heinemann, 491 p.

Köhler, A., Pallarès, D. & Johnsson, F. (2017). Modelling axial mixing of char - application to the dense bottom bed in CFB boilers, Proceedings of 12th International Conference on Fluidized Bed Technology, Halifax, pp. 385–392.

La Nauze, R.D. (1987). A review of the fluidized bed combustion of biomass, Journal of the Institute of Energy, Vol. 60, pp. 66–76.

Lackermeier, U. & Werther, J. (2002). Flow phenomena in the exit zone of a circulating fluidized bed, Chemical Engineering and Processing: Process Intensification, Vol. 41, Issue 9, pp. 771–783.

Lebowitz, J. L. (1964). Exact solution of generalized Percus-Yevick equation for a mixture of hard spheres. Physical Review, Vol. 133, Issue 4A, pp. A895-A899.

Lee, J.S. & Choi, E.C. (2018). CO_2 leakage environmental damage cost – A CCS project in South Korea, Renewable and Sustainable Energy Reviews, Vol. 93, pp. 753–758.

Leva, M. et al. (1948). Chem. Eng. Prog., 44, 511, 707 (1948); Ind. Eng. Chem., 41, 1206 (1949).

Levendis, Y., Joshi, K., Khatami, R. & Sarofim, A.F. (2011). Combustion behavior in air of single particles from three different coal ranks and from sugarcane bagasse, Combustion and Flame, Vol. 158, Issue 3, pp. 452–465.

Li, J. & Kato, K. (2001). Effect of electrostatic and capillary forces on the elutriation of fine particles from a fluidized bed, Advanced Powder Technol., Vol. 12, No. 2, pp. 187–205.

Li, J. & Kuipers, J.A.M. (2003). Gas-particle interactions in dense gas-fluidized beds, Chemical Engineering Science, Vol. 58, Issue 3–6, pp. 711–718.

Liley, P.E., Thomson, G.H., Friend, D.G., Daubert, T.E. & Buck, E. (1997). Physical and Chemical data, Perry's chemical engineers' handbook edited by Perry, R.H., Green, D.W. & Maloney, J.O., 7th edition, The McGraw-Hill Companies.

Lind, T., Kauppinen, E.I., Kurkelam J., Maenhaut, W., Shah, A. & Huggins, F. (1995). Mineral, Sorbent and Sulfur Interactions in Real-Scale CFBC, Proceedinges of the 13th International Conference in Fluidized bed Combustion. Heinschel, ASME, pp. 1129–1136.

Lind, T. (1999). Ash formation in circulating fluidized bed combustion of coal and solid biomass, dissertation, VTT Publications 378, 80 p. + app. 83 p.

Loth, E. (2008). Drag of non-spherical solid particles of regular and irregular shape, Powder Technology, Vol. 182, Issue 3, pp. 342–353.

Lu. H., Ip, E., Scott, J., Foster, P., Vickers, M. & Baxter, L. (2010). Effects of particle shape and size on devolatilization of biomass particle, Fuel, Vol. 89, Issue 5, pp. 1156–1168.

Luckos, A. & Koekemoer, A. (2014). On the sphericity of coal and char particles, Proceedings of IFSA 2014 conference, pp. 267–276.

Luecke, K., Hartge, E.U., Werther, J. (2004). A 3-dimensional model of combustion in large-scale circulating fluidized bed boilers, International Journal of Chemical Reactor Engineering, Vol. 2, Issue 1.

Macedo, I.C., Nassar, A.M., Cowie, A.L., Seabra, J.E.A., Marelli, L., Otto, M., Wang, M.Q. & Tyner, W.E. (2015). Greenhouse Gas Emissions from Bioenergy, Bioenergy & Sustainability: bridging the gaps edited by Souza, G.M., Victoria, R.L., Joly, C.A. & Verdade, L.M., SCOPE, 735 p.

Mandø, M. (2009). Turbulence Modulation by Non-Spherical Particles, dissertation, Aalborg University, 234 p.

Mandø, M. & Rosendahl, L. (2010). On the motion of non-spherical particles at high Reynolds number, Powder Technology, Vol. 202, Issue 1–3, pp. 1–13.

Mao, G., Huang, N., Chen, L. & Wang, H. (2018). Research on biomass energy and environment from the past to the future: A bibliometric analysis, Science of The Total Environment, Vol. 635, pp. 1081–1090.

Mclaren, D. (2012). A comparative global assessment of potential negative emissions technologies, Process Safety and Environmental Protection, Vol. 60, Issue 6, pp. 489–500.

Momeni, M., Yin, C., Kær, S. K., Hansen, T. B., Jensen, P. A., & Glarborg, P. (2013). Experimental Study on Effects of Particle Shape and Operating Conditions on Combustion Characteristics of Single Biomass Particles, Energy & Fuels, Vol. 27, Issue 1, pp. 507-514.

Myöhänen, K., (2011). Modelling of combustion and sorbent reactions in three-dimensional flow environment of a circulating fluidized bed furnace, dissertation, Lappeenranta University of Technology, Acta Universitatis Lappeenrantaensis 449, 161 p.

Myöhänen, K. & Hyppänen, T. (2011). A Three-Dimensional Model Frame for Modelling Combustion and Gasification in Circulating Fluidized Bed Furnaces, International Journal of Chemical Reactor Engineering, Vol. 9, Issue 1.

Nasa, Drag of a Sphere, webpage, Available (accessed 17.1.2018): https://www.grc.nasa.gov/www/k-12/airplane/dragsphere.html

Nikku, M., Jalali, P., Ritvanen, J. & Hyppänen, T. (2014). Characterization method of average gas–solid drag for regular and irregular particle groups, Powder Technology, Vol. 253, pp. 284–294.

Nikku, M. (2015). Three-dimensional modeling of biomass fuel flow in a circulating fluidized bed furnace, dissertation, Lappeenranta University of Technology, Acta Universitatis Lappeenrantaensis 644, 99 p.

Nikku, M., Myöhänen, K., Ritvanen, J., Hyppänen, T. & Lyytikäinen, M. (2016). Three-dimensional modeling of biomass fuel flow in a circulating fluidized bed furnace

with an experimentally derived momentum exchange model, Chemical Engineering Research and Design, Vol. 115, Part A, pp. 77–90.

Nikku, M., Jalali, P. & Hyppänen, T. (2017). Comparison of Ansys Fluent and OpenFOAM in Simulation of Circulating Fluidized Bed Riser, Proceedings of the 12th International Conference of Fluidized Bed Technology, pp. 349–356.

Niklasson, F., Thunman, H., Johnsson, F. & Leckner, B. (2002). Estimation of Solids Mixing in a Fluidized-Bed Combustor, Ind. Eng. Chem. Res, Vol. 41, pp. 4663–4673.

Niklasson, F., Pallarès, D. & Johnsson, F. (2006). Biomass co-firing in a CFB boiler – The influence of fuel and bed properties on in-furnace gas-concentration profiles, Proceedings of the 19th Fluidized Bed Combustion Conference, Vienna.

Nuortimo, K. (2015). State of the art CFB technology for flexible large scale utility power production, PowerGen Russia, Moscow.

Oka, S.N. (2004). Fluidized Bed Combustion, Marcel Dekker, Inc., 590 p.

Olowson, P.A. & Almstedt, A.E. (1990). Influence of pressure and fluidization velocity on the bubble behaviour and gas flow distribution in a fluidized bed, Chemical Engineering Science, Vol. 45, No. 7, pp. 1733–1741.

Orasuo, V. (2018). Bioenergian merkitys ja kestävyys - Suomelle ja globaalisti, Master's thesis, Tampere University of Technology, 81 p. + app. 3 p.

Palchonok, G.I., Breitholtz, C., Thunman, H. & Leckner B. (1997). Impact of heat and mass transfer on combustion of a fuel particle in CFB boilers. Proceedings of the 14th international conference on FBC, pp. 871–888.

Pallarès, D. & Johnsson, F. (2006a). Macroscopic modelling of fluid dynamics in large-scale circulating fluidized beds, Progress in Energy and Combustion Science. Vol. 32, Issue 5–6, pp. 539–569.

Pallarès, D. & Johnsson, F. (2006b). A novel technique for particle tracking in cold 2-dimensional fluidized beds—simulating fuel dispersion, Chemical Engineering Science, Vol. 61, pp. 2710 – 2720.

Pallarès, D. (2008a). Fluidized bed combustion – modeling and mixing, dissertation, Chalmers University of Technology, Ny serie nr. 2823, 50 p.

Pallarès, D. & Johnsson, F. (2008b). Modeling of fuel mixing in fluidized bed combustors, Chemical Engineering Science, Vol. 63, Issue 23, pp. 5663–5671.

Pallarès, D., Johnsson, F. (2009). Dynamical modeling of the gas phase in fluidized bed combustion – accounting for fluctuations, Proceedings of the 20th International Conference on Fluidized Bed Combustion, Xi'an.

Pallarès, D., Palonen, M., Ylä-Outinen, V & Johnsson, F. (2012). Modeling of the heat transfer in large-scale fluidized bed furnaces, Proceedings of the 21st International Conference on Fluidized Bed Combustion, Naples.

Pallarès, D. & Johnsson, F. (2013). Modeling of fluidized bed combustion processes, Fluidized Bed Technologies for Near-Zero Emission Combustion and Gasification edited by Scala, F., Woodhead Publishing, 1088 p.

Pallarès, D. & Johnsson, F. (2015). Time-resolved modeling of gas mixing in fluidized bed units, Fuel Processing Technology, Vol. 134, pp. 73–84.

Palonen, M., Pallarès, D., Ylä-Outinen, V., Larsson, A., Laine, J. & Johnsson, F. (2011). Circulating fluidized bed combustion – build-up and validation of a three-dimensional model, Proceedings of the 10th International Conference on Circulating Fluidized Beds, Oregon.

Paris Agreement (2015). United Nations, Available (accessed 22.10.2018): https://unfccc.int/files/essential_background/convention/application/pdf/english_paris_agreement.pdf

Priyanto, D.E., Ueno, S., Hashida, K. & Kasai, H. (2017). Energy-efficient milling method for woody biomass, Advanced Powder Technology, Vol. 28, Issue 7, pp. 1660–1667.

Raiko, R. (2002). Palamisen termodynaamiset perusteet, Poltto ja Palaminen, 2nd edition edited by Raiko, R., Saastamoinen, J., Hupa, M. & Kurki-Suonio, I., Internationl Flame Research Foundation – Finnish Flame Research Committee, 750 p.

Ratschow, L. (2009). Three-Dimensional Simulation of Temperature Distributions in Large-Scale Circulating Fluidized Bed Combustors, dissertation, Hamburg University of Technology.

Rautiainen, A., Lintunen, J. & Uusivuori J. (2018). How harmful is burning logging residues? Adding economics to the emission factors for Nordic tree species, Biomass and Bioenergy, Vol. 108, pp. 167–177.

Riaza, J., Khatami, R., Levendis, Y.A., Álvarez, L., Gil, M.V., Pevida, C., Rubiera, F. & Pis, J.J. (2014). Single particle ignition and combustion of anthracite, semi-anthracite and bituminous coals in air and simulated oxy-fuel conditions, Combustion and Flame, Vol. 161, Issue 4, pp. 1096–1108.

Riaza, J., Gibbins, J. & Chalmers, H. (2017). Ignition and combustion of single particles of coal and biomass, Fuel, Vol. 202, pp. 650–655.

Riley, N.A. (1941). Projection sphericity, Journal of Sedimentary Research, Vol. 11, No. 2, pp. 94–97.

Roni, M.S., Chowdhury, S., Mamun, S., Marufuzzaman, M., Lein, W. & Johnson, S. (2017). Biomass co-firing technology with policies, challenges, and opportunities: A global review, Renewable and Sustainable Energy Reviews, Vol. 78, pp. 1089–1101.

Rootzén, J. & Johnsson, F. (2015). CO_2 emissions abatement in the Nordic carbon-intensive industry – An end-game in sight?, Energy, Vol. 80, pp. 715–730.

Saraber, A.J. & van den Berg, J.W. (2004). Influence of Co-Combustion on the Quality of Coal Fly Ash, ACI Special Publications, Vol. 735.

Schiller, L. & Naumann, Z. (1935). Über die grundlegenden Berechnungen bei der Schwerkraftaufbereitung, Zeitschrift Des Vereines Deutscher Ingenieure, 77, pp. 318–320.

Schulz, E.F., Wilde, R.H. & Albertson, M.L. (1954). Report for the Missouri River Div., Corps of Engineers, U.S. Army, through Colorado A&M Research Foundation, Fort Collins, CO.

Shellard, J.E. & Macmillan, R.H. (1978). Aerodynamic properties of threshed wheat materials, Journal of Agricultural Engineering Research, Vol. 23, pp. 273–281.

Skrifvars, B.J. & Hupa, M. (2002). Tuhka, kuonaantuminen, likaantuminen ja korroosio, Poltto ja Palaminen, 2nd edition edited by Raiko, R., Saastamoinen, J., Hupa, M. & Kurki-Suonio, I., Internationl Flame Research Foundation – Finnish Flame Research Committee, 750 p.

Song, X., Xu, Z., Li, G., Pang, Z. & Zhu, Z. (2017). A new model for predicting drag coefficient and settling velocity of spherical and non-spherical particle in Newtonian fluid, Powder Technology, Vol. 321, pp. 242–250.

Soriano Sánchez, I. (2019). Effective velocity of biomass particles in a fluidized bed reactor, Master's thesis, Chalmers University of Technology, 33 p.

Souza, G.M., Ballester, M.V.R., de Brito Cruz, C.H., Chum, H., Dale, B., Dale, V.H., Fernandes, E.C.M., Foust, T., Karp, A., Lynd, L., Filho, R.M., Millanez, A., Nigro, F., Ossenweijer, P., Verdade, L.M., Victoria, R.L. & Van der Wielen, L. (2017). Environmental Development, Vol. 23, pp. 57–64.

Spliethoff, H. (2010). Power Generation from Solid Fuels, Springer-Verlag Berlin Heidelberg, 674 p.

Steenari, B.M., Åmand, L.E. & Bohwalli, J. (2019). Agglomeration of the bed material in fluidized bed reactors for thermal conversion of biomass -A threat for the development of the technology.

Steer, J.M., Marsch, R., Morgan, D. & Greenslade, M. (2015). The effects of particle grinding on the burnout and surface chemistry of coals in a drop tube furnace, Fuel, Vol. 160, pp. 413–423.

Sternéus, J., Johnsson, F. & Leckner, B. (2000a). Gas mixing in circulating fluidised-bed risers, Chemical Engineering Science, Vol. 55, Issue 1, pp. 129–148.

Sternéus, J., Johnsson, F., Leckner, B., Wiesendorf, V. & Werther, J. (2000b). Measurements of fluid dynamics and reaction conditions in the bottom zone of large-scale CFB combustors, Journal of the Institute of Energy, Vol. 73, Issue 497, pp. 184–190.

Sternéus, J., Johnsson, F. & Leckner, B. (2002). Characteristics of gas mixing in a circulating fluidised bed, Powder Technology, Vol. 126, Issue 1, pp. 28–41.

Stringham, G.E., Simons, D.B. & Guy, H.P. (1969). The behaviour of large particles falling in quiescent liquids, United States Geological Survey professional paper, 562-C, pp. C1–C36.

Sun, L., Lin, J., Wu, F. & Chen, Y. (2004). Effect of non-spherical particles on the fluid turbulence in a particulate pipe flow, Journal of Hydrodynamics, Ser. B, 16 (6), pp. 721–729.

Suopajärvi, H., Umeki, K., Mousa, M., Hedayati, A., Romar, H., Kemppainen, A., Wang, C., Aekjuthon, P., Tuomikoski, S., Norberg, N., Andefors, A., Öhman, M., Lassi, U. & Fabritius, T. (2018). Use of biomass in integrated steelmaking – Status quo, future needs and comparison to other low-CO2 steel production technologies, Applied Energy, Vol. 213, pp. 384–407.

Svensson, A., Johnsson, F. & Leckner, B. (1996). Bottom bed regimes in a circulating fluidized bed boiler, Int. J. Multiphase Flow, Vol. 22, No. 6, pp. 1187–1204.

Swamee, P.K. & Ojha, C.P. (1991). Drag coefficient and fall velocity of nonspherical particles, Journal of Hydraulic Engineering, Vol. 117, Issue 5, pp. 660–667.

Syamlal, M. (1985). Multiphase hydrodynamics of gas-solids flow, dissertation, Illinois Institute of Technology.

Syamlal, M., Rogers, W. & O'Brien, T.J. (1993). MFIX Documentation Theory Guide, U.S. Department of Energy, 52 p.

Teir, S., Pikkarainen, T., Kujanpää, L., Tsupari, E., Kärki, J., Arasto, A. & Aatos, S. (2011). Hiilidioksidin talteenotto ja varastointi (CCS): Teknologiakatsaus, VTT Working Papers 161, 103 p. + app. 3 p.

Thunman, H., Davidsson, K. & Leckner, B. (2004). Separation of drying and devolatilization during conversion of solid fuels, Combustion and Flame, Vol. 137, Issue 1–2, pp. 242–250.

Tolvanen, H., Kokko, L. & Raiko, R. (2013). Fast pyrolysis of coal, peat and torrefied wood: Mass loss study with a drop-tube reactor, particle geometry analysis, and kinetics modeling, Fuel, Vol. 111, pp. 148–156.

Tourunen, A.S., Saastamoinen, J.J., Hämäläinen, J.P., Paakkinen, K.M., Hyppänen, T.E. & Kettunen, A.M. (2003). Study of operation of a pilot CFB-reactor in dynamic conditions, Proceedings of the 17th International Conference on Fluidized Bed Combustion, Jacksonville, pp. 353–361.

Ulusoy, U. & Igathinathane, C. (2014). Dynamic image based shape analysis of hard and lignite coal particles ground by laboratory ball and gyro mills, Fuel Processing Technology, Vol. 126, pp. 350–358.

United Nations Climate Change, Paris Agreement - Status of Ratification, web page, Available (accessed 11.07.2019): https://unfccc.int/process/the-paris-agreement/status-of-ratification

Usui, H., Li, L. & Suzuki, H. (2001). Rheology and pipeline transportation of dense fly ash-water slurry, Korea-Australia Rheology Journal, Vol. 13, No. 1, pp. 47–54.

Utt, J. & Giglio, R. (2012). Technology comparison of CFB versus pulverized-fuel firing for utility power generation, Journal of the Southern African Institute of Mining and Metallurgy, Vol. 112, No. 6, pp. 449–454

Uusitalo, M., Kinnunen, H. & Luomaharju, T. (2018). Material solutions in FBC boilers with challenging fuels, 23rd International Conference on Fluidized Bed Combustion, Seoul.

Vakkilainen, E.K. (2017). Solid Biofuels and Combustion - Steam Generation from Biomass, Butterworth-Heinemann, 322 p.

Valmet MyAcademy, CFB Boiler, (internal website).

Vassilev, S.V., Baxter, D., Andersen, L.K. & Vassileva, C.G. (2010). An overview of the chemical composition of biomass, Fuel, Vol. 89, Issue 5, pp. 913–933.

Vepsäläinen, A., Myöhänen, K., Hyppänen, T., Leino, T. & Tourunen, A. (2009). Development and Validation of a 3-Dimensional CFB Furnace Model, Proceedings of the 20th International Conference on Fluidized Bed Combustion, Xi'an, pp. 757–763.

Versteeg, H.K. & Malalasekera, W. (2007). An Introduction to Computational Fluid Dynamics: The Finite Volume Method, 2nd edition, Pearson Education Limited, 503 p.

Wadell, H. (1933). Sphericity and Roundness of Rock Particles, The Journal of Geology, Vol. 41, No. 3, pp. 310–331.

Wall, T., Liu, Y. & Bhattacharya, S. (2012). A scoping study on Oxy-CFB technology as an alternative carbon capture option for Australian black and brown coals, Australian National Low Emissions Coal Research & Development (ANLEC R&D), 57 p.

Wang, D. & Fan, L.-S. (2013). Particle characterization and behavior relevant to fluidized bed combustion and gasification systems, Fluidized Bed Technologies for Near-Zero Emission Combustion and Gasification edited by Scala, F., Woodhead Publishing, 1088 p.

Wang, Q., Luo, Z., Li, X., Fang, M., Ni, M. & Cen, K. (1999). A mathematical model for a circulating fluidized bed (CFB) boiler, Energy, Vol. 24, Issue 7, pp. 633–653.

White, F.M. (2016). Fluid Mechanics, 8th edition, McGraw-Hill Education, 848 p.

Wiesendorf, V., Hartge, E.U., Werther, J., Johnsson, F., Sternéus, J., Leckner, B., Montat, D., Briand, P. (1999). The CFB Boiler in Gardanne - An Experimental Investigation of its Bottom Zone, Proceedings of the 15th International Conference on Fluidized Bed Combustion, Savannah.

Win, K.K., Nowak, W., Matsuda, H., Hasatani, M., Bis, Z., Krzywanski, J. & Gajewski, W. (1995). Transport Velocity of Coarse Particles in Multi-Solid Fluidized Bed, Journal of Chemical Engineering of Japan, Vol. 28, Issue 5, pp. 535–540.

Wischnewski, R. (2008). Simulation of large-scale circulating fluidized bed combustors, dissertation, Hamburg University of Technology.

Yang, H., Wirsum, M., Guangxi, Y., Fett, F.N. & Youning, X. (2003). A six-parameter model to predict ash formation in a CFB boiler, Powder Technology, Vol. 134, Issue 1–2, pp. 117–122.

Yang, H., Wirsum, M., Lu, J., Xianbin, X. & Guangxi, Y. (2004). Semiempirical technique for predicting ash size distribution in CFB boilers, Fuel Processing Technology, Vol. 85, Issue 12, pp. 1403–1414.

Yates, J.G. (1996). Effects of temperature and pressure on gas-solid fluidization, Chemical Engineering Science, Vol. 51, Issue 2, pp. 167–205.

Yin, C., Rosendahl, L.A. & Kær, S.K. (2008). Grate-firing of biomass for heat and power production, Progress in Energy and Combustion Science, Vol. 34, Issue 6, pp. 725–754.

Yin, C. & Li, S. (2017). Advancing grate-firing for greater environmental impacts and efficiency for decentralized biomass/wastes combustion, Energy Procedia, Vol. 120, pp. 373–379.

Young, H.D. & Freedman, R.A. (2012). Sears and Zemansky's University Physics with Modern Physics, 13th edition, Pearson Education, Inc., 1521 p.

Yow, H.N., Pitt, M.J. & Salman, A.D. (2005). Drag correlations for particles of regular shape, Advanced Powder Technology, Vol. 16, No. 4, pp. 363–372.

Zhang, W., Johnsson, F. & Leckner, B. (1995). Fluid-dynamic boundary layers in CFB boilers, Chemical Engineering Science, Vol. 50, Issue 2, pp. 201–210.

Zhang, Y., Zhang, M., Yao, X., Lyu, J. & Yang, H. (2018). The exit impact on segregation of binary particles in the CFB system, Powder Technology, Vol. 339, pp. 930–938.

Zhao, B., Zhou, Q., Wang, J. & Li, J. (2015). CFD study of exit effect of high-density CFB risers with EMMS-based two-fluid model, Chemical Engineering Science, Vol. 134, pp. 477–488.

Zhou, T., Gong, Z., Lu, Q., Na, Y. & Sun, Y. (2015). Experimental Study on Enhanced Control of NO Emission from Circulating Fluidized Bed Combustion, Energy & Fuels, Vol. 29, Issue 6, pp. 3634–3639.